NASA Contractor Report 179537
Garrett 21-5278-1

Oxide-Dispersion-Strengthened Turbine Blades

Volume I

P.P. Millan, Jr. and J.C. Mays
Garrett Turbine Engine Company
Phoenix, Arizona

October 1986

Prepared for
Lewis Research Center
Under Contract NAS3-20073

National Aeronautics and
Space Administration

TABLE OF CONTENTS

TABLE OF CONTENTS (Contd)

FOREWORD

This Project Completion Report was prepared for the National Aeronautics and Space Administration, Lewis Research Center. It presents the results of a program conducted to establish the advantages of using uncooled, oxide-dispersion- and gamma-prime-strengthened MA6000 turbine blades. The program was conducted as part of the Materials for Advanced Turbine Engines (MATE) Program under Contract NAS3-20073.

The authors wish to acknowledge the assistance and guidance of S. Grisaffe, C. P. Blankenship, and R. L. Dreshfield of the NASA - Lewis Research Center. In addition, the authors acknowledge the efforts of individuals who have made significant contributions to this NASA MATE Project 4: G.S. Hoppin, F.A. Schweizer, M. Egan, J. Clark, T.G. Beatty, R.E. Dennis, D.K. Winstanley, A. Ansari, and V.H. Long.

SECTION I

1.0 SUMMARY

Uncooled turbine blades of the oxide-dispersion and gamma-prime strengthened alloy MA6000 have good stress rupture properties at low stresses and elevated temperatures, resulting in a significant improvement in metal-temperature capability. This, in turn, tends to maximize the turbine efficiency in small- to medium-sized turbofan engines for business and commuter aircraft. Due to the unique combination of strengthening mechanisms in this International Nickel Company (INCO) developed alloy, it offers a 100 to 150F improvement in temperature capability over cast single-crystal turbine blades in the maximum temperature/stress-rupture limited regions of advanced turbine blades. This project includes a demonstration of the advantages of using uncooled, oxide-dispersion and gamma-prime strengthened alloy MA6000 turbine blades as compared with uncooled, cast, directionally solidified (DS) MAR-M 247 turbine blades (as demonstrated in Project 1) in the TFE731 engine. Specific objectives of the program were:

- Scale up and optimize processing of oxide-dispersion strengthened MA6000 alloy
- Determine key material properties and compare to DS MAR-M 247 and single crystal CMSX-3 alloys
- Develop blade manufacturing techniques
- Design low-stress blade
- Evaluate blades through component testing

- Demonstrate uncooled MA6000 turbine blades through engine testing

The initial work focused on refining the process employed to produce MA6000 bar stock such that uniform, high quality, properly sized material required to produce TFE731 HP turbine blades can be reproducibly manufactured by INCO. The optimum processing parameters for MA6000 barstock were identified and a fair degree of tolerance to nonoptimum processing was indicated. A schematic of the process is shown in Figure 1.

The MA6000 barstock was then characterized for mechanical, environmental, and physical properties. This evaluation consisted of microstructure and grain size metallographic examination and tensile and stress-rupture testing. Figures 2 and 3 show a comparison of these properties with DS MAR-M 247 and SC CMSX-3.

Investigations were conducted to determine which machining process was the most cost effective for producing turbine blades from MA6000. Machining methods studied included electrical-discharge-machining (EDM), electro-chemical machining (ECM), milling, and grinding. The ECM process was found to be superior for the airfoil, while conventional grinding was selected for the firtree.

The design requirement of low blade stress for MA6000 material requires a high taper ratio blade (7.1 to 1). Based on two-dimensional blade-to-blade flow solutions and boundary layer analyses, no performance penalty was identified for the new high taper ratio blade design when compared to the previous blade design.

Analyses and component tests performed in the mechanical design of the blades included:

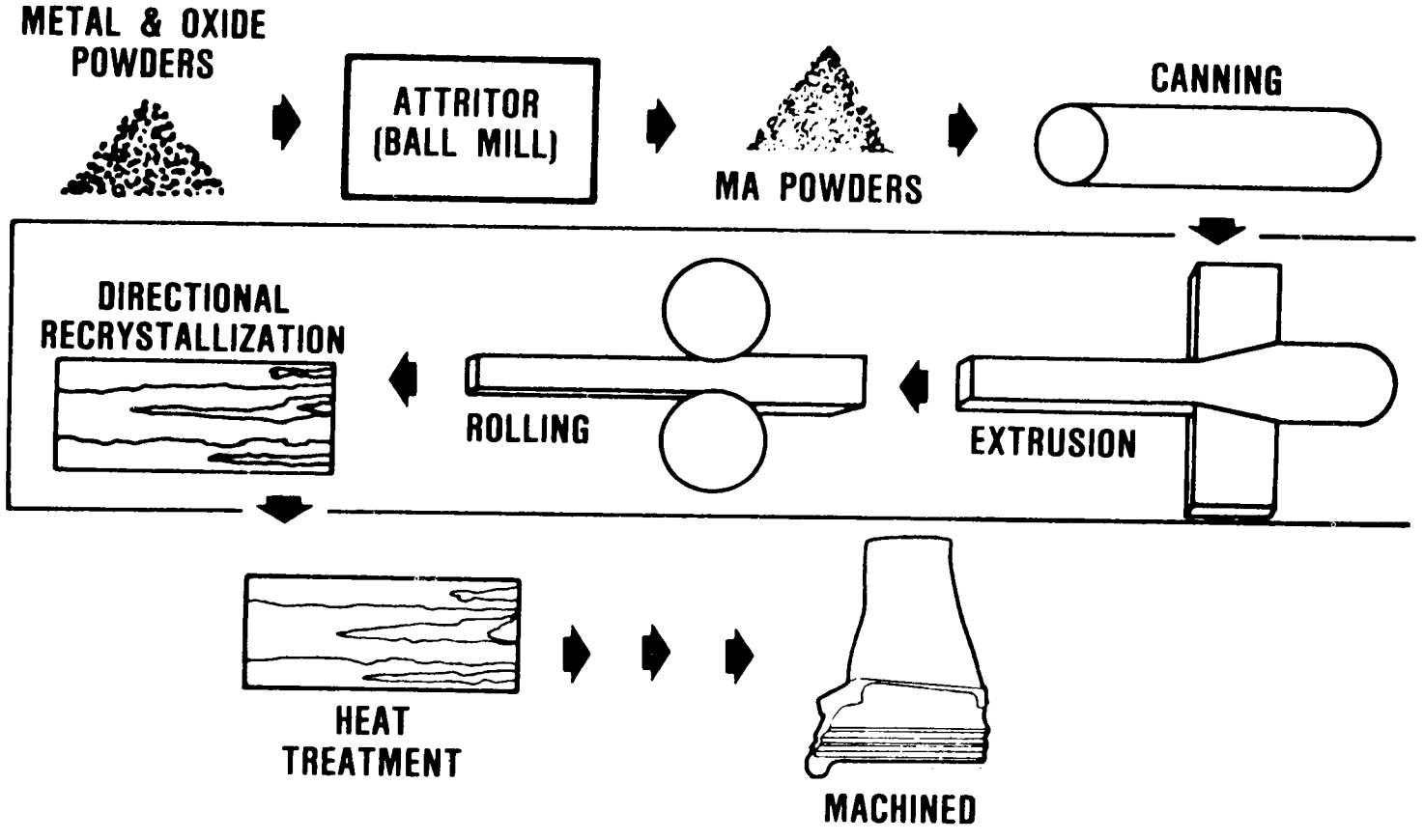

Figure 1. Mechanical Alloying Process.

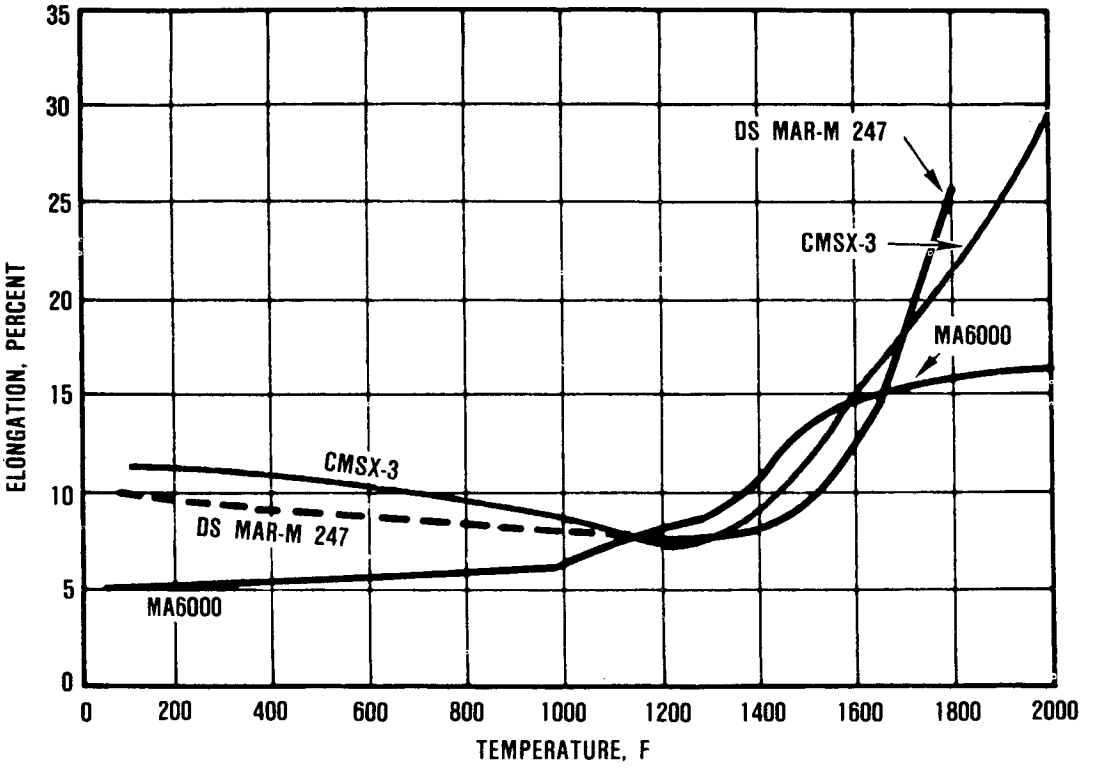

G5-000-20

Figure 2. Tensile Properties Versus Temperature of MA6000, SC CMSX-3, and DS MAR-M 247, Longitudinal Orientation.

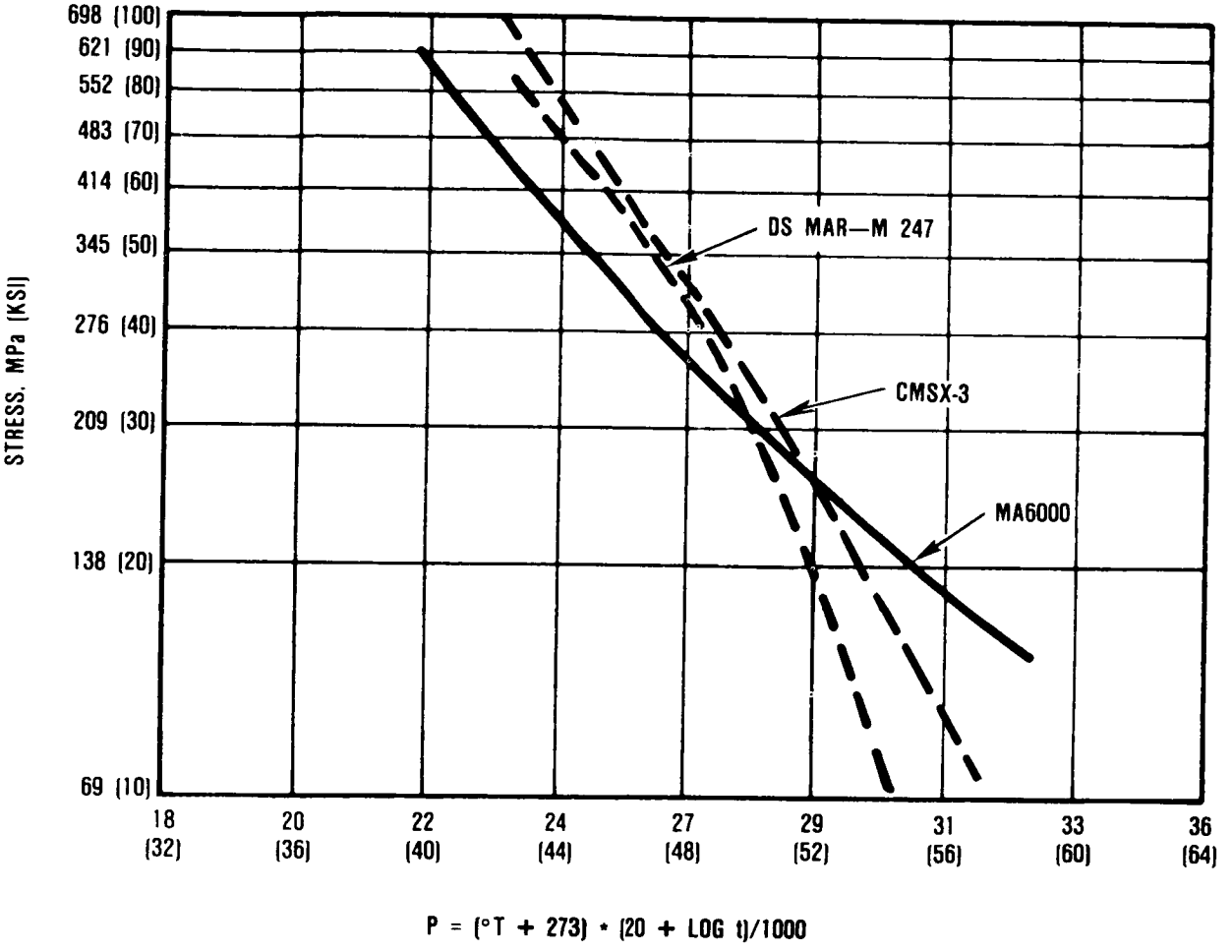

Figure 3. Stress-Rupture Data for MA6000, SC CMSX-3, and DS MAR-M 247, Longitudinal Orientation.

- Thermal and stress analysis
- Blade life analysis
- Vibration tests
- Whirlpit tests
- High rotor rig test

A 2-D thermal analysis was performed on the HP rotor. Stresses in the airfoil and attachment were analyzed using 3-D and 2-D finite element models, respectively.

A detailed blade life analysis was performed based on the planned 200-hour engine test. Results indicated acceptable lives for the test cycles planned. Comparison of the rupture life of the MA6000 blade with the CMSX-3 single crystal at T_4 = 1054C (1930F), and 29,700 rpm indicates that the MA6000 blade has 44 percent longer life than the single crystal blade.

Holography and shaker tests of strain gaged blades were conducted to determine the frequency, mode shapes, and blade critical strain locations. Strain gages were subsequently mounted on the blades at the critical locations and tested in a core engine at the design speed and temperature. The results of the test indicated that the maximum alternating strains were well within the acceptable level.

A whirlpit test was conducted to verify the structural integrity of the MA6000 blade airfoil and its firtree attachment. Pre- and posttest examinations indicated no significant distress or critical distortion.

MA6000 airfoil vibratory strains under engine conditions were evaluated in a high-rotor-rig test. The posttest fluorescent penetrant inspection indicated no signs of blade or disk defects.

Preliminary and final cost analyses which compared the finished costs of the following three TFE731-3B uncooled blade designs were completed:

- o DS MAR-M 247 production
- o Single crystal CMSX-3 blades
- o ODS MA6000 blades

The cost projections are for lots of 2000 to 3000 blades per month for the 1985 to 1990 time period.

The results of the preliminary cost comparison indicated that the material cost for a MA6000 blade was approximately the same as the total cost of a DS blade. The finished cost of the MA6000 blade was 2.9 times that of a DS blade and 1.7 times that of a SC blade.

The results of the final cost study indicate that the cost of a MA6000 blade is approximately twice (1.95) that of a DS cast blade. The final cost projection reflects the experience gained with MA6000 and is substantially lower than the preliminary analysis (1.95 versus 2.91).

SECTION II

2.0 INTRODUCTION

One of the driving parameters that affects the successful design and development of advanced, high-performance gas turbine engines is turbine inlet temperature. The ability to increase this critical temperature results in a gain in the thrust-to-weight ratio and a potential reduction in specific fuel consumption. These gains are achieved by significant design improvements in the turbine section directly affecting the turbine blades and vanes. Sophisticated cooling schemes offering high cooling effectiveness and/or advanced material systems that have improved mechanical properties at elevated temperatures are approaches that are commonly employed to improve component capability. However, the use of cooling air entails a performance penalty attributed to aerodynamic losses and to the thicker airfoils to provide room for cooling passages. In addition, cooled turbines involve complex construction that may lead to increased cost for small turbine components. Thus, the use of advanced material systems for uncooled turbine blades operating at higher temperatures clearly is a desirable approach.

The NASA Materials for Advanced Turbine Engines (MATE) Program supported by the NASA - Lewis Research Center is a cooperative effort with industry to accelerate the introduction of new material technologies into aircraft turbine engines. As part of this effort, the Garrett Turbine Engine Company (GTEC) was authorized under NASA Contract NAS3-20073 to conduct Project 4, which is concerned with determining the performance/life potential and problems associated with the application of oxide-dispersion-strengthened (ODS) alloys in gas turbine engines. Specifically, the project focuses on the development of a high-temperature, uncooled gas turbine blade using

INCONEL MA6000* alloy from the feasibility stage through the engine demonstration test. The performance of the oxide-dispersion- and gamma-prime-strengthened MA6000 alloy turbine blades compared with cast, directionally solidified (DS) MAR-M 247** (established in Project 1 of this program) will be demonstrated in a Garrett Model TFE731 turbofan engine.

This report constitutes Volume 1 of a two-volume Project Completion Report presenting the results of the investigations performed under MATE Project 4, Oxide-Dispersion-Strengthened Turbine Blades. This volume contains all of Project 4 except the full-scale engine testing and posttest analysis. These are the subjects of Volume 2 of this report.

The intent of Project 4 was to develop an optimum method to manufacture ODS turbine blades from the INCO MA6000 barstock and to design and compare this blade with the DS MAR-M 247 turbine blade.

Project goals associated with this program include the following:

- Scale up and establish commercial production capability for MA6000 barstock and the associated blade manufacturing process

- Define material properties and design a high-pressure turbine blade from this data base

- Demonstrate uncooled MA6000 blade performance through component and engine tests

*Trademark - INCO Alloys International
**Trademark - Martin Marietta Company

Project 4 was subdivided into the following ten tasks:

Task I - Alloy Process Optimization
Task II - Blade Manufacturing Process Optimization
Task III - Blade Cost Analysis
Task IV - Material Property Characterization
Task V - Blade Design
Task VI - Component Manufacture
Task VII - Component Testing
Task VIII - Subcontractor Activity
Task IX - Engine Test
Task X - Posttest Analysis

In Task I, the optimum processing parameters for MA6000 barstock were identified. A fair degree of tolerance to nonoptimum processing was indicated.

Task II led to the selection of a grinding process for the fir-tree area and the use of electrochemical machining (ECM) to generate the blade airfoil shape.

In Task III, blade costs, including material and processing costs, were analyzed and projected.

The mechanical, environmental, and physical property evaluations of MA6000 were conducted during Task IV. Mechanical property testing included tensile, creep-rupture, stress-rupture, and high- and low-cycle fatigue tests. Environmental characterization included coated and uncoated oxidation and hot-corrosion tests. Physical properties measured included density, thermal expansion, thermal conductivity, and elastic modulus.

During Task V, the ODS blade was designed to use the improved manufacturing process and mechanical properties of MA6000.

In Task VI, three complete sets of MA6000 blades and one set of all components needed to test these blades were manufactured.

Task VII included three phases of component testing: bench tests, high-rotor-rig tests, and whirlpit tests.

As part of Task VIII, INCO Alloys International (formerly Wiggin Alloys Ltd, U.K.) furnished the MA6000 material for Tasks IV and VI. Processing parameters were developed by the INCO Research and Development Center (IRDC) as part of Task I.

The engine testing, test results, and posttest evaluation (Tasks IX and X) are described in Volume 2 of this report.

SECTION III

3.0 OXIDE-DISPERSION-STRENGTHENED TURBINE BLADE TECHNOLOGY DEVELOPMENT

MA6000, developed at INCO, Ltd., specifically for turbine blade application, is a nickel-base superalloy that derives its strength from the oxide-dispersion-strengthening phase, yttrium oxide, solid solution strengthening of the face-centered cubic gamma (γ) matrix, and the precipitation hardening of the gamma matrix by the ordered gamma-prime (γ') phase. The alloy derives additional strength from the coarse, highly directional grain structure (grain aspect ratio greater than 10:1 in the longitudinal direction) developed by directional zone annealing.

The manufacture of MA6000, like other ODS alloys, involves a series of conventional as well as unconventional powder metallurgy processing steps. INCO developed the mechanical alloying (MA) process, schematically shown in Figure 4, to produce the ODS alloy systems. Typical of the process, MA6000 starts out as a mixture of elemental metal powders, master alloy powders, and very fine refractory oxide particles. These are charged into a high-energy ball mill or attritor, where mechanical alloying takes place. The individual particles are cold-welded and fractured by repeated high-energy mechanical impact until the alloy consists of a uniform dispersion of a highly refractory oxide (Y_2O_3) in a metallic superalloy matrix.

The MA powders are then consolidated by canning, vacuum outgassing, and hot extrusion, followed by hot working operations (primarily hot rolling), and subsequent zone annealing to develop a highly textured microstructure. A final solution heat treatment and two-step aging is performed to optimize the strength properties. Turbine blades can then be machined from this barstock.

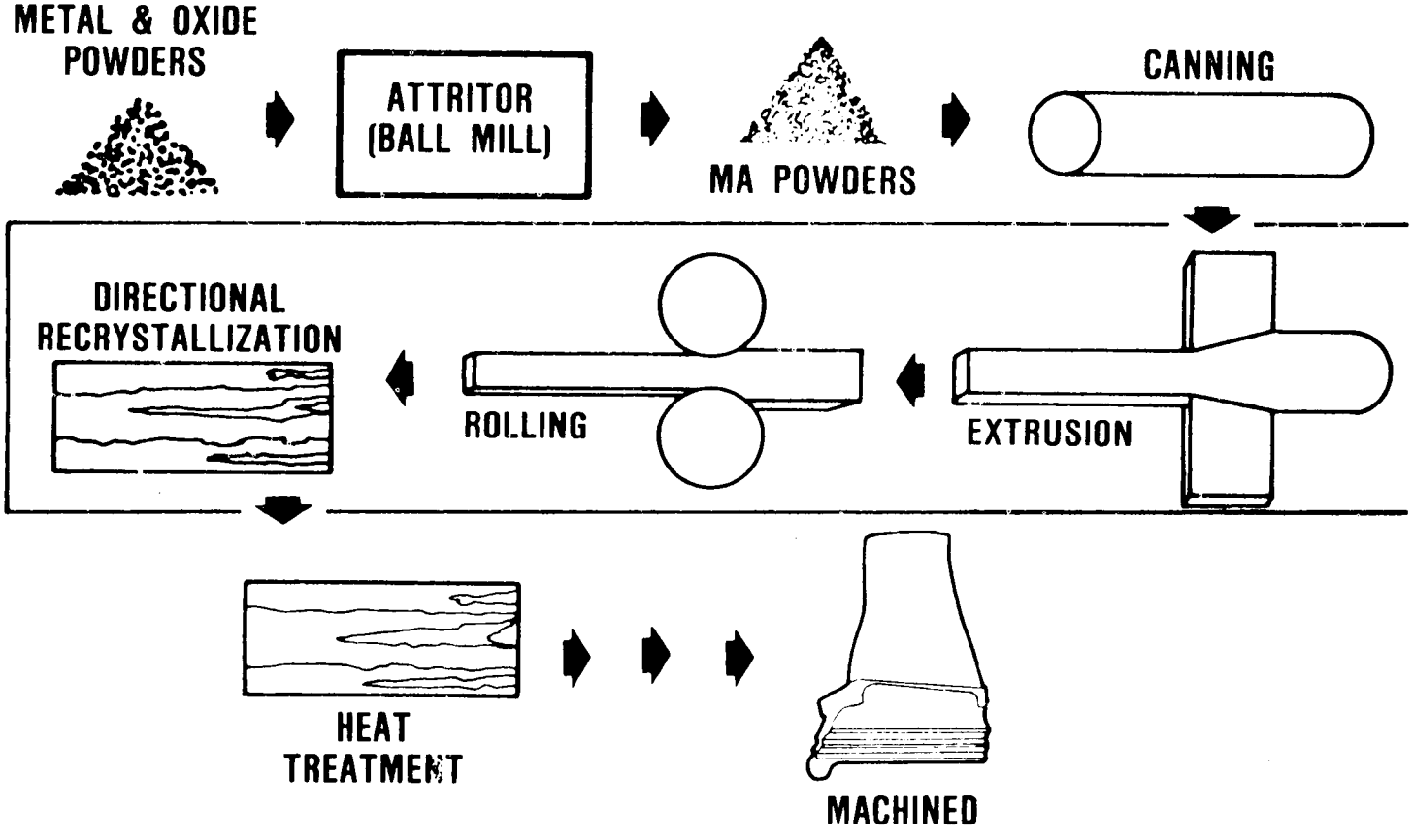

Figure 4. Mechanical Alloying Process.

Details of the ODS alloy processing development are discussed in the following subsections. The process parameters to be used in the commercial production of MA6000 barstock were subsequently identified.

3.1 Powder Production

The powder raw materials listed in Table 1 were attrited in 34 kg (75 lb) heats in a Szegvari Model 100S attritor. The nominal composition of MA6000 is also given in Table 1. Attrited powder was examined to monitor the attritor processing and to ensure that well-processed homogeneous powder was produced. Heat record numbers and typical screen, chemical, and microstructural analyses are presented in Table 2. Representative powder microstructures are shown in Figure 5. A completely processed powder would show, at a higher magnification examination, a uniform particle microstructure consisting of a very fine, even dispersion of highly refractory oxide in a metallic matrix.

Thirty-one heats of MA6000 powder were attrited during the development phase of Project 4. Of these, 25 were judged acceptable. The remainder either contained unacceptable -325 mesh fractions due to internal water leaks in the attritor tank or were used as wash heats after weld repairs of these leaks. The production of powder was the most critical and difficult task of this project and represented nearly 50 percent of the effort.

3.2 Consolidation/Extrusion

3.2.1 Consolidation

Powder blends were prepared from the attrited powder heats to fill the large extrusion cans needed for Project 4. Therefore, each blend was the result of cone blending three attritor heats for three

TABLE 1. MA6000 RAW MATERIALS AND PARTICLE SIZE DISTRIBUTION

Component	Size
Ni, Type 123	4.7 micron
Cr, elemental	-200 mesh
Mo, elemental	-325 mesh
W, elemental	-325 mesh
Ta, elemental	-325 mesh
Ni-17Al-28Ti	-200 mesh
Ni-46Al	-200 mesh
Ni-18B	-200 mesh
Ni-28Zr	-200 mesh
Y_2O_3	0.02-0.04 micron

Nominal Composition of MA6000 (Weight Percent)	
Ni - Balance	Ti - 2.50
Cr - 15.0	C - 0.05
Mo - 2.0	B - 0.01
W - 4.0	Zr - 0.15
Ta - 2.0	Y_2O_3 - 1.10 (2.5 v/o)
Al - 4.5	Fe - 2.5

TABLE 2. MA6000 TYPICAL POWDER ANALYSIS.

Heat Record No.	Chemistry, Wt. Percent				Screen Analysis, Mesh Size, Percent						Micro-structure
	C	O	N	Fe	+20	-20/+60	60/100	100/200	200/325	-325	
81621	0.048	0.52	0.25	0.71	NA					15	Good
84207	0.043	0.45	0.27	0.81	NA					18	Good
84212	NA				NA					NA	NA
84213	Scrapped due to water leak										
84214	Scrapped due to water leak										
84216	NA				0.9	25	17	30	15	13	Good
84359	0.045	0.79	0.34	0.74	1	47	16	18	10	7	Good
84360	0.045	0.51	0.32	0.66	0.5	15	14	45	15	11	Good
T84368	0.045	0.56	0.31	0.86	1	40	21	26	6	4	Good
T84369	0.045	0.59	0.31	0.85	1	41	19	23	7	9	Good
T84370	0.049	0.48	0.27	0.94	2	35	23	24	9	8	Good
T84371	0.050	0.68	0.35	0.93	3	33	21	25	8	9	Good
T84372	0.051	0.41	0.28	1.00	NA	24	27	31	9	9	Good
T84373	0.058	0.62	0.32	0.86	NA	9	19	40	17	15	Good
T84374	0.049	0.69	0.36	0.82	NA	10	24	43	13	10	Good
T84375	0.050	0.65	0.33	0.85	NA	12	19	37	19	13	Good
84376	0.051	0.54	0.32	0.84	0	22	19	27	19	13	Good
84377	0.052	0.43	0.28		2	6	12	36	29	17	Good
84378	0.049	0.34	0.28		7	9	13	40	19	11	Good
84379	0.047	0.70	0.38		3	6	15	45	19	13	Good
84380	Scrapped due to water leak										
84496	Wash run										
84497	Wash run										
84498	0.043	0.81	0.32	0.67	0	24	17	31	16	12	Good
84499	0.047	0.75	0.32	0.76	0	25	22	25	17	11	Good
84500	0.045	0.79	0.35	0.66	1	48	23	17	5	7	Good
84501	0.047	0.78	0.37	0.60	1	39	21	16	12	11	Good
84502	0.048	0.59	0.30	0.79	0	12	19	36	18	15	Good
84503	0.045	0.85	0.56	0.54	0	3	8	22	24	44	NA

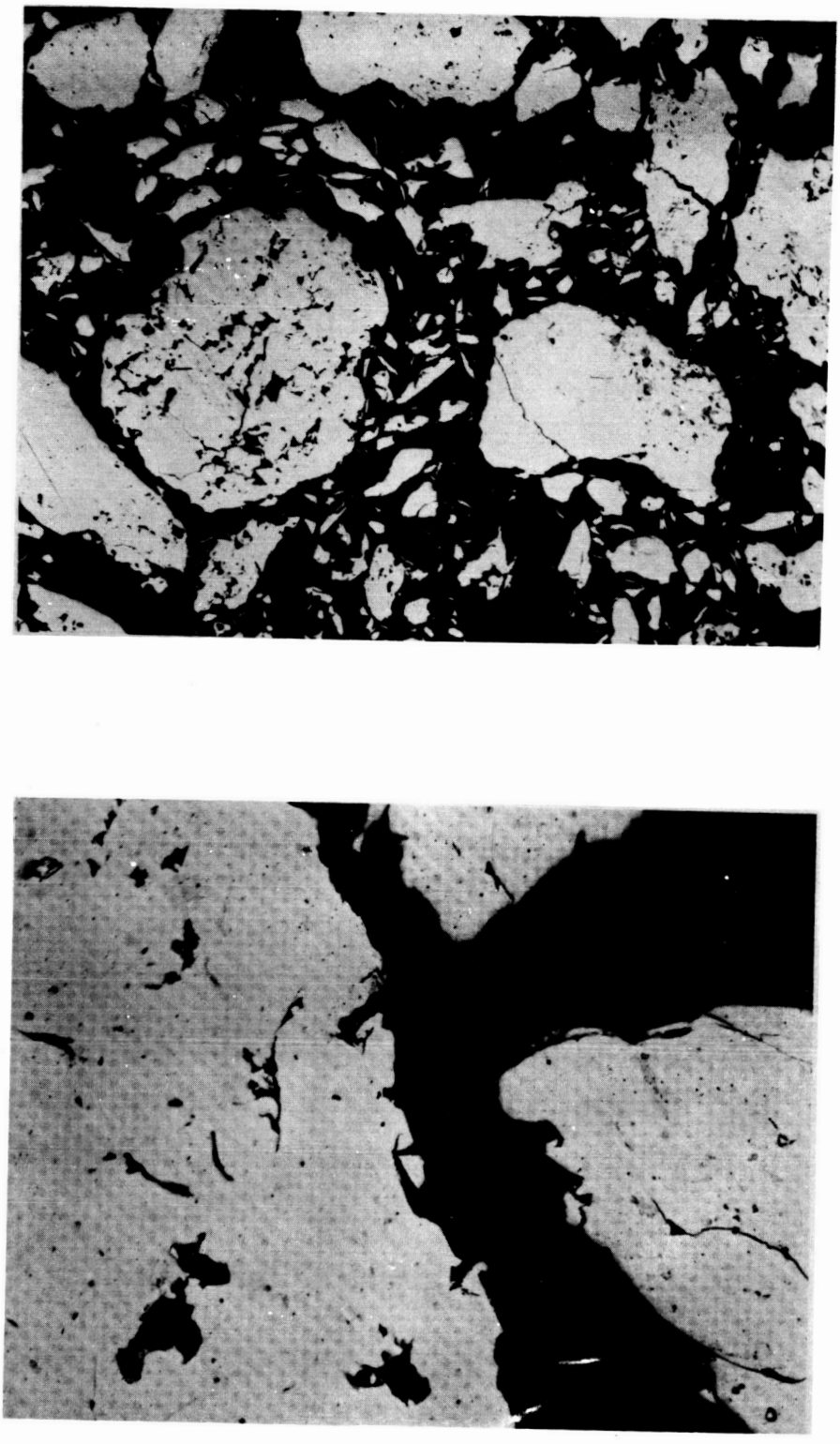

Figure 5. Typical Microstructure of Completely Processed MA6000 Powder, (a) 100X, (b) 500X. Attritor Heat T-84359.

hours. Each extrusion can was identified by the record number of the powder blend used to fill the can.

Mild steel extrusion cans, having the following dimensions, were prepared:

203 mm (8.0 in) outside diameter
6.4 mm (0.25 in) wall thickness
610 mm (24.0 in) length
51 mm (2.0 in) long nose plug
13 mm (0.5 in) long tail plug

Each can was filled from the tail end after screening and using the -20 mesh fraction. The powder was settled by vibrating for one minute. After filling, the tail plug was welded to the can. An evacuation stem was fitted to this plug.

The filled cans were leak-checked by pressurization with nitrogen and immersion in water. No leaks were detected. To degas each extrusion can, the can was placed in a cold electric furnace and connected to a mechanical vacuum pump. The furnace controller was set to 260C (500F). At two-hour intervals, the controller was reset to 399C (750F), to 538C (1000F), and finally to "off." The evacuation stem was sealed while the can remained under evacuation 16 hours after the furnace was shut off. Pressure during heating, as measured at the pumping station, was generally less than 26 Pa (200 μmHg); pressure just before sealing was about 2.0 Pa (15 μmHg).

3.2.2 Extrusion

At laboratory scale, MA6000 is usually extruded at 1010C (1850F) at a 7.2:1 extrusion ratio using a 6.7 MN (750 ton) press with an 89-mm (3.5-in) diameter liner. The required extrusion pressure of 827 MPa (120 ksi) is near the available capacity for the

small press [1000 MPa (145 ksi)]. The maximum extrusion force that can be developed with the nominal 26.7 MN (3000 ton) Brush-Wellman press using a 210-mm (8.25-in) diameter liner is 724 MPa (105 ksi). The stalling of cans heated to 1010C (1850F) indicates that the lessened proportion of friction involved in the extrusion of larger cans does not adequately counter the lower available pressure of the Brush-Wellman press. For this press, therefore, cans must be heated to a higher temperature 1038C (1900F), to allow extrusion at a lower pressure.

Production extrusion was performed on a 26.7 MN (3000 ton) press during two sessions at Brush-Wellman, Inc., Elmore, Ohio. Similar MA6000 cans were extruded for other INCO projects during these two sessions and were helpful in choosing extrusion conditions for this project. The original plan called for the evaluation of four combinations of two extrusion ratios and two extrusion temperatures. The attempt at the lower temperature, 1010C (1850F), and high extrusion ratio (13.6:1) was abandoned after a similar can for another project stalled the press. Only one of the two attempts at the same ratio and a higher temperature, 1038C (1900F) resulted in a successful extrusion. However, a bar was extruded successfully at 10.1:1 at the higher temperature. Thus, bars were obtained from two extrusion ratios, but only at the higher temperature.

Details of the extrusions, including heating times, temperatures, ram force, ram speed, and lubrication, are presented in Table 3. Bar from the low extrusion ratio measured 82.6 x 41.4 mm (3.25 x 1.63 in). The high extrusion ratio yielded bar with approximately the same thickness, but narrower width, 57.2 x 44.5 mm (2.25 x 1.75 in). These dimensions include the mild steel can material.

TABLE 3. MA6000 EXTRUSION CONDITIONS

Can	Furnace Times/Temp.	Die Size	Ram Force	Ram Speed
T84490	140 min/1010C (1850F) plus 105 min/1038C (1900F)	44.5 x 57.2 mm (1.75 x 2.25 in)	24.0 MN (2700 tons)	stall
T84492	140 min/1010C (1850F) plus 129 min/1038C (1900F)	44.5 x 57.2 mm (1.75 x 2.25 in)	23.6 MN (2650 tons)	13-38 mm/s (0.5-1.5 in/s)
T84494	240 min/1010C (1850F)	41.4 x 82.6 mm (1.63 x 3.25 in)	24.9 MN (2800 tons)	stall
T84495	30 min/1010C (1850F) plus 255 min/1038C (1900F)	41.4 x 82.6 mm (1.63 x 3.25 in)	22.7 MN (2550 tons)	64 mm/s (2.5 in/s)

NOTES:
1. Cans were heated in graphite sleeves in gas furnace.
2. Lubrication was provided by Fiske 604D (graphite in oil base) and glass wrap and nose pad.
3. Dies had conical entrances.
4. Transfer times were less than two minutes.
5. Throttle was set to 100 percent.

3.3 Hot Rolling

Ten extrusion ratio/rolling reduction/rolling temperature combinations were evaluated in Project 4. The two rolling temperatures used were 1038C (1900F) and 1066C (1950F). The low-extrusion-ratio bar was rolled 43 percent and 49 percent at both temperatures. The high-extrusion-ratio bar was rolled 45 percent and 55 percent at both temperatures and 65 percent at the higher temperature only. Edge cracking was a problem at the lower rolling temperature, so the attempt to roll 65 percent at this temperature was abandoned, leaving nine combinations to be evaluated.

Rolling schedules and other details are presented in Table 4. Roll diameter was 508 mm (20 in); mill speed was 279 mm/s (11 in/s). Four passes were used in all cases except the 65-percent reduction, which used five passes. The latter reduction was to the width of the bars; all others were to the thickness. The reduction schedules were designed to give a constant reduction per pass. Bars were reheated between the second and third pass (also between the fourth and fifth pass for the 65-percent reduction). All rolling was performed with the canning material surrounding the alloy so that roll surface chilling and cracking would be minimized. The rolled bars were then sandblasted and pickled to remove the can material.

3.4 Zone-Annealing

The large bars produced for this project could not be zone-annealed in the IRDC existing zone-annealing units, which consisted of small-diameter Inconel tubes and traveling platinum-wound resistance furnaces. A larger tube with a matching furnace was obtained that was capable of zone-annealing bars of the minimum size required for this project. Early evaluation of some bars were of material zone-annealed in this equipment at 76 mm/h (3 in/h) with maximum temperatures

TABLE 4. MA6000 HOT ROLLING SCHEDULE

Extrusion Ratio	10.1:1		13.6:1		
Rolling Reduction Ratio	43 Percent	49 Percent	45 Percent	55 Percent	65 Percent
Starting Stock	41.4 mm (1.63 in)	41.4 mm (1.63 in)	44.5 mm (1.75 in)	44.5 mm (1.75 in)	57.2 mm (2.25 in)
First Pass	34.5 mm (1.36 in)	33.6 mm (1.32 in)	38.4 mm (1.51 in)	35.6 mm (1.40 in)	49.0 mm (1.93 in)
Second Pass	29.0 mm (1.14 in)	27.2 mm (1.07 in)	33.0 mm (1.30 in)	28.4 mm (1.12 in)	37.6 mm (1.48 in)
	Reheat	Reheat	Reheat	Reheat	Reheat
Third Pass	24.4 mm (0.96 in)	21.9 mm (0.86 in)	28.4 mm (1.12 in)	22.9 mm (0.90 in)	30.5 mm (1.20 in)
Fourth Pass	20.3 mm (0.80 in)	17.8 mm (0.70 in)	24.4 mm (0.96 in)	20.3 mm (0.80 in)	24.4 mm (0.96 in)
					Reheat
Fifth Pass					20.3 mm (0.80 in)

NOTES: 1. The above dimensions include can material.
2. Soak time was 30-40 minutes; reheat time was 10-15 minutes.

of about 1260C (2300F) (Figure 6). Simultaneously, a different type of zone-annealing apparatus was developed that consists of a 20 kW radio-frequency induction power supply, an eight-turn induction coil, a 102-mm (4-in) diameter by 102-mm (4-in) height SiC-coated graphite susceptor with a 25-mm (1.0-in) wide slot, and a suitable travel mechanism. This unit allowed better temperature control and a twofold improvement in thermal gradient at the recrystallization temperature. Bars from all thermomechanical processing (TMP) combinations were ultimately zone-annealed in this unit at 76 mm/h (3 in/h) at a maximum temperature of 1260C (2300F), which provided a 135C/mm (275F/in) gradient at 1191C (2175F). One bar, zone-annealed at a higher rate [153 mm/h (6 in/h)], revealed no significant effect of recrystallization rate on rupture strength.

3.5 Thermomechanical Processing Optimization

One of the primary objectives of Project 4 was to optimize the TMP of scaled-up MA6000 barstock for maximum 1093C (2000F) stress-rupture strength while efficiently producing barstock to a specified size requirement, 41.9 x 14.0 mm (1.65 x 0.55 inch). Based on the preceding studies, these principal parameters were varied: (1) extrusion ratio, (2) extrusion temperature, (3) hot-rolling reduction, and (4) hot-rolling temperature. The capacity of the Brush-Wellman press was insufficient to extrude material at 1010C (1850F), the lower of the two chosen temperatures, so extrusion temperature became a constant 1038C (1900F) for Project 4. Size constraints limited the possible rolling reductions to a modest range. The final test matrix contained two extrusion ratios (10.1:1 and 13.6:1), two or three rolling reductions (43 percent and 49 percent for the low extrusion ratio; 45 percent, 55 percent, and 65 percent for the high extrusion ratio), and two rolling temperatures 1038C (1900F) and 1066C (1950F). The lower of the two rolling temperatures often caused serious transverse cracking and led to the

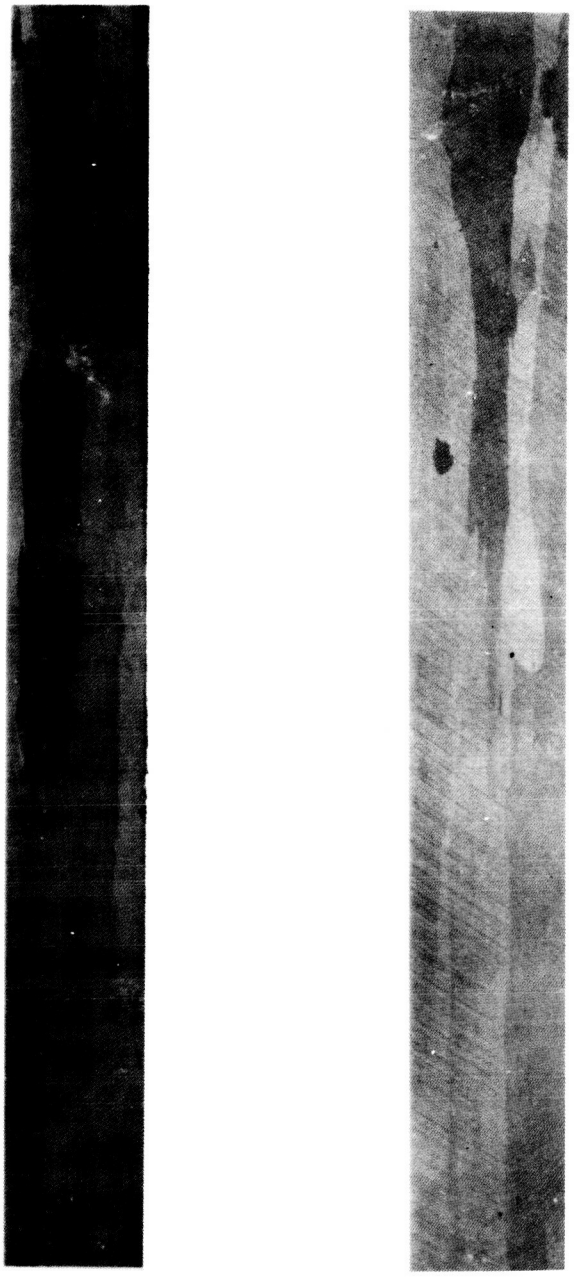

Figure 6. Coarse, Elongated Grain Structure of Bars Hot-Rolled at 1038C (1900F) to 55-Percent (right) and 65-Percent (left) Reduction and Zone-Annealed at 1260C (2300F).

elimination of the high extrusion ratio/65-percent rolling reduction/low rolling temperature combination. Of the remaining nine TMP combinations, one yielded bar that would not recrystallize properly and exhibited poor rupture strength. This combination (high extrusion ratio/65-percent rolling reduction/high rolling temperature) was not considered further in this study, leaving eight combinations of two extrusion ratios, two rolling reductions, and two rolling temperatures. The stress-rupture data that are most useful for comparison are the estimated 100-hour rupture strengths of specimens that were either (1) loaded initially to 138 MPa (20 ksi) or (2) loaded initially to 152 MPa (22 ksi) after a 243-hour aging at the test temperature to reduce the coaxing effect. The short-lived specimens that were loaded initially to 152 MPa (22 ksi) without a test temperature aging were not considered.

Examination of the averaged estimated 100-hour rupture strength for each of the eight TMP routes, as presented in Table 5, reveals small but consistent trends for each of the two extrusion ratios. For both ratios, lower strengths result from the high temperature/high rolling reduction and the low temperature/low rolling reduction combinations. Higher rupture strengths result from the low temperature/high rolling reduction and the high temperature/low rolling reduction combinations. The high temperature/low rolling reduction combination gives the best rupture strength for both extrusion ratios. This is fortunate, since cracking is a problem during rolling at the lower rolling temperature.

3.5.1 Stress-Rupture Tests

Initially, stress-rupture tests were performed on zone-annealed material that was given a gamma-prime solutioning treatment, 1232C (2250F)/0.5 h/air cool. No aging treatment was given since gamma-

TABLE 5. AVERAGED ESTIMATED 100-HOUR RUPTURE STRENGTHS

Processing	Rolling Temperature	
	1038C (1900F)	1066C (1950F)
10.1:1 Extrusion	MPA (ksi)	MPa (ksi)
43-percent Rolling Reduction	137 (19.9)	149 (21.6)
49-percent Rolling Reduction	143 (20.8)	143 (20.7)
13.6:1 Extrusion		
45-percent Rolling Reduction	150 (21.7)	154 (22.3) (highest)
55-percent Rolling Reduction	152 (22)	148 (21.5)

*Does not include specimens loaded initially to 152 MPa (22 ksi) without a test temperature age.

prime precipitation strengthening was not expected to be significant at the test temperature of 1093C (2000F) and, in any event, would rapidly precipitate and coarsen upon heating to the test temperature. However, a "coaxing" phenomenon was observed: test results of specimens step-loaded to 152 MPa (22 ksi) after about 150 hours at 138 MPa (20 ksi) had significantly longer stress rupture life than specimens directly loaded to 152 MPa (22 ksi). To determine whether this effect was due to stress or thermal history, some specimens were held nominally unloaded for 24 hours at the test temperature before the full test load was applied. This resulted in longer stress rupture life, indicating the effect was thermal.

Because of this observation, it was decided that all remaining tests would be performed on material given the standard aging treatment, 954C (1750F)/2 h/air cool + 843C (1550F)/24 h/air cool. The coaxing effect was not reduced by this treatment, however, as will be discussed later.

Stress-rupture testing was performed in accordance with applicable American Society for Testing and Materials (ASTM) specifications. Specimens had 6.4 mm (0.25 inch) gage diameters and 31.8 mm (1.25 inch) gage lengths. All testing was done in air at 1093C (2000F). Two or three specimens from each bar were tested at various stress levels with at least one at 138 MPa (20 ksi). Step-loading was often required to obtain specimen failures in reasonable times due to the high stress sensitivity of MA6000.

Stress-rupture test results for low and high extrusion ratio processing show a wide scatter of times to failure (also due largely to stress sensitivity), which makes direct comparison of the raw data difficult. Therefore, an estimated stress for failure in 100 hours was calculated by the following procedure.

Calculation of Estimated 100-Hour Rupture Strength

This calculation involves the summation of the fractions of expected life at each stress imposed on a specimen (Equation 1). The expected lives were determined from inspection of available MA6000 data. For specimens that were not step-loaded, only one stress and one fraction are involved. Specimens of this project were subject to up to four increasing stress levels for various times before failure.

The sum of the expected life fractions is converted to a stress that is estimated to cause failure in 100 hours (Equation 2) by assuming a slope of 20 in the plot of log rupture life versus log stress. Table 6 shows the expected rupture lives at various stresses.

(1) $F = \sum_{\sigma} \frac{t_f}{t_\sigma}$,

σ = stress
t_f = specimen time at σ
t = expected life at σ
F = sum of fractional lives

(2) $\sigma_t = \sigma \frac{t_\sigma}{t} F^{1/20}$

t_σ = desired life
σ_t = stress for life of t

TABLE 6. EXPECTED RUPTURE LIVES AT VARIOUS STRESSES

Stress, MPa (ksi)	Expected Life, Hours
138 (20)	300
145 (21)	113
152 (22)	45
159 (23)	18.3
165 (24)	7.8

Example

Test Number 37604:

$$F = \frac{140}{300} + \frac{70}{45} + \frac{13}{18.3} = 2.73$$

$$\sigma_{100 \text{ hours}} = 138 \text{ MPa} \left(\frac{300 \text{ hours}}{100 \text{ hours}}\right) 2.73^{1/20}$$

= 153 MPa (or 22.2 ksi, if 20 ksi is substituted for 138 MPa above)

Test Number 37604 presents a typical result (refer to the first listed specimen in Table 7). This specimen was loaded initially to 138 MPa (20 ksi). After 140 hours without failure, the load was increased to 152 MPa (22 ksi). After an additional 70 hours without failure, the load was further increased to 159 MPa (23 ksi), after which failure occurred in 13 hours. For this specimen, the estimated stress for failure in 100 hours is 153 MPa (22.2 ksi).

3.5.2 Coaxing Phenomenon

It was observed that specimens initially loaded to 152 MPa (22 ksi) had unexpectedly short lives when compared to specimens that were step-loaded to this same stress from a lower stress. The second specimen listed in Table 7, Test Number 37605, is a good example of this behavior when compared with Test Number 37604, which was used in the example. Test 37605 resulted in a failure after only 1.1 hours at 152 MPa (22 ksi). The specimen of Test 37604 endured 70 hours without failure at the same stress after having been loaded for 140 hours at 138 MPa (20 ksi). This "coaxing" phenomenon has been noted before in the stress-rupture testing of ODS materials, but not to this extent. An initial hypothesis was that gamma-prime

TABLE 7. 1093C (2000F) STRESS-RUPTURE TEST RESULTS, EXTRUSION CAN T84495 (10.1:1 EXTRUSION RATIO).

Test No.	Hot Rolling Reduction/Temp C(F)	Heat Treatment	Stress, MPa (ksi)	Life, H	100 Hour Strength MPa (ksi)	Elong., percent
37604	43%/ 1066 (1950F)	solution	138/152/159 (20/22/23)	140/70/13	152 (22)	6.4
37605	"	"	152 (22)	1.1	124 (18)	12.0
37623	"	1093 (2000F) age	152 (22)	35	145 (21)	4.8
37606	49%/ 1066 (1950F)	solution	138/152 (20/22)	1139/47	152 (22)	5.6
37607	"	"	152 (22)	0.2	110 (16)	4.8
37624	"	1093 (2000F) age	152 (22)	13	138 (20)	6.4
37872	43% 1066 (1900F)	full	138 (20	3	117 (17)	10.4
37873	"	"	138 (20)	140	138 (20)	5.6
37884	"	"	138 (20)	102	138 (20)	4.0
37581	"	solution	138 (20)	16	124 (18)	4.8
37582	"	"	152 (22)	38	145 (21)	8.0
37622	"	1093 (2000F) age	138/152/159/165 (20/22/23/24)	137/24/24/22	159 (23)	4.8
39266	49% 1066 (1900F)	full	138 (20)	85	131 (19)	4.0
39267	"	"	138/152/159 (20/22/23)	168/24/14	152 (22)	4.0

precipitation occurs during the low-stress loading and provides significant strengthening during later loading at a higher stress. This was seemingly demonstrated by tests in which specimens were left nominally unloaded (actually, preloaded to 10 percent of intended test stress) at temperature in test stands for 24 hours before the full test stress was applied. In terms of estimated 100-hour strength, the average decrement due to loading initially to 152 MPa (22 ksi) rather than 138 MPa (20 ksi) is 30 MPa (4.4 ksi). This decrement was reduced to 6 MPa (0.9 ksi) when specimens were aged in test stands at the test temperature for 24 hours before full loading.

Prior to testing, these specimens had been given a solutionizing heat treatment only, 1232C (2250F)/0.5 h/air cool, because gamma-prime strengthening was not expected to be significant at the test temperature. In any event, gamma-prime was expected to precipitate in a relatively short time and begin to coarsen during the early part of a test, probably during heating to the test temperature. These presumptions were apparently contradicted by the early test results. Therefore, all further testing was performed with material given a two-stage aging heat treatment, 954C (1750F)/2 h/air cool + 843C (1550F)/24 h/air cool. However, the average strength decrement due to loading initially to 152 MPa (22 ksi) rather than 138 MPa (20 ksi) was 23 MPa (3.3 ksi) after this full heat treatment. This means either that aging at the test temperature simply provides better rupture strength at the test temperature than aging treatments at lower temperatures or that the 10-percent preload that was applied during the test temperature age develops a gamma-prime structure that is stress oriented in some manner and is beneficial to rupture strength. Oxide-dispersion-coarsening is unlikely at temperatures as low as 1093C (2000F). Oriented gamma-prime morphologies have been observed previously in failed MA6000

rupture specimens.[1] Also, a somewhat analogous effect has been observed in an advanced single-crystal superalloy for which a rafted gamma-prime structure that results from testing a solutionized material exhibits greater rupture strength than unrafted material.[2]

3.5.3 Structure Evaluation

Failed stress-rupture specimens of material from all nine TMP routes were sectioned longitudinally, polished, and etched in glyceregia to reveal grain structures (Figure 7). Eight of the TMP routes yielded structures typical of MA6000 barstock. Typically, two or three grains appear in the gage sections of these specimens. Grain aspect ratio is generally greater than 10.

One TMP route, which exhibited poor rupture strength, yielded regions of fine, low-aspect-ratio grains that provided an intergranular fracture path. This TMP route involved the greatest amount of hot working--the high extrusion ratio and 65-percent rolling reduction.

In the absence of more useful theoretical knowledge about the relationships between deformation, recrystallization, and rupture strength, an energy concept was used in the past to explain the recrystallization behavior of mechanically alloyed ODS materials. This concept involves the amount of substructural energy retained in

---

[1] Y.G. Kim and H.F. Merrick, "Characterization of an Oxide-Dispersion-Strengthened Superalloy, MA6000E, for Turbine Blade Applications," Final Report (NASA CR-159492, NASA Contract No. NAS3-20093, May 1979.

[2] D.D. Pearson, F.D. Lemkey, and B.H. Kear, "Stress Coarsening of Gamma-Prime and Its Influence on Creep Properties of a Single-Crystal Superalloy." Superalloys, 1980, Tien, et al., eds, Am. Soc. Metals, Metals Park, OH, 1980, p. 513.

(a)

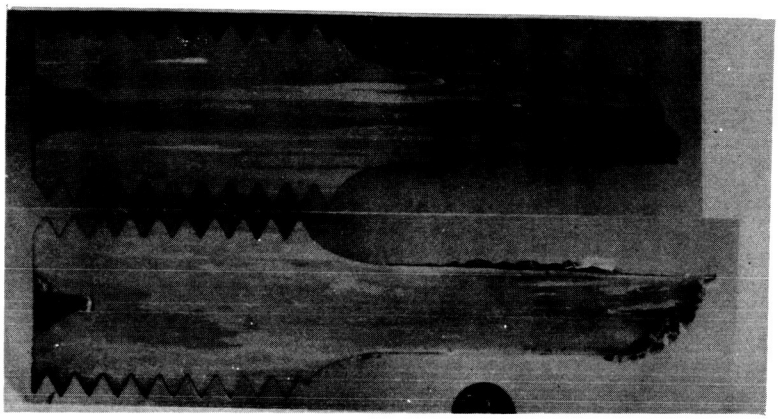

43 Percent/1066C (1950F), Tests 37623 (top) and 37604 (bottom)

(b)

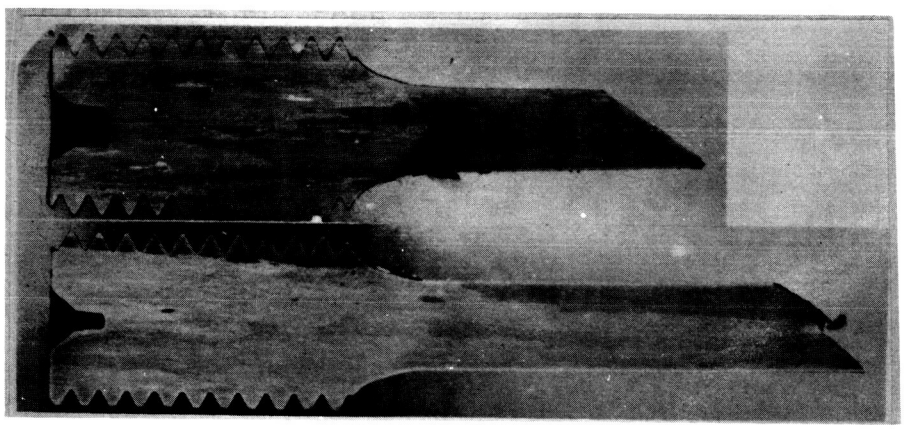

49 Percent/1066C (1950F), Tests 37624 (top) and 37606 (bottom)

Figure 7. Polished and Etched (Glyceregia) Sections of Stress Ruture Specimens Revealing Typical Grain Structure of Laboratory Scale MA6000, Except for Specimen (g). (2X)

(c)

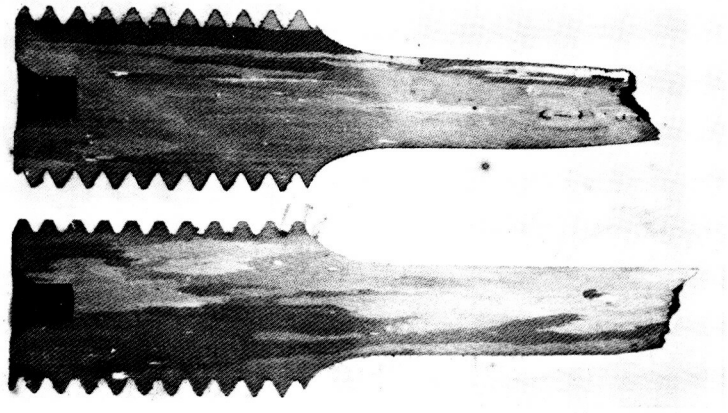

43 Percent/1038C (1900F), Tests 37872 (top) and 37873 (bottom)

(d)

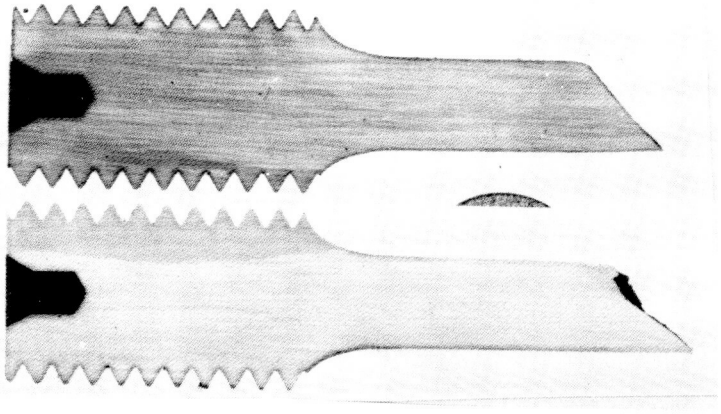

49 Percent/1038C (1900F), Tests 39266 (top) and 39267 (bottom)

Figure 7. Polished and Etched (Glyceregia) Sections of Stress Ruture Specimens Revealing Typical Grain Structure of Laboratory Scale MA6000, Except for Specimen (g). (2X) (Contd)

(e)

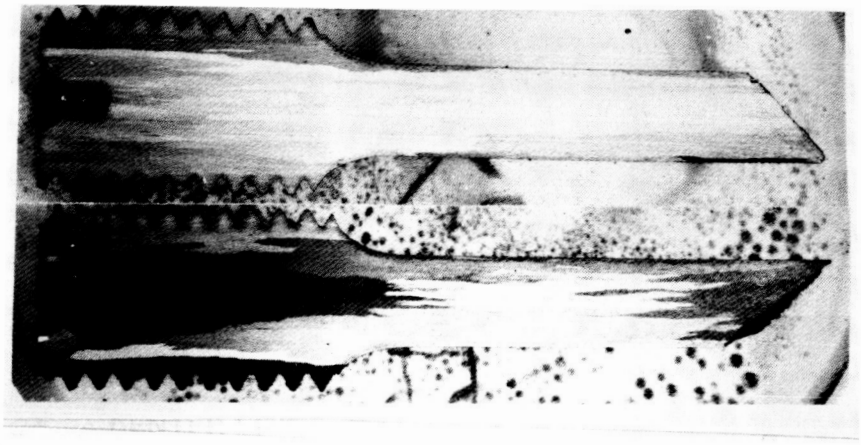

45 Percent/1066C (1950F), Tests 37866 (top) and 37867 (bottom)

(f)

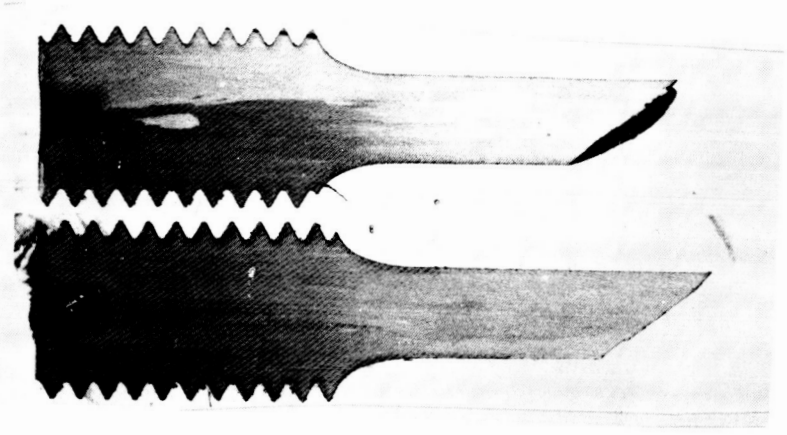

55 Percent/1066C (1950F), Tests 37870 (top) and 37871 (bottom)

Figure 7. Polished and Etched (Glyceregia) Sections of Stress Ruture Specimens Revealing Typical Grain Structure of Laboratory Scale MA6000, Except for Specimen (g). (2X) (Contd)

(g)

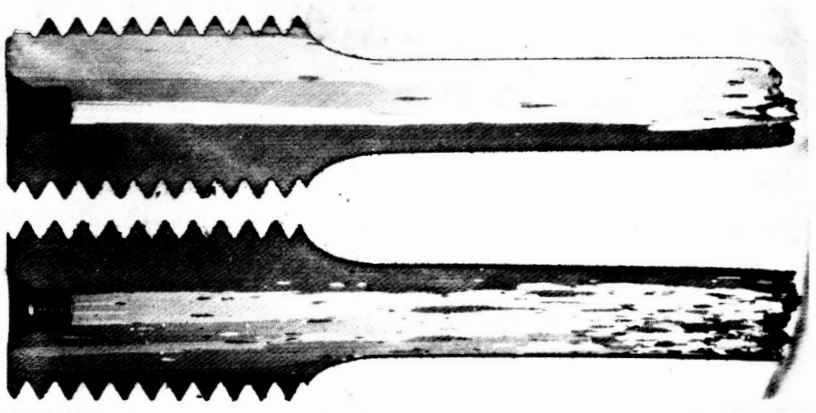

65 Percent/1066C (1950F), Tests 37868 (top) and 37883 (bottom)

(h)

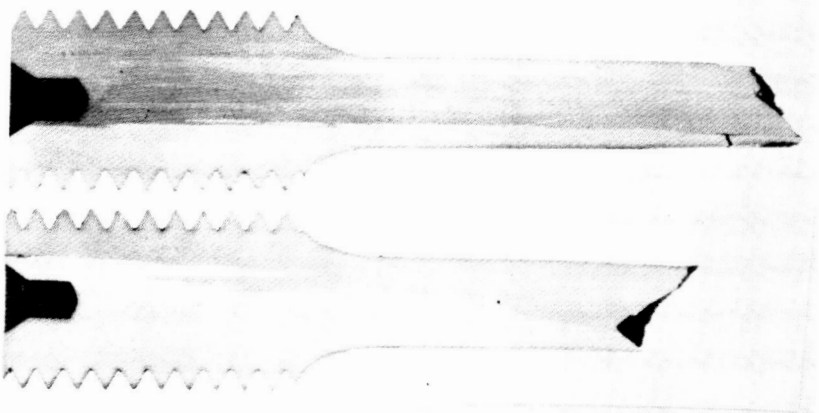

45 Percent/1038C (1900F), Tests 39264 (top) and 39265 (bottom)

Figure 7. Polished and Etched (Glyceregia) Sections of Stress Ruture Specimens Revealing Typical Grain Structure of Laboratory Scale MA6000, Except for Specimen (g). (2X) (Contd)

(i)

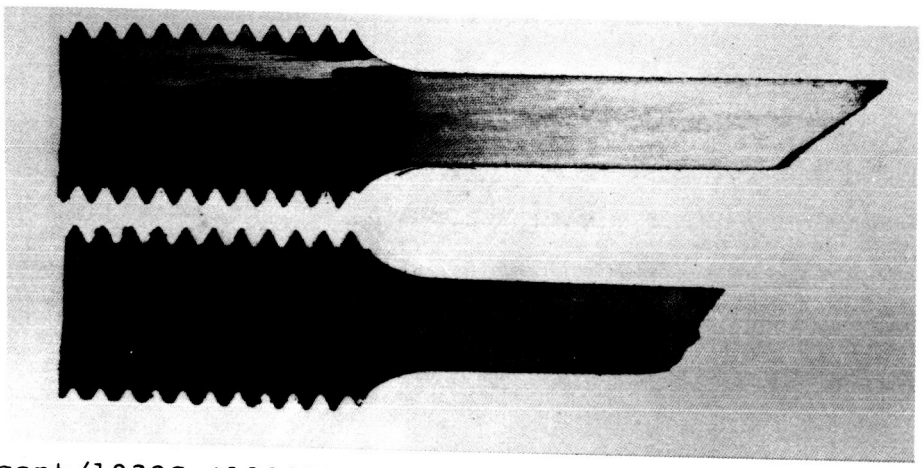

55 Percent/1038C (1900F), Tests 37864 (top) and 37865 (bottom)

Figure 7. Polished and Etched (Glyceregia) Sections of Stress Ruture Specimens Revealing Typical Grain Structure of Laboratory Scale MA6000, Except for Specimen (g). (2X) (Contd)

the deformed material. Such energy is expected to increase with deformation and to decrease with temperature of deformation. For best recrystallized structure and properties, the energy must be within a critical range, neither too high nor too low.

This energy concept, however, is not useful to explain the trends of the present results. An equivalence of high temperature/low reduction, and vice versa, is not expected from the energy concept. The observed differences in rupture strengths are quite small, and it is unknown at present what macro- and microstructural differences are responsible for these differences. No significant structural differences among the eight TMP routes with good rupture strengths have been detected.

The high-extrusion-ratio material exhibited generally superior rupture strength over the low-extrusion-ratio material. The strength of the former is 154 MPa (22.3 ksi) for 100-hour life, which is 5 MPa (0.7 ksi) better than the low-extrusion-ratio material. This difference may, in fact, be due to the extrusion ratio or to normal variations in the powder makeup of each extrusion. In any case, the strength for each extrusion ratio exceeds the project goal of 138 MPa (20 ksi) for 100-hour life.

Thus, the best 1093C (2000F) rupture strength was obtained for the TMP combination with the higher extrusion ratio (13.6:1); the higher extrusion temperature, 1038C (1900F); the lowest rolling reduction (45 percent); and the higher rolling temperature, 1066C (1950F). Material produced by this optimum TMP combination exhibited an average estimated 100-hour rupture strength of 154 MPa (22.3 ksi), greatly exceeding the goal of 138 MPa (20 ksi).

Most of the other TMP combinations also exceeded the stress-rupture goal, indicating a fair degree of tolerance to nonoptimum processing.

Certain workability constraints were found, such as inadequate press capacity for extrusion at the lower temperature, 1010C (1850F), and significant cracking during rolling at the lower rolling temperature, 1040C (1900F). Fortunately, these constraints do not involve the optimum processing route determined by this project.

SECTION IV

4.0 PROPERTY CHARACTERIZATION

The MA6000 barstock was characterized for mechanical, environmental, and physical properties prior to component and engine testing of the turbine blades machined from this alloy.

The original program required GTEC's evaluation of material produced by the IRDC process. However, after the program was established, Wiggin Alloys Limited* replaced IRDC as the MA6000 production material supplier. Therefore, GTEC conducted a preliminary evaluation of commercially produced MA6000 barstock from Wiggin. Evaluation of the Wiggin material consisted of microstructure and grain size metallographic examination and tensile and stress-rupture testing.

4.1 Evaluation of Preliminary Wiggin Material

Macrostructure and microstructure examination of MA6000 barstock representative of commercial grade Wiggin material were conducted. Grain inspection (Figure 8) revealed a structure consisting of elongated grains between 20 to 100 mils wide with a grain-aspect-ratio (GAR) of ten or greater. This macrostructure morphology was similar to the acceptable structure produced by IRDC.

Microstructural examination (Figure 9) in the longitudinal direction showed the presence of chains of fine equiaxed grains. The chains appeared to be the result of incomplete recrystallization and growth during zone annealing. Incomplete recrystallization may have been due to compositional variations. Wiggin suggested that powder particles, having significantly different composition, may

*Now INCO Alloys International

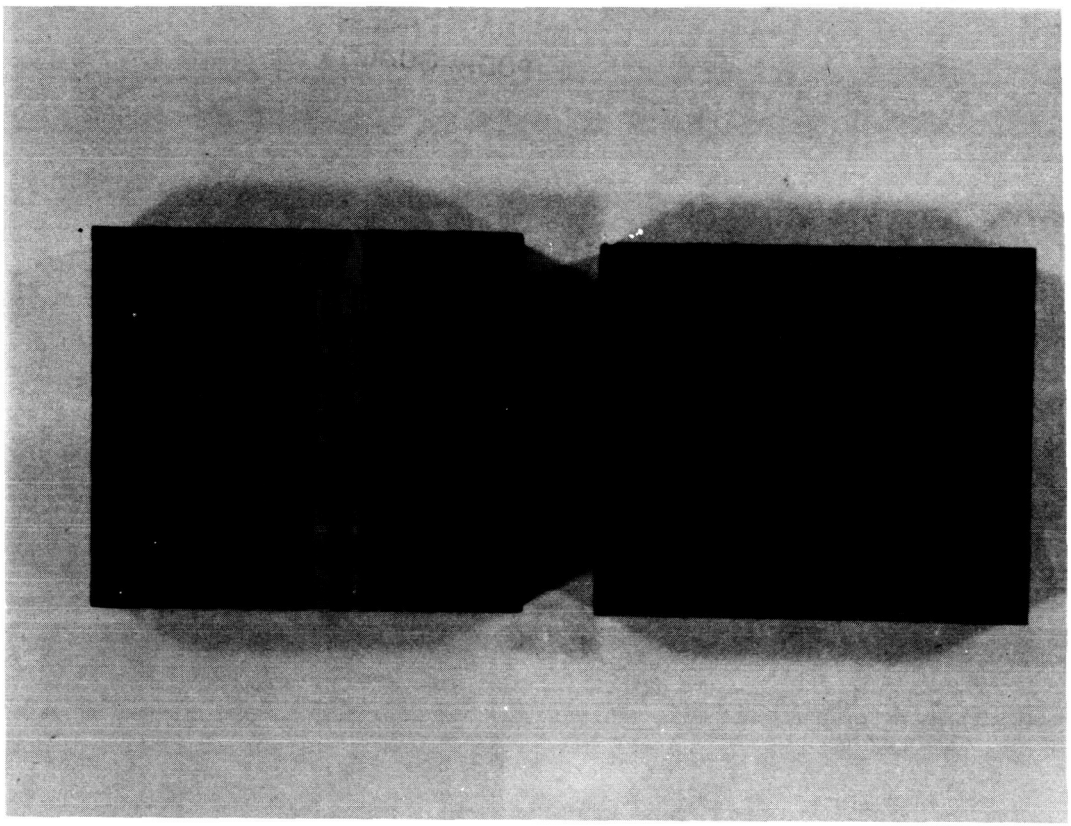

P73790-1

ETCHANT-HC1-H_2O_2 MAG-0.8x

Figure 8. Grain Structure of Preliminary Wiggin MA6000.

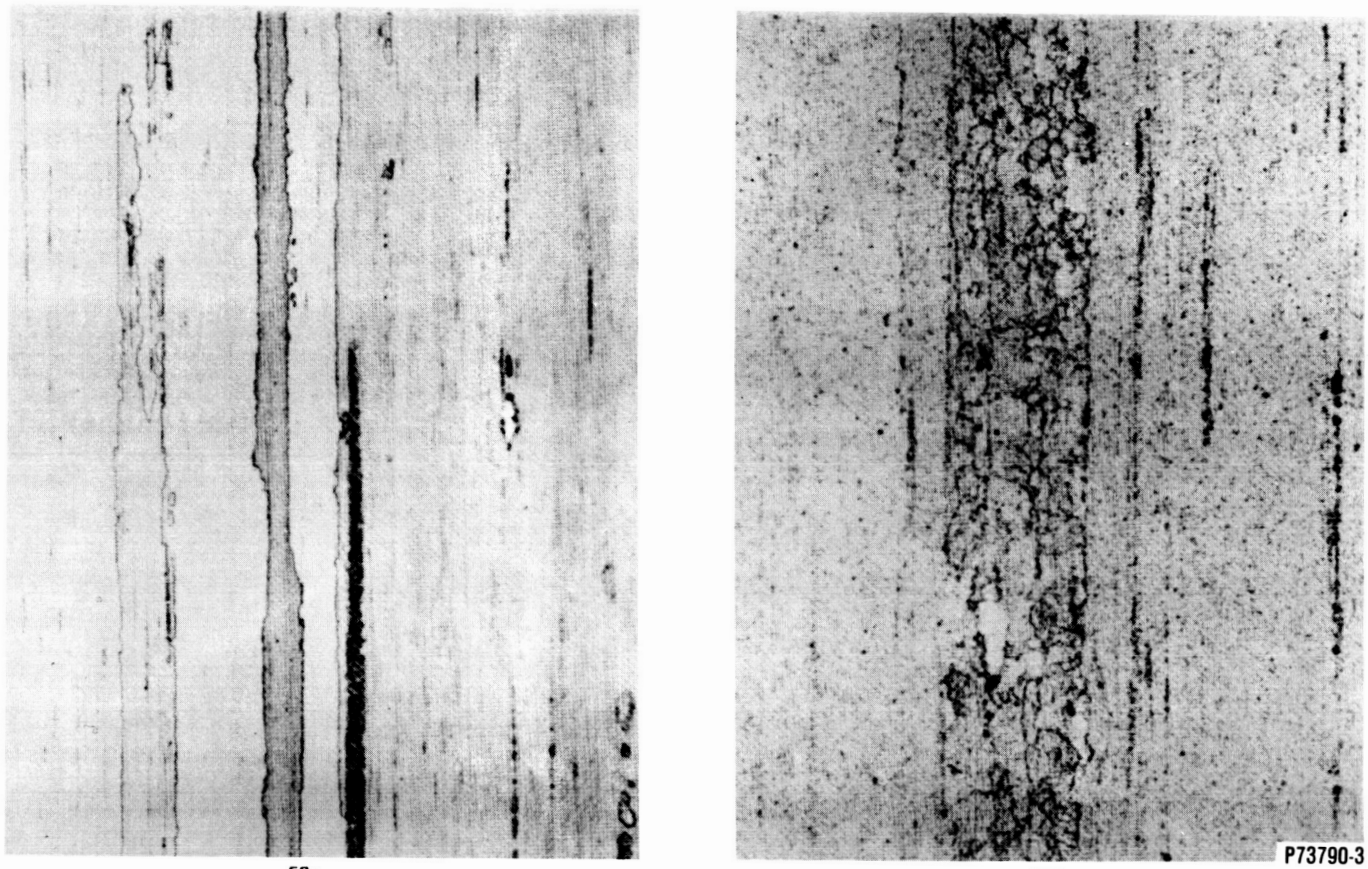

Figure 9. Longitudinal Microstructure of Preliminary Wiggin MA6000 Showing Chain of Small Equiaxed Grains.

produce regions in the extruded and rolled bar that require a higher recrystallization temperature and result in areas of fine equiaxed grains. Another possible explanation was the use of improper zone-annealing parameters. Wiggin used a prototype zone-annealing unit to manufacture this initial material. To determine if a variation in composition existed between the fine equiaxed grains and the elongated grains, a microprobe examination of the specimens was performed.

A probe scan, with a 10-micron wide line, was performed for Al, Ti, Cr, Mo, W, Ta, and Fe, traversing from a coarse, elongated grain through a fine-grained area and back into a coarse, elongated grain. The results shown in Figure 10 were recorded using an X-Y plotter and are given in Figure 11. The scans show a depletion of Ti and a variation of Al and Cr concentration in the fine-grained area. These results suggested minor compositional variations in the MA6000 powder. These chemistry variations may have been due to attritor wear, which increases the gap between the wall and arms, resulting in small variation in powder chemistry. Tensile testing of the preliminary Wiggin MA6000 material was conducted independently of this program at NASA. The results are compared with IRDC properties in Table 8. Stress rupture and LCF testing were also conducted at NASA on this preliminary Wiggin MA6000 material.

The effect of fine equiaxed grains on mechanical properties was evaluated by Wiggin. Wiggin's data suggested that neither longitudinal nor transverse stress-rupture and tensile properties are degraded due to the presence of fine equiaxed grains. Wiggin, however, did not evaluate the effect of these grains on fatigue properties.

A commercial 2-kHz induction heated zone-annealing unit was subsequently fabricated and installed at Wiggin to manufacture the commercial quality MA6000.

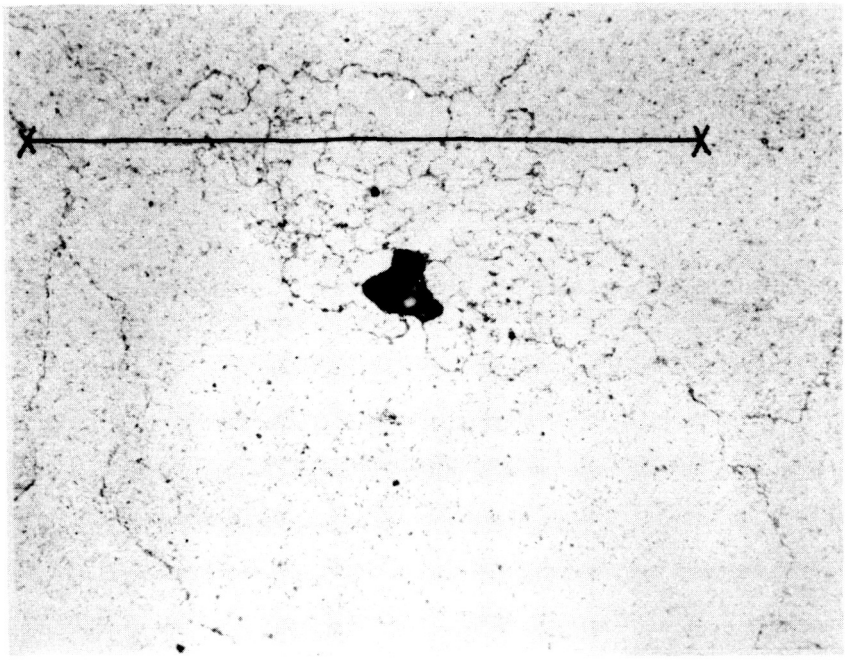

Figure 10. Microprobe Trace of Fine-Grain Area in Preliminary Wiggin MA6000 Barstock.

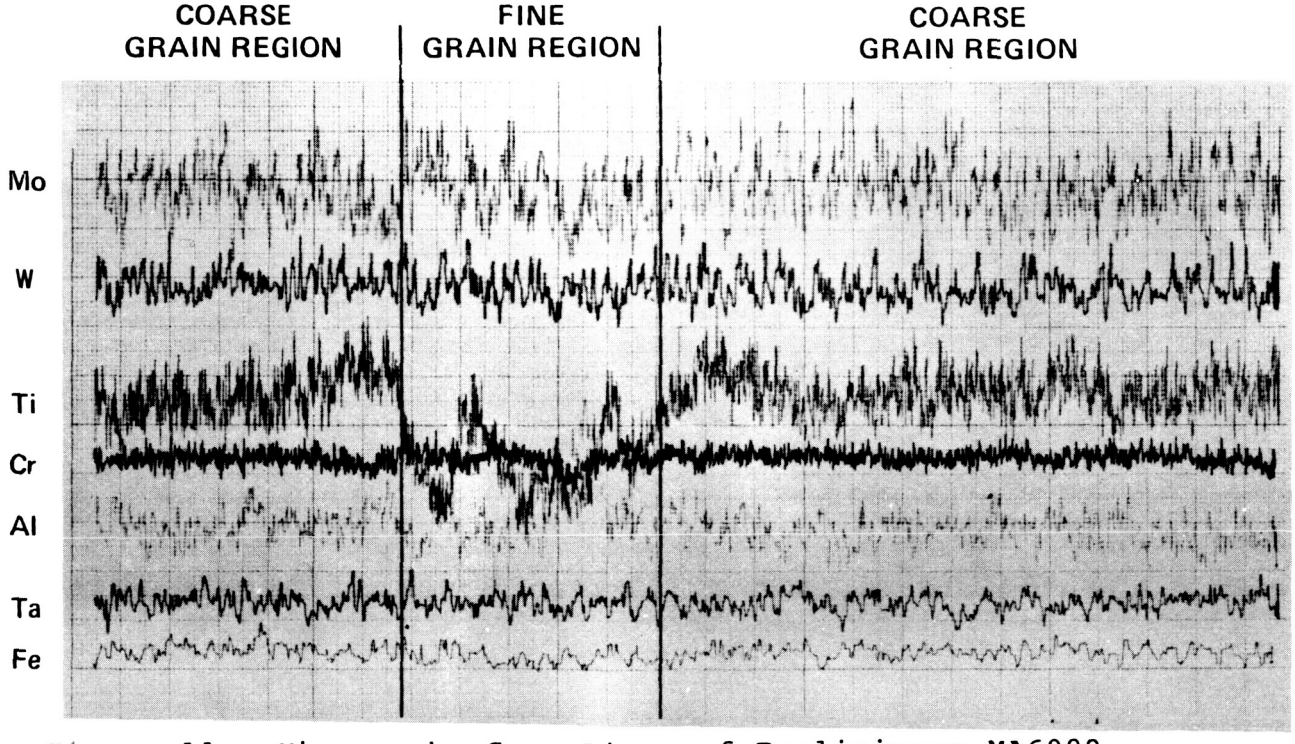

Figure 11. Microprobe Scan Lines of Preliminary MA6000 Wiggin Material.

TABLE 8. MA6000 TENSILE TEST RESULTS

Room Temperature Tensile Properties				
Material	0.2% YS, MPa (ksi)	UTS, MPa (ksi)	Elongation Percent	RA Percent
Preliminary Wiggin*	1158 (168)	1248 (181)	2	4
IRDC	1192 (173)	1199 (174)	4	5
760C (1400F) Tensile Properties				
Preliminary Wiggin*	1014 (147)	1041 (151)	NA	5
IRDC	945 (137)	993 (144)	8	7

*Testing conducted by NASA.

4.2 Mechanical Properties

4.2.1 Tensile Testing

Results of tensile testing at room and elevated temperatures in both the longitudinal and transverse directions are shown in Tables 9 and 10, respectively. The data combines the results of both the preliminary Wiggin material and the commercial production lot. In general, the data for these sets of tests are comparable. They compare favorably with previously reported results by Inco.

The comparative tensile properties of MA6000, DS MAR-M 247, and CMSX-3 single crystal alloys are plotted as a function of temperature in Figures 12 and 13. The ultimate tensile strength of MA6000 is higher, to about with 704C (1300F), but with a corresponding lower tensile elongation compared with DS MAR-M 247. This behavior can be explained by considering the strengthening mechanisms of these alloys. During plastic deformation at lower temperatures, both MA6000 and DS MAR-M 247 appear to behave similarly due to the solid-solution strengthening of the gamma (γ) matrix and by precipitation strengthening of the gamma-prime (γ') phase. MA6000 gains some additional strength from oxide-dispersion-strengthening. From 704 to 982C (1300 to 1800F), the cast alloy surpasses MA6000 in tensile strength due to its higher volume fraction of gamma-prime. However, above 982C (1800F), MA6000 tensile strength does not decrease as rapidly as DS MAR-M 247 because the ODS mechanism still remains active. At these temperatures, the gamma-prime is coarsening and begins to dissolve. The tensile elongation remains relatively low for the ODS alloy but is considered adequate for the temperature range of 1200 to 1400F where the blade root attachment operates.

TABLE 9. LONGITUDINAL TENSILE PROPERTIES OF MA6000

Temperature C (F)	0.2% Yield Strength MPa (ksi)	Ultimate Strength MPa (ksi)	Elongation Percent	R of A Percent	Static Modulus X GPa (10^6 psi)
24 (75)	1151 (167)	1227 (178)	4.9	5.2	233 (32.4)
	1103 (160)	1186 (172)	6.4	8.5	209 (30.3)
	1186 (172)	1207 (175)	5.4	6.1	--
	1180 (171)	1186 (172)	3.7	4.5	--
	1200 (174)	1200 (174)	3.4	4.6	--
	1193 (173)	1207 (175)	4.6	4.5	--
	1110 (161)	1151 (167)	3.7	4.0	217 (31.4)
	1076 (156)	1158 (168)	4.6	7.5	223 (32.4)
538 (1000)	1000 (145)	1186 (172)	7.3	8.6	161 (23.4)
	1007 (146)	1165 (169)	3.8	3.8	161 (23.3)
	958 (139)	1131 (164)	5.6	4.8	181 (26.2)
	938 (136)	1110 (161)	5.4	7.0	157 (22.7)
649 (1200)	986 (143)	1138 (165)	9.0	9.6	145 (21.1)
	1014 (147)	1165 (169)	4.7	6.6	159 (23.0)
	979 (142)	1138 (165)	7.0	7.9	140 (20.3)
	993 (144)	1117 (162)	10.1	12.0	150 (21.8)
760 (1400)	938 (136)	958 (139)	20.9	34.1	--
	958 (139)	1000 (145)	6.3	6.4	--
	924 (134)	1020 (148)	8.8	6.5	--
	946 (137)	986 (143)	11.0	9.4	--
	758 (110)	979 (142)	9.1	9.0	152 (22.0)
	662 (96)	979 (142)	10.5	11.0	147 (21.3)
	800 (116)	951 (138)	9.9	11.0	131 (19.0)
	765 (111)	938 (136)	12.2	16.6	128 (18.6)
	841 (122)	986 (143)	10.8	14.7	--
	827 (120)	986 (143)	7.0	8.1	--
	903 (131)	931 (135)	8.4	9.9	--
	800 (116)	931 (135)	8.3	8.9	--
	848 (123)	986 (143)	6.4	8.8	--
	820 (119)	979 (142)	5.8	6.1	--
	827 (120)	965 (140)	9.0	9.1	--
	827 (120)	965 (140)	9.9	11.9	--
871 (1600)	469 (68)	662 (96)	9.5	13.6	128 (18.6)
	517 (75)	641 (93)	17.2	28.1	130 (18.9)
	517 (75)	669 (97)	15.2	23.6	118 (17.1)
	503 (73)	676 (98)	12.3	19.1	117 (16.9)
982 (1800)	331 (48)	414 (60)	12.4	31.7	110 (15.9)
	331 (48)	427 (62)	14.6	27.4	108 (15.6)
	331 (48)	427 (62)	17.5	30.3	125 (18.1)
	365 (53)	421 (61)	15.5	28.1	117 (16.9)
	365 (53)	414 (60)	16.8	26.6	--
	338 (49)	407 (59)	15.5	28.2	--
	365 (53)	421 (61)	11.7	25.8	--
	324 (47)	407 (59)	22.1	30.9	--
	317 (46)	400 (58)	11.8	14.8	--
	255 (37)	421 (61)	12.0	22.3	--
	348 (50)	414 (60)	22.8	36.9	--
	331 (48)	400 (58)	21.0	29.2	--
1093 (2000)	193 (28)	228 (33)	18.6	31.3	90 (13.1)
	200 (29)	228 (33)	17.0	32.9	90 (13.0)
	186 (27)	228 (33)	16.5	28.7	103 (15.0)
	193 (28)	228 (33)	18.0	33.2	94 (13.6)

TABLE 10. TRANSVERSE TENSILE PROPERTIES OF MA6000

Temperature C (F)	0.2% Yield Strength MPA (ksi)	Ultimate Strength MPa (ksi)	Elongation percent	R of A (percent)	Static Modulus (x GPa (10^6 psi)
24 (75)	1089 (158)	1165 (169)	2.4	4.8	216 (31.3)
	1082 (157)	1145 (166)	1.4	5.1	224 (32.5)
	1055 (153)	1096 (159)	1.4	3.6	217 (31.4)
	1069 (155)	1110 (161)	1.1	2.0	217 (31.4)
538 (1000)	972 (141)	1110 (161)	1.9	3.2	157 (22.7)
	945 (137)	1069 (155)	1.4	3.1	159 (23.0)
	1020 (148)	1165 (169)	3.4	4.3	147 (21.3)
	1027 (149)	1055 (153)	1.9	2.0	159 (23.1)
649 (1200)	1000 (145)	1158 (168)	3.3	5.5	148 (21.5)
	1020 (148)	1158 (168)	2.3	2.3	146 (21.2)
	979 (142)	1165 (169)	3.2	4.4	160 (23.2)
	979 (142)	1186 (172)	3.5	5.2	143 (20.8)
760 (1400)	758 (110)	972 (141)	3.7	5.8	124 (18.0)
	772 (112)	1014 (147)	3.4	2.3	125 (18.2)
	800 (116)	1014 (147)	3.5	2.7	152 (22.0)
	779 (113)	1000 (145)	0.9	2.3	149 (21.6)
871 (1600)	517 (75)	738 (107)	4.6	4.7	131 (19.0)
	496 (72)	724 (105)	2.4	3.6	129 (18.7)
	483 (70)	731 (106)	3.1	3.6	117 (16.9)
	490 (71)	731 (106)	3.2	4.4	119 (17.3)
982 (1800)	324 (47)	400 (58)	1.3	2.7	110 (15.9)
	345 (50)	352 (51)	--	--	110 (16.0)
	331 (48)	455 (66)	3.3	3.6	112 (16.2)
	338 (49)	448 (65)	2.2	2.7	117 (17.0)
1093 (2000)	193 (28)	193 (28)	1.5	1.2	90 (13.0)
	193 (28)	193 (28)	1.3	1.2	105 (15.2)
	--	193 (28)	1.4	1.2	96 (13.9)

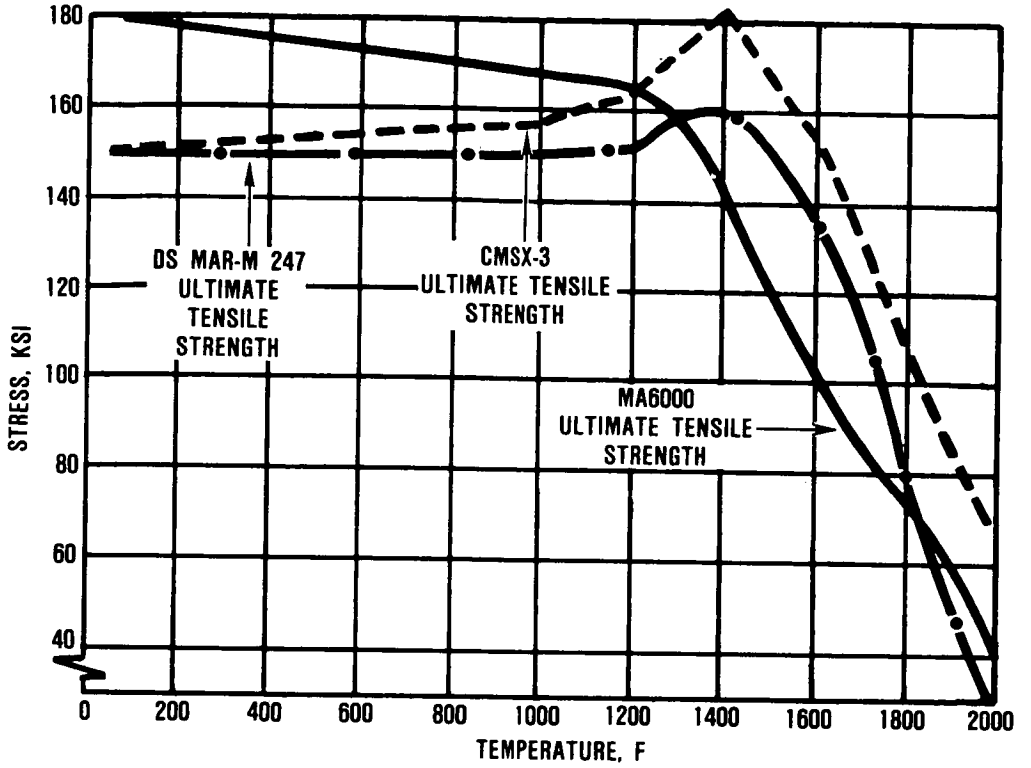

Figure 12. Tensile Properties Versus Temperature of MA6000, DS MAR-M 247, and CMSX-3, Longitudinal Orientation.

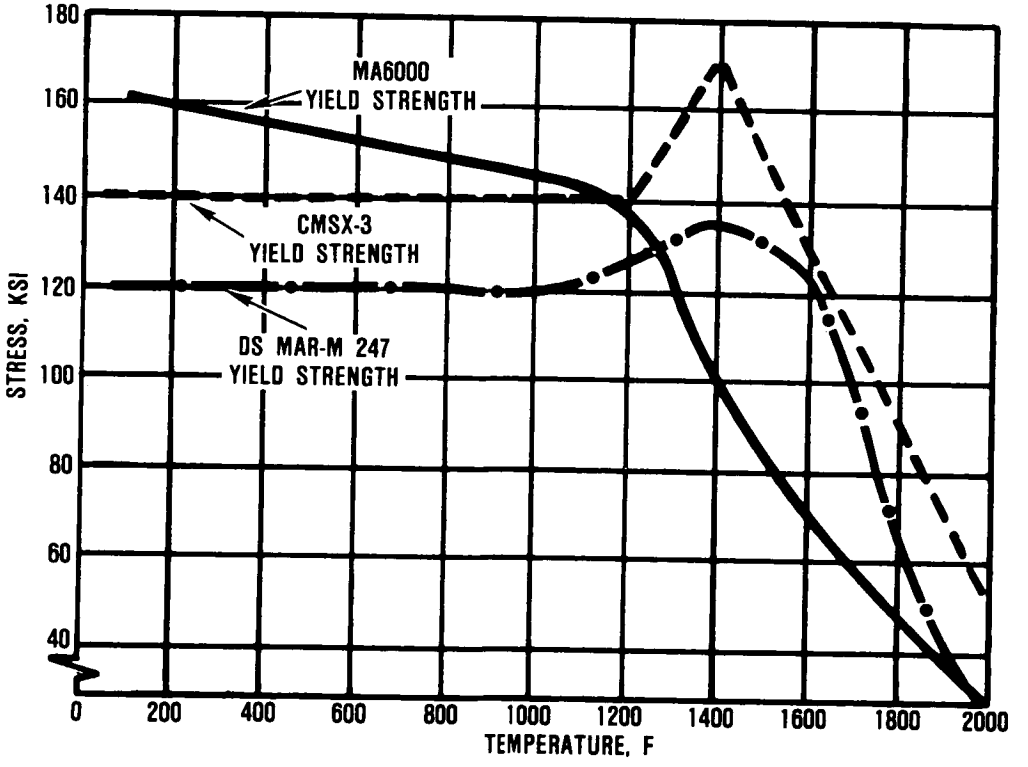

Figure 13. Tensile Properties Versus Temperature of MA6000, DS MAR-M 247, and CMSX-3, Longitudinal Orientation.

Analysis of the failed room-temperature and 1400F tensile specimens found that both macrostructure and microstructure appeared similar to typical MA6000 structure. Figure 14 shows typical fracture surfaces of the tensile specimens. At room temperature, the fracture is noncrystallographic, while at 1400F, crystallographic cracking is the failure mode.

4.2.2 Creep-Rupture Testing

Results of creep-rupture testing of the combined preliminary Wiggin material and the commercial production lots are shown in Table 11. The MA6000 creep elongations are relatively low compared with those of conventional nickel-base superalloys. This low MA6000 ductility produces creep behavior in which third-stage creep initiates below 1.0-percent elongation. Thus, times to 1-percent creep are a substantial fraction (85 percent) of the rupture life.

Comparing the average 1-percent creep capability of DS MAR-M 247 with the data average for MA6000 shows a 66C (150F) creep advantage of MA6000 (Figure 15) at 25 ksi stress levels. At higher stresses--(greater than 276 Mpa (40 ksi)--the DS alloy is slightly better, which, as discussed below under stress-rupture testing, is characteristic behavior of the two alloy systems.

Data analyses of the 0.5- and 1.0-percent creep for MA6000, both longitudinal and transverse direction, are shown in Figures 18 through 19. These figures also present the data generated by INCO during the development phase of MA6000.

4.2.3 Stress-Rupture Testing

Paragraph 3.6, which discussed the stress-rupture testing conducted during the process optimization task, established that properly processed MA6000 barstock will meet a 100-hour minimum life at

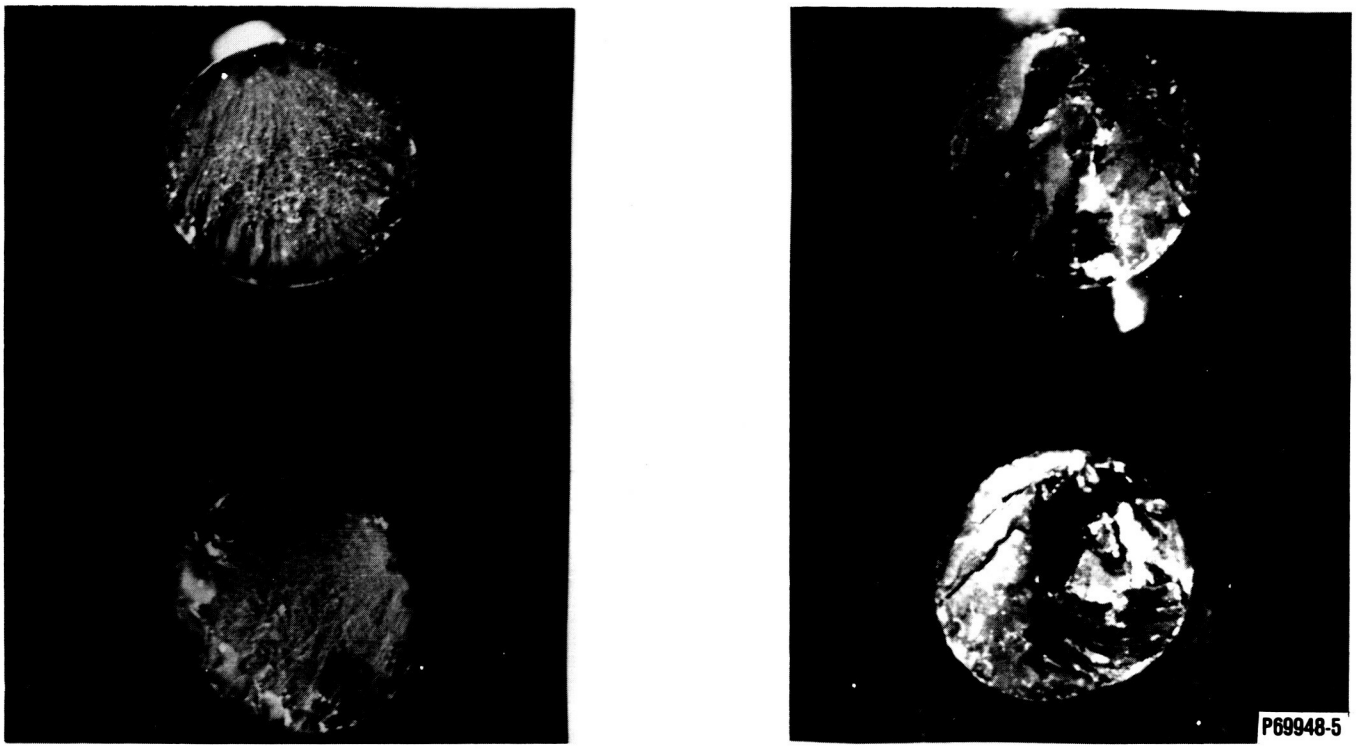

Figure 14. Fracture Surfaces of (A) Room Temperature and (B) 760C (1400F) MA6000 Tensile Specimens.

TABLE 11. MA6000 CREEP-RUPTURE RESULTS

Temperature C (F)	Stress MPa (ksi)	Rupture Time Hours	Elongation Percent	R of A Percent	Time to Percent Creep, Hours			
					0.5	1.0	1.5	2.0
760 (1400)	586 (85)	21.2	7.7	12.0	3	8	12	15
	552 (80)	46.2	4.8	9.0	6	15	24	31
	538 (78)	86.2	9.3	15.1	13	33	48	61
	517 (75)	111.4	4.4	5.0	21	49	70	86
	483 (70)	409.9	6.5	10.5	100	213	291	335
	455 (66)	812.4	5.3	6.6	250	460	598	688
	427 (62)	1604.0	4.7	9.3	489	929	1209	1385
871 (1600)	359 (52)	32.8	8.5	14.9	9	19	24	27
	345 (50)	74.9	9.5	17.1	26	45	57	63
	331 (48)	103.6	6.7	14.1	44	69	82	89
	317 (46)	164.3	8.4	15.0	77	117	137	147
	290 (42)	330.9	6.5	10.6	151	235	277	299
	276 (40)	711.6	5.4	11.3	267	528	621	660
	262 (38)	1105.2	5.1	11.0	260	695	911	1004
982 (1800)	241 (35)	13.5	10.5	24.8	4	8	10	11
	221 (32)	37.9	6.4	12.1	17	29	35	--
	214 (31)	55.5	6.4	15.9	16	38	48	52
	207 (30)	54.1	6.8	16.9	25	44	49	51
	207 (30)	135.2	2.1	3.8	66	116	134	--
	207 (30)	93.5	4.1	5.3	56	81	89	--
	207 (30)	73.9	3.4	6.5	44	63	71	--
	200 (29)	338.2	3.2	5.5	78	245	316	336
	193 (28)	659.5	2.6	5.1	170	624	--	--
	193 (28)	185.5	2.2	4.1	33	121	172	--
	193 (28)	372.8	1.7	2.8	155	319	368	--
	193 (28)	398.4	1.4	2.6	61	263	--	--
	193 (28)	611.3	1.8	2.7	125	514	611	--
	186 (27)	915.1	1.2	1.7	423	910	--	--
	186 (27)	554.2	1.6	2.7	316	528	--	--
	186 (27)	838.6	3.0	5.0	293	533	679	--
	186 (27)	791.4	2.2	2.4	432	785	--	--
1038 (1900)	207 (30)	4.4	11.6	31.0	2	--	--	--
	186 (27)	20.1	8.0	18.3	8	16	--	--
	179 (26)	70.5	5.3	9.9	22	57	67	--
	179 (26)	122.7	3.4	6.8	39	106	120	--
	172 (25)	165.9	2.7	3.3	99	162	--	--
	172 (25)	959.8	2.0	2.9	65	942	--	--
	165 (24)	504.6	1.0	2.3	361	--	--	--
1093 (2000)	152 (22)	9.1	5.3	16.2	4	--	--	--
	152 (22)	112.0	3.6	5.3	45	--	--	--
	145 (21)	165.7	4.1	7.5	94	162	--	--
	145 (21)	370.4	2.8	7.0	309	--	--	--
	138 (20)	612.7	4.5	5.1	27	392	606	--
	131 (19)	2186.6	3.9	4.4	673	2088	--	--
1149 (2100)	124 (18)	18.2	8.4	25.3	0.2	1	8	16
	124 (18)	72.9	7.7	19.1	14	44	66	72
	117 (17)	157.7	6.3	9.5	146	--	--	--
	117 (17)	198.7	7.9	17.3	157	186	194	197
	110 (16)	324.4	6.6	9.0	242	323	--	--
	103 (15)	655.4	4.0	6.4	55	349	608	645

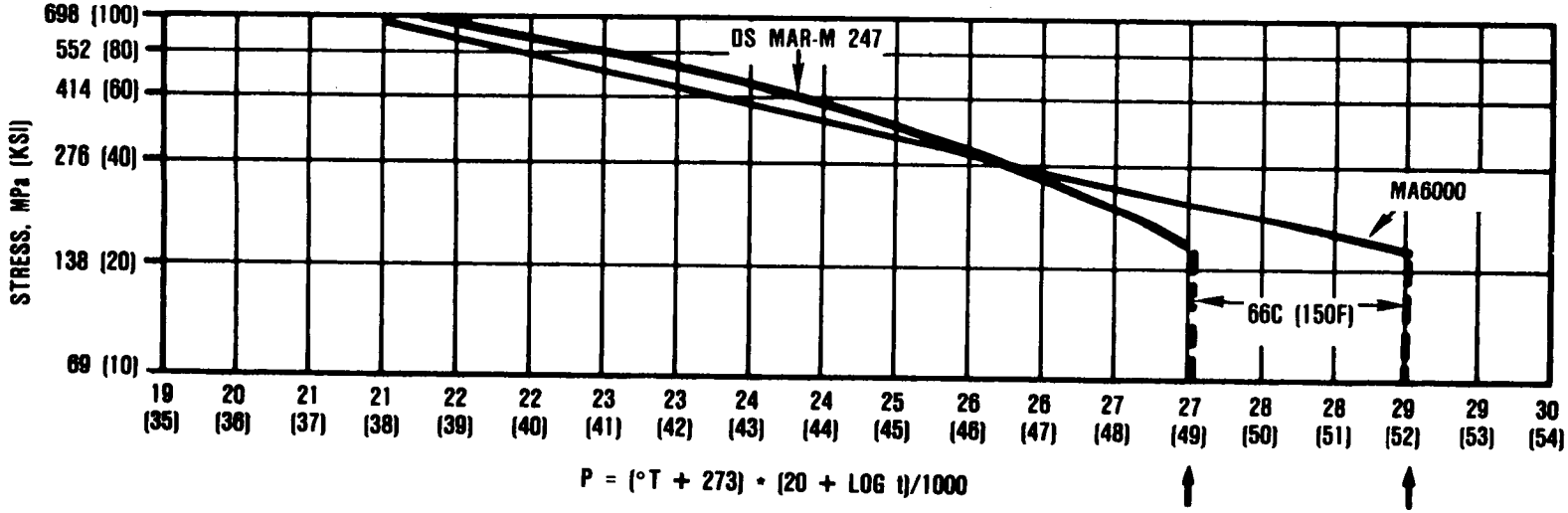

Figure 15, One-Percent Creep Data for MA6000 and DS MAR-M 247 (Longitudinal Direction).

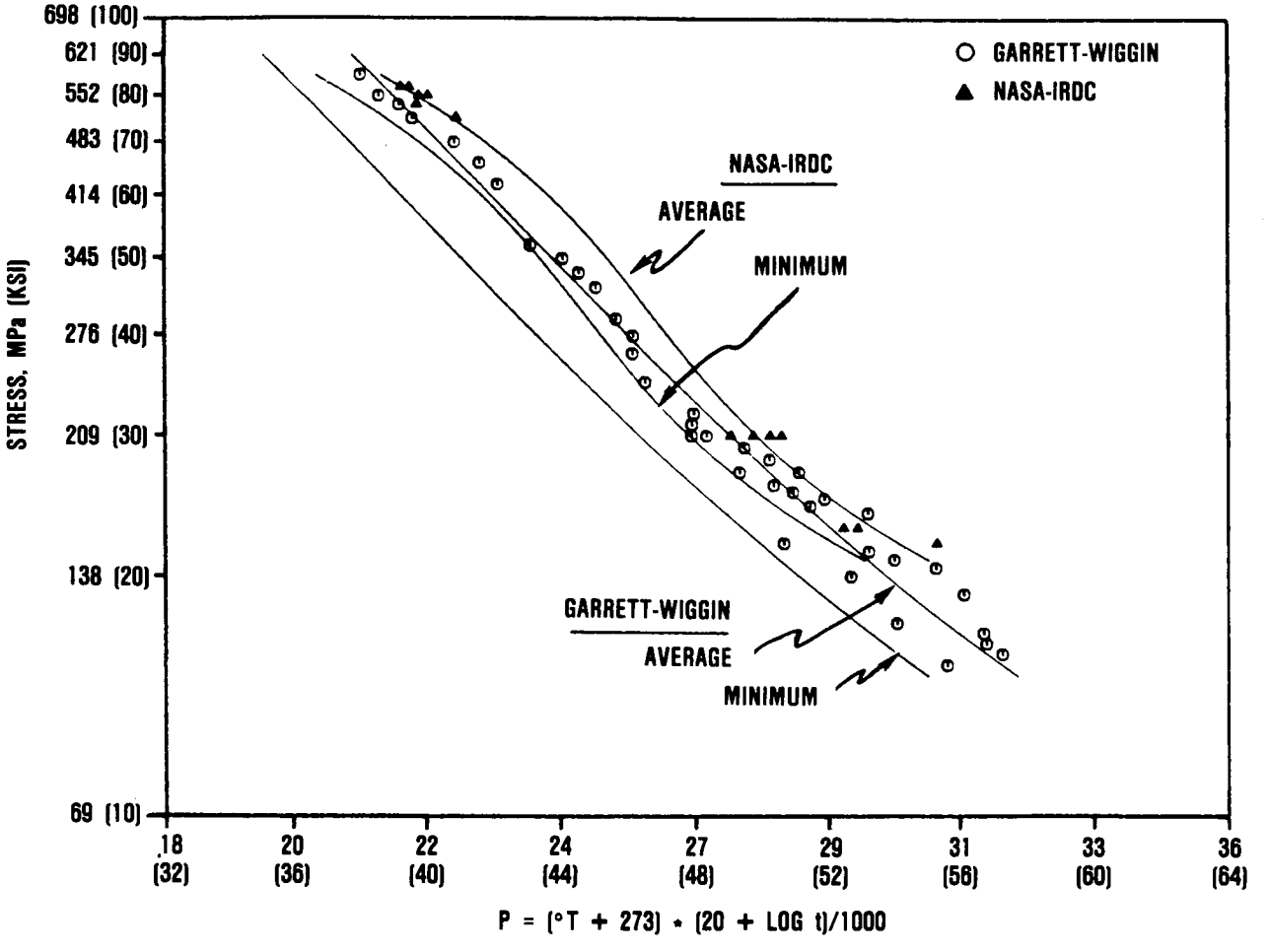

Figure 16. 0.5-Percent Creep of NASA-IRDC MA6000 Compared to Wiggin Commercial Material Lots 1 and 2, Longitudinal Direction.

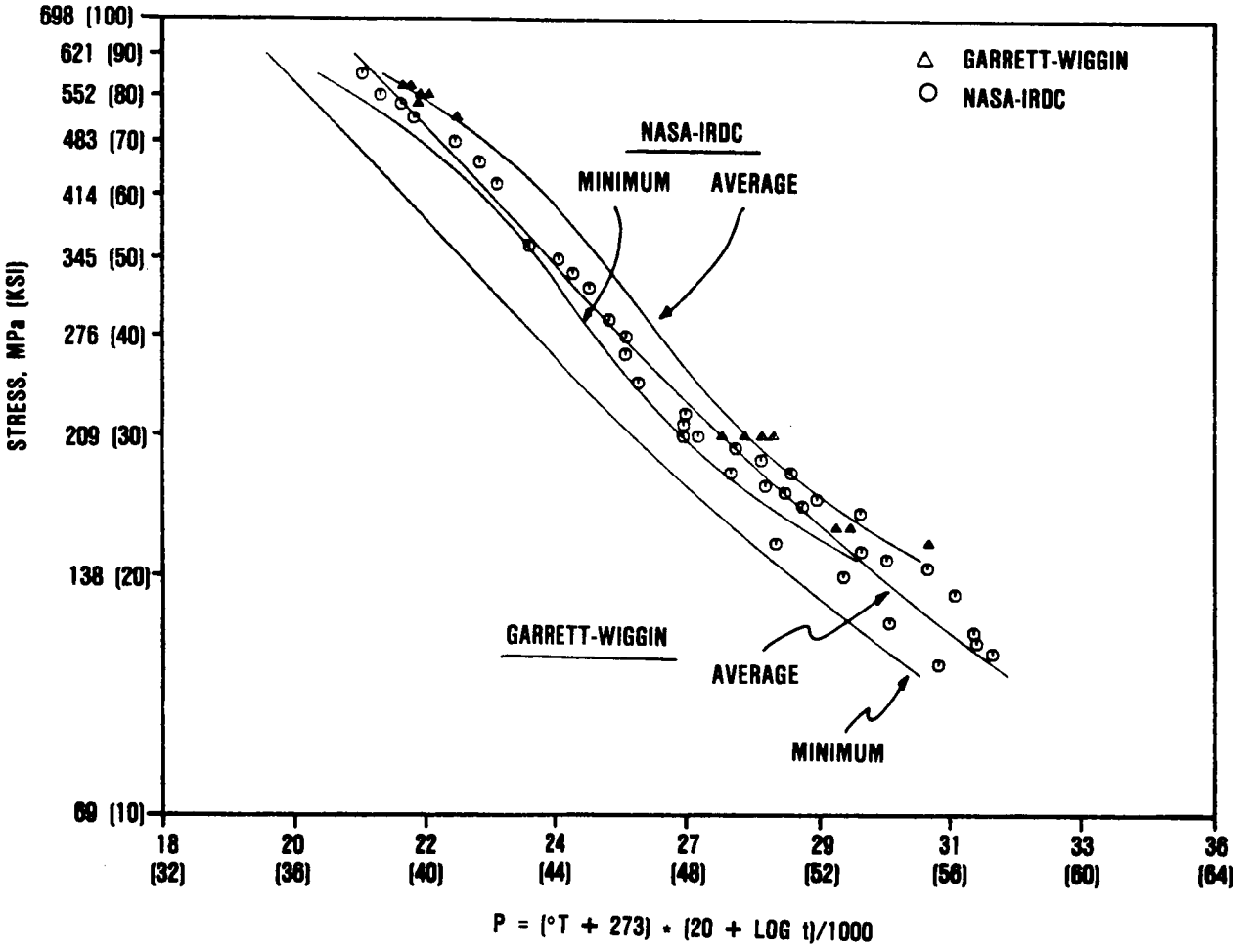

Figure 17. 1.0-Percent Creep of NASA-IRDC MA 6000 Compared to Wiggin Commercial Material Lots 1 and 2, Longitudinal Direction.

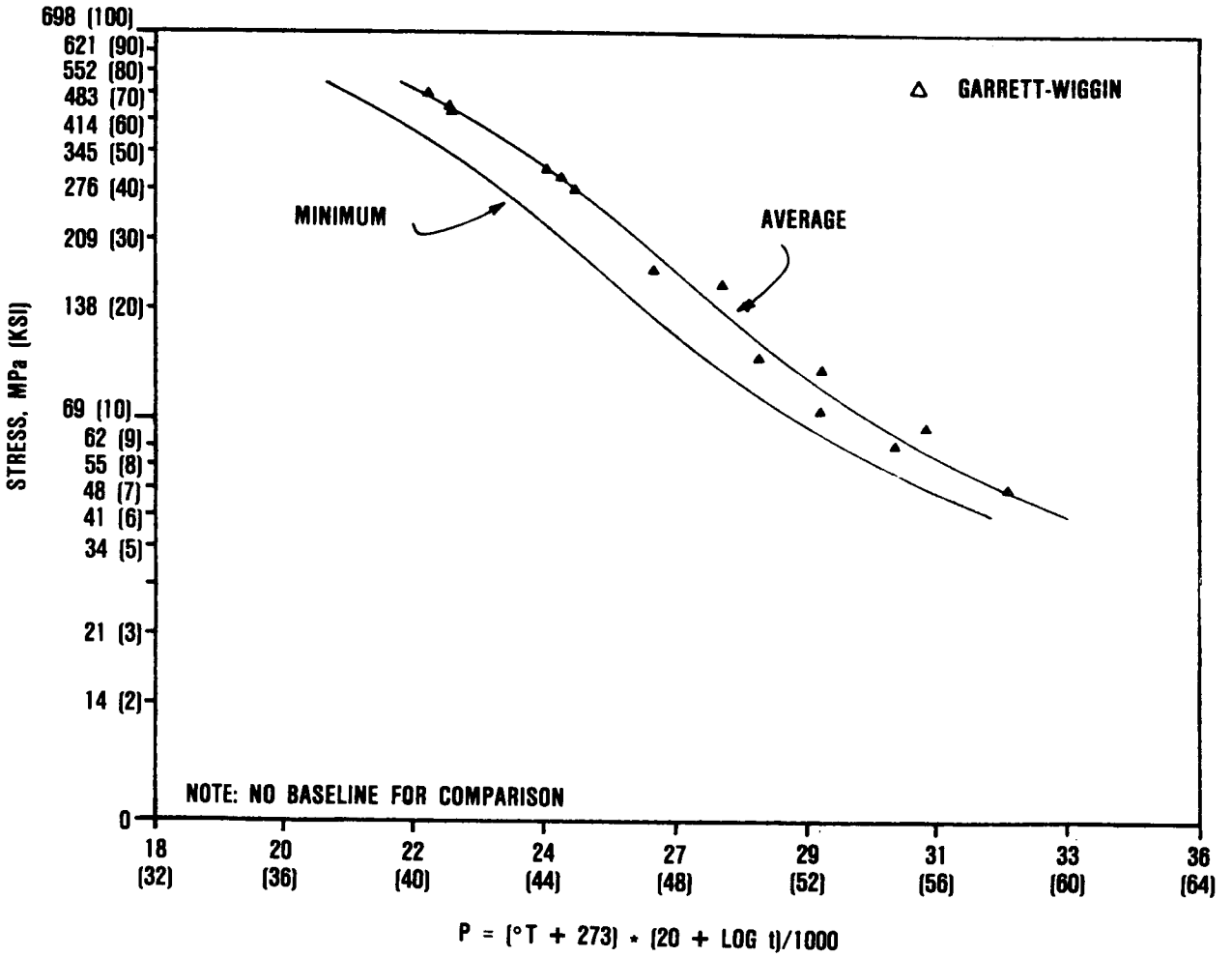

Figure 18. 0.5-Percent Creep of MA 6000 (Lot No. 2) Produced by Wiggin, Transverse Direction.

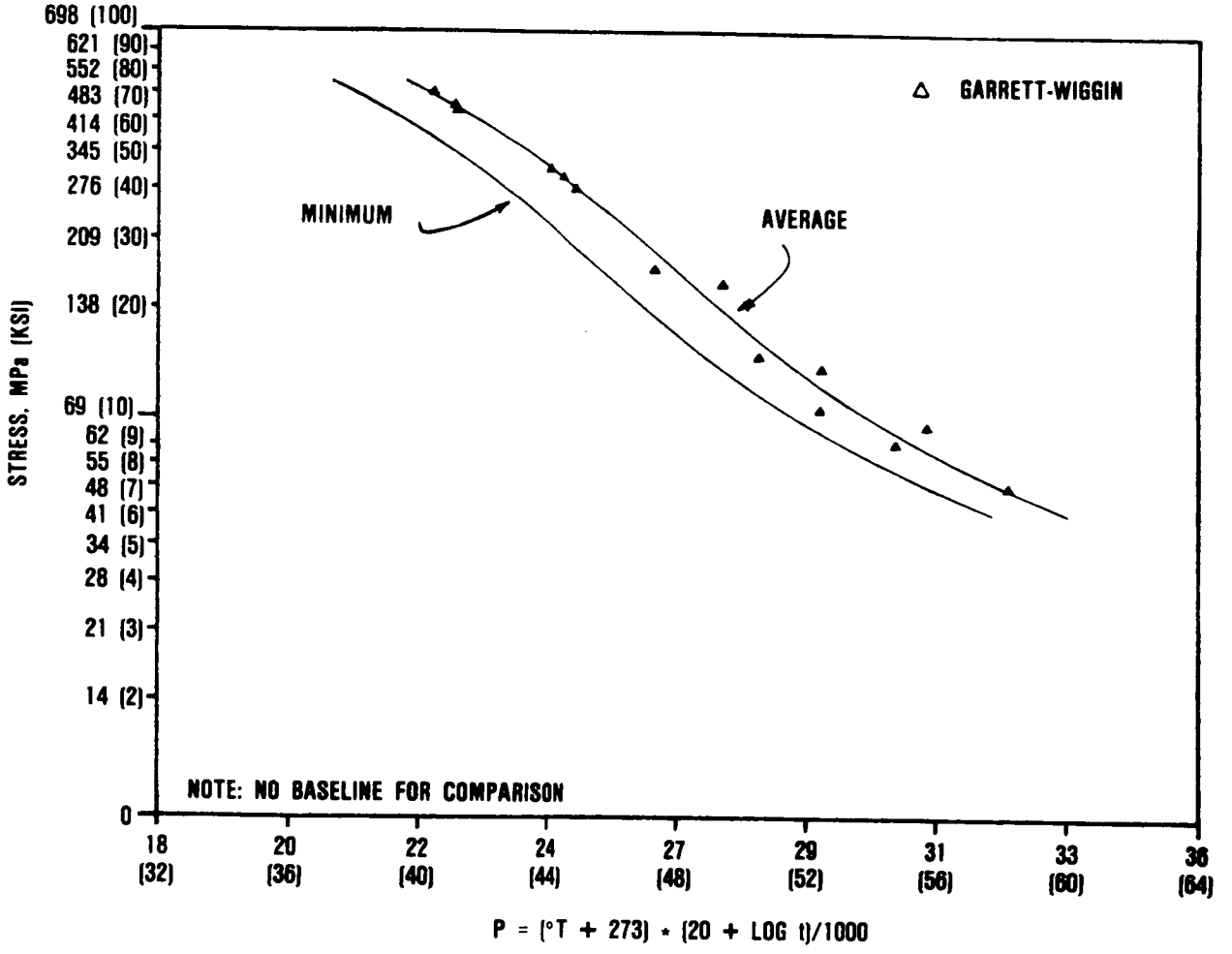

Figure 19. 1.0-Percent Creep of MA6000 (Lot No. 2) Produced by Wiggin, Transverse Direction.

1093C (2000F) and 138 MPa (20 ksi) stress level in the longitudinal orientation and 1093C (2000F)/41 MPa (6 ksi) in the transverse direction. All subsequent commercial barstock used in this program was tested to this minimum life requirement as part of the acceptance testing imposed on incoming material. Stress rupture tests were generally uploaded by 2 ksi and run to failure once the specimens reached the 100-hour minimum life.

Figures 20 and 21 show the longitudinal and transverse stress-rupture data plots for MA6000. The longitudinal data shows good correlation to earlier INCO results. Table 12 shows the stress-rupture data of commercially produced MA6000.

Based on the observed tensile and rupture strength behavior of MA6000, mathematical analysis was performed on the stress-rupture data accumulated from all the commercial lot materials tested, and the analysis was plotted to characterize the upper and lower bounds of the curve (Figure 22). In addition, the optimum Larson-Miller constant, C, was determined to establish whether the C value of 20, conventionally used for nickel-base superalloys, also was valid for MA6000. The mathematical model used in this study is given in terms of a regression analysis:

$$P = a_o + a_1x + a_2x^2 + a_3x^3 + \ldots.$$

where: a_o, a_1, a_2, a_3 are constants

$x = \text{Log}_{10}$ (stress, ksi)

p = (Temperature, degrees T + 273)
(20 + Log t)/1000

C = Larson-Miller constant

The optimized Larson-Miller constant for the full-spectrum curve of MA6000 was determined to be 29.81 (Figure 23). A similar

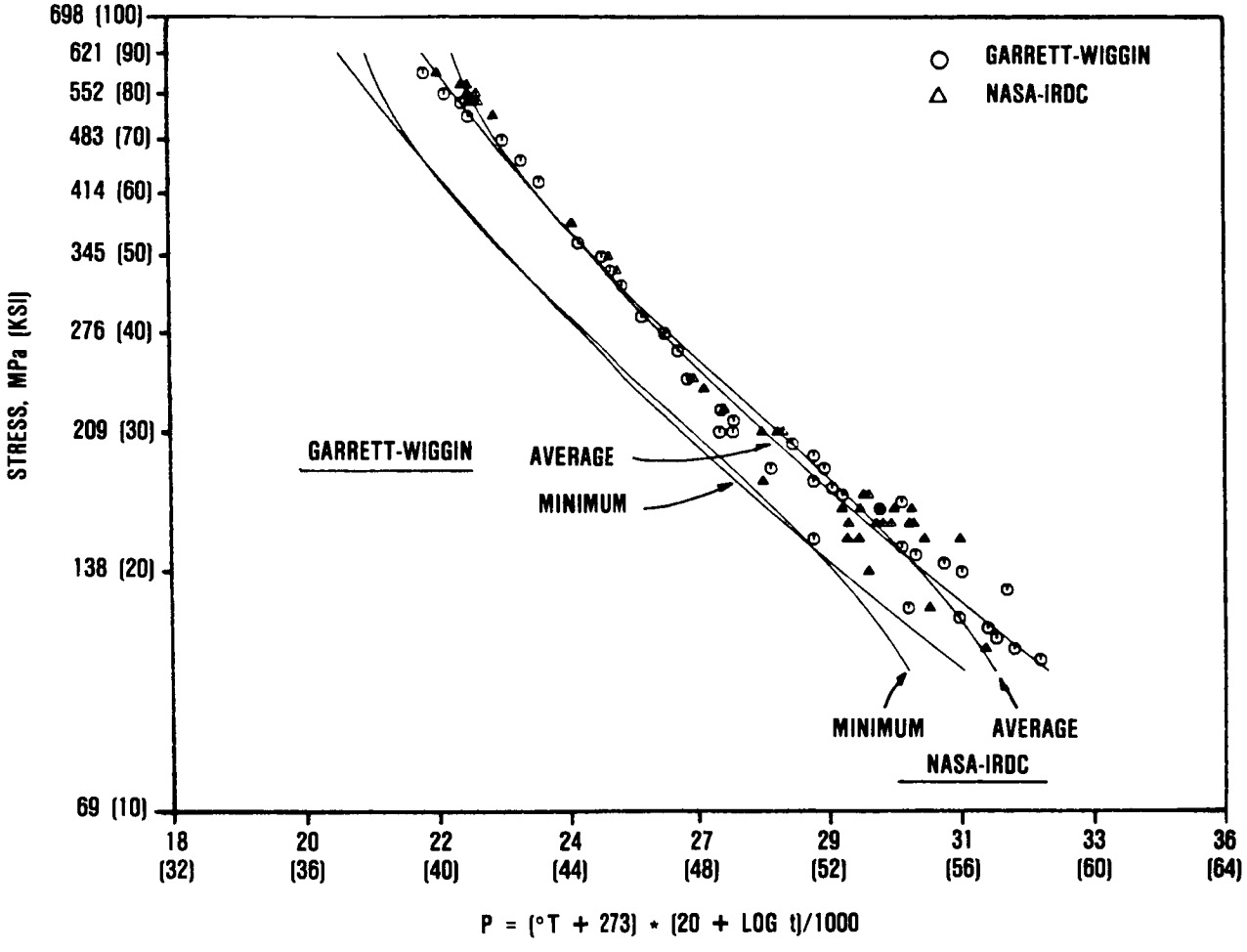

Figure 20. Stress Rupture of NASA-IRDC MA6000 Compared to Wiggin Commercial Material Lots 1 and 2, Longitudinal Direction.

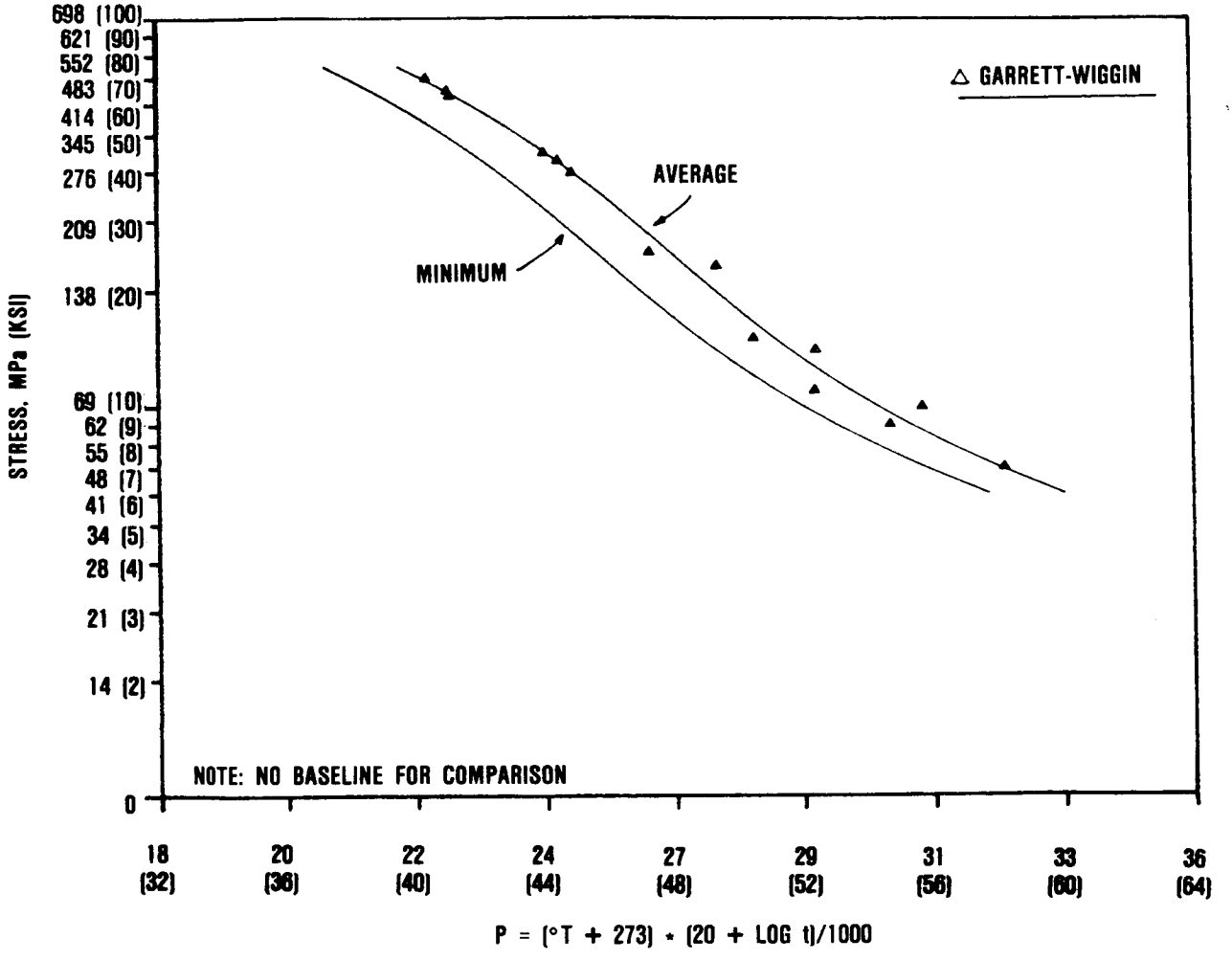

Figure 21. Stress Rupture of MA6000 (Lot No. 2) Produced by Wiggin, Transverse Direction.

TABLE 12. MA6000 STRESS-RUPTURE RESULTS

Test Orientation	Temperature C (F)	Stress MPa (ksi)	Rupture Time Hours	Elongation percent	R of A percent
Transverse	760 (1400)	483 (70)	55.9	2.2	2.7
	760 (1400)	448 (65)	124.6	0.7	0.9
	760 (1400)	434 (60)	136.3	0.9	1.5
	871 (1600)	310 (45)	24.5	1.4	2.0
	871 (1600)	296 (43)	40.2	1.6	1.5
	871 (1600)	276 (40)	64.5	0.6	1.2
	982 (1800)	172 (25)	8.6	0.7	1.1
	982 (1800)	159 (23)	71.1	0.8	1.0
	1038 (1900)	103 (15)	25.3	1.2	1.6
	1038 (1900)	97 (14)	165.0	0.3	0.4
	1093 (2000)	76 (11)	19.8	1.6	2.0
	1093 (2000)	69 (10)	432.1	0.4*	---
	1093 (2000)	41 (6)	164.0*	3.5	---
	1149 (2100)	62 (9)	23.3	1.7	1.5
	1149 (2100)	48 (7)	543.2	2.0	2.3
Longitudinal	1093 (2000)	138 (20)*	142.3	7.7	14.2
	1093 (2000)	138 (20)*	107.2	5.0	11.3
	1093 (2000)	138 (20)*	124.1	5.3	11.3
	1093 (2000)	138 (20)*	108.6	6.5	13.8
	1093 (2000)	138 (20)*	103.9	5.6	11.8
	1093 (2000)	138 (20)*	122.7	5.5	9.1
	1093 (2000)	138 (20)*	123.9	5.0	9.0
	1093 (2000)	138 (20)*	122.2	7.5	11.9
	1093 (2000)	138 (20)*	113.0	10.0	---
	1093 (2000)	138 (20)*	107.0	11.0	---
	760 (1400)	490 (71)	173.0	5.2	---

*Tests were uploaded to 152 MPa (22 ksi) after 100 hours.

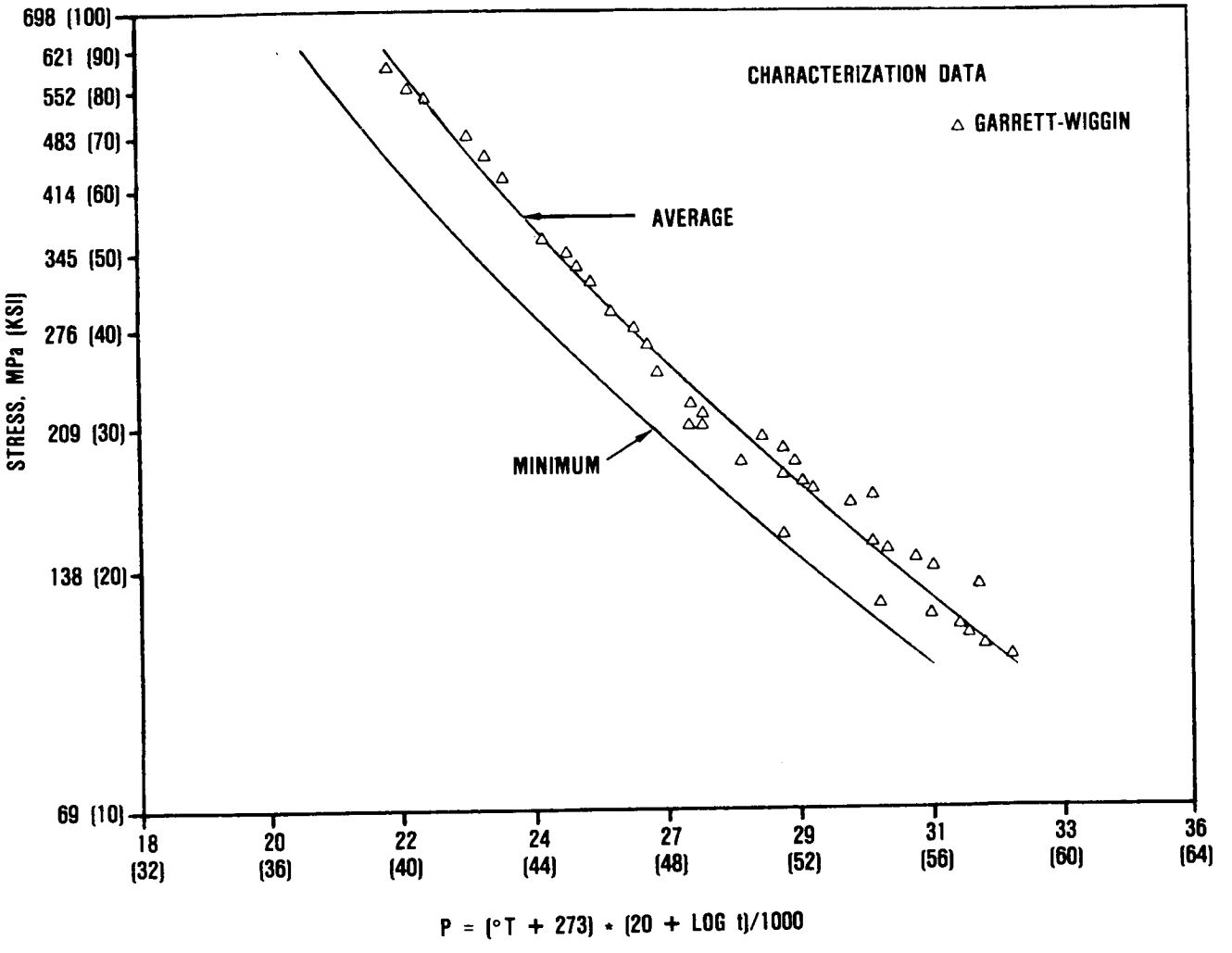

Figure 22. Stress-Rupture of MA6000 GTEC Data for C=20.

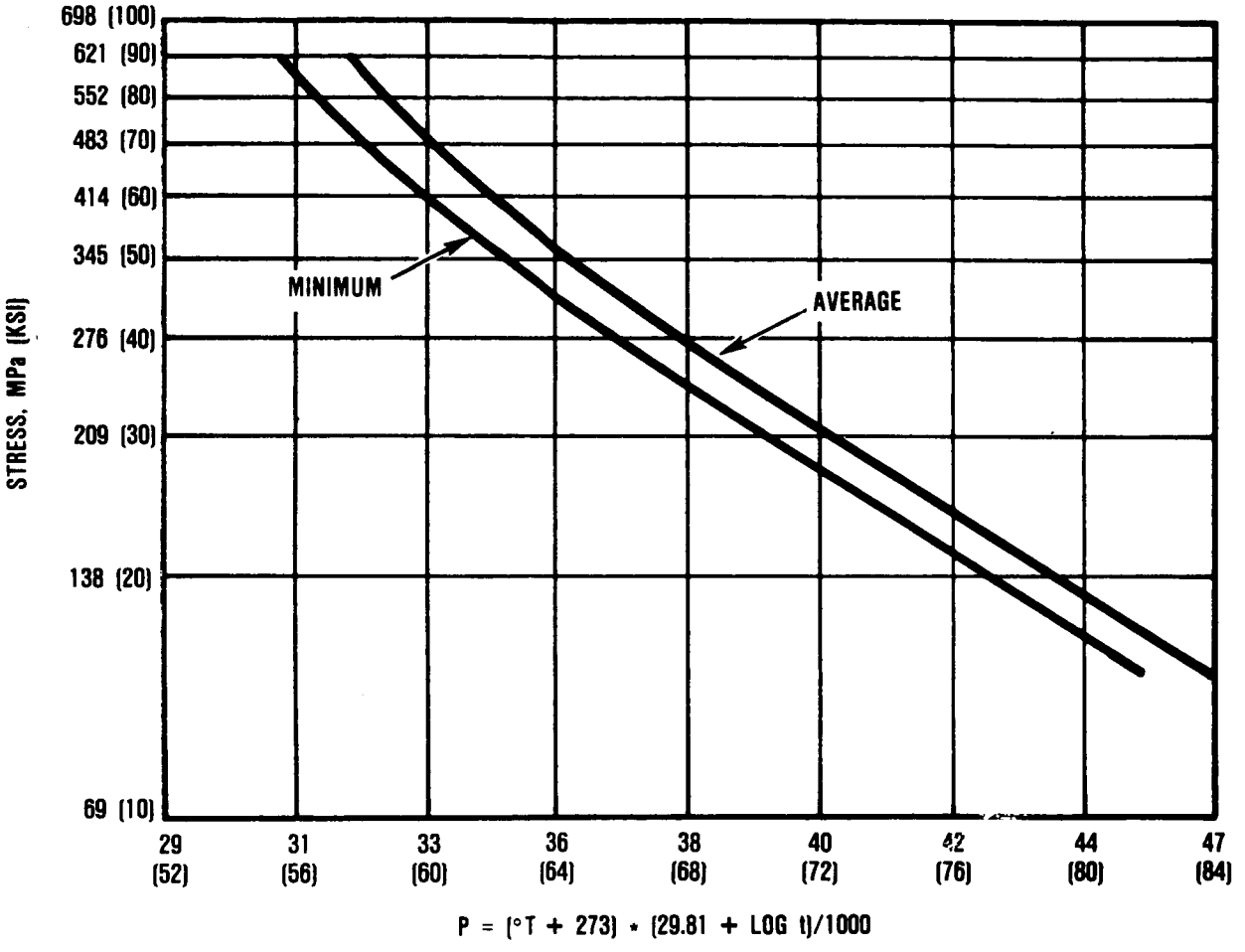

Figure 23. Stress-Rupture Behavior of MA6000 Replotted Using the Optimized Larson-Miller Constant of 29.81, Longitudinal Orientation.

analysis of the data above and below 30 ksi stress level yields C values of 22.75 and 49.96, respectively. Figure 24 compares the stress rupture plots above 30 ksi using the conventional C = 20 and the optimized C = 22.75 while Figure 25 repeats this analysis below 30 ksi using the optimum value of C = 49.96.

The analysis suggest the dual-strengthening mechanisms operative in the MA6000 alloy. At low and intermediate temperatures and higher stresses, the alloy behaves as a conventional nickel-base superalloy deriving its strength primarily from the precipitation hardening effect of the gamma-prime phase. At high temperatures and lower stresses, dispersion strengthening of the oxide phase becomes the dominant mechanism, thus giving the alloy its superior high temperature capability.

A comparative stress-rupture plot between MA6000, DS MAR-M 247, and single-crystal CMSX-3 is shown in Figure 26. At lower temperatures and higher stresses, DS MAR-M 247 shows better stress rupture capability. However, at higher temperatures and lower stresses, the ODS alloy clearly becomes superior. This behavior is characteristic of the ODS alloy, as has been observed in its tensile and creep behavior. The ODS mechanism operates at higher temperatures, thus giving the alloy the decided advantage for elevated temperature applications over the conventional DS-cast nickel base superalloys.

4.2.4 Low-Cycle-Fatigue Testing

Results of the strain-controlled LCF tests (Lot Nos. 1 and 2) are presented in Table 13. The load-controlled LCF tests (Lot Nos. 1 and 2) are presented in Table 14. Table 15 shows LCF results on test specimens produced by using ECM methods to simulate blade surface.

Figure 27 shows the comparative results of strain-controlled axial LCF tests of Lots No. 1 and 2 material, and Figure 28 gives the comparative results of load-controlled LCF tests of Lots No. 1 and 2 material.

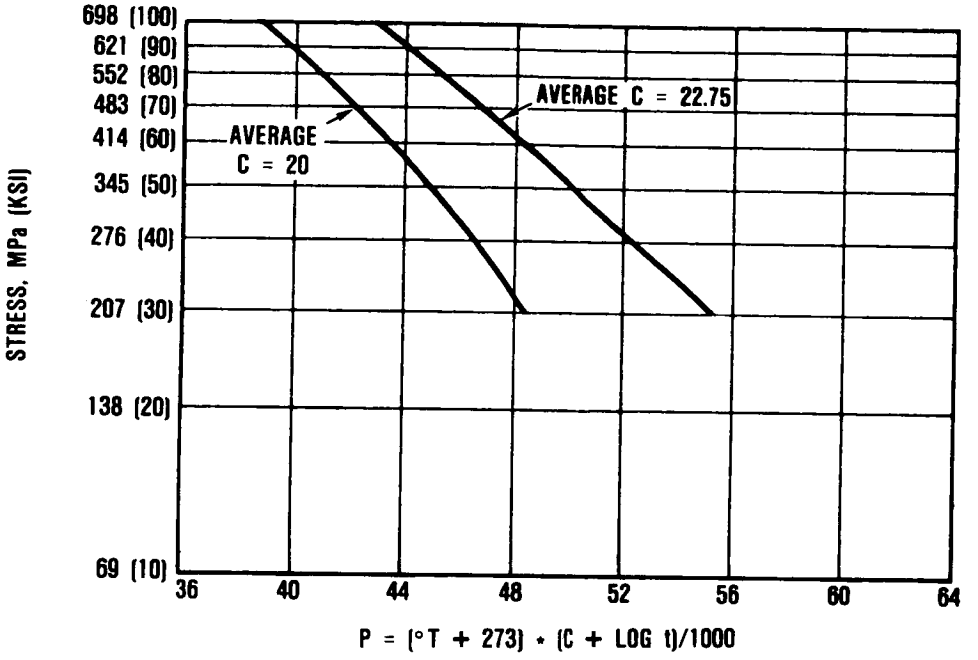

Figure 24. Stress-Rupture of MA6000 for All Stress Greater Than or Equal to 207 MPa (30 ksi).

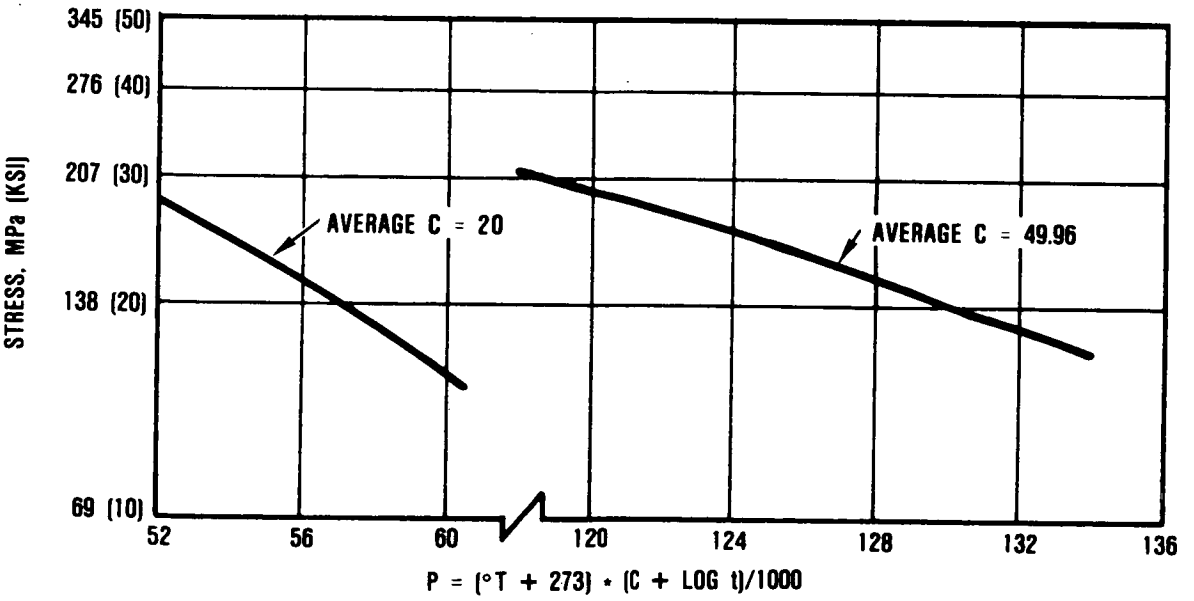

Figure 25. Stress Rupture of MA6000 for All Stresses Below 207 MPa (30 ksi).

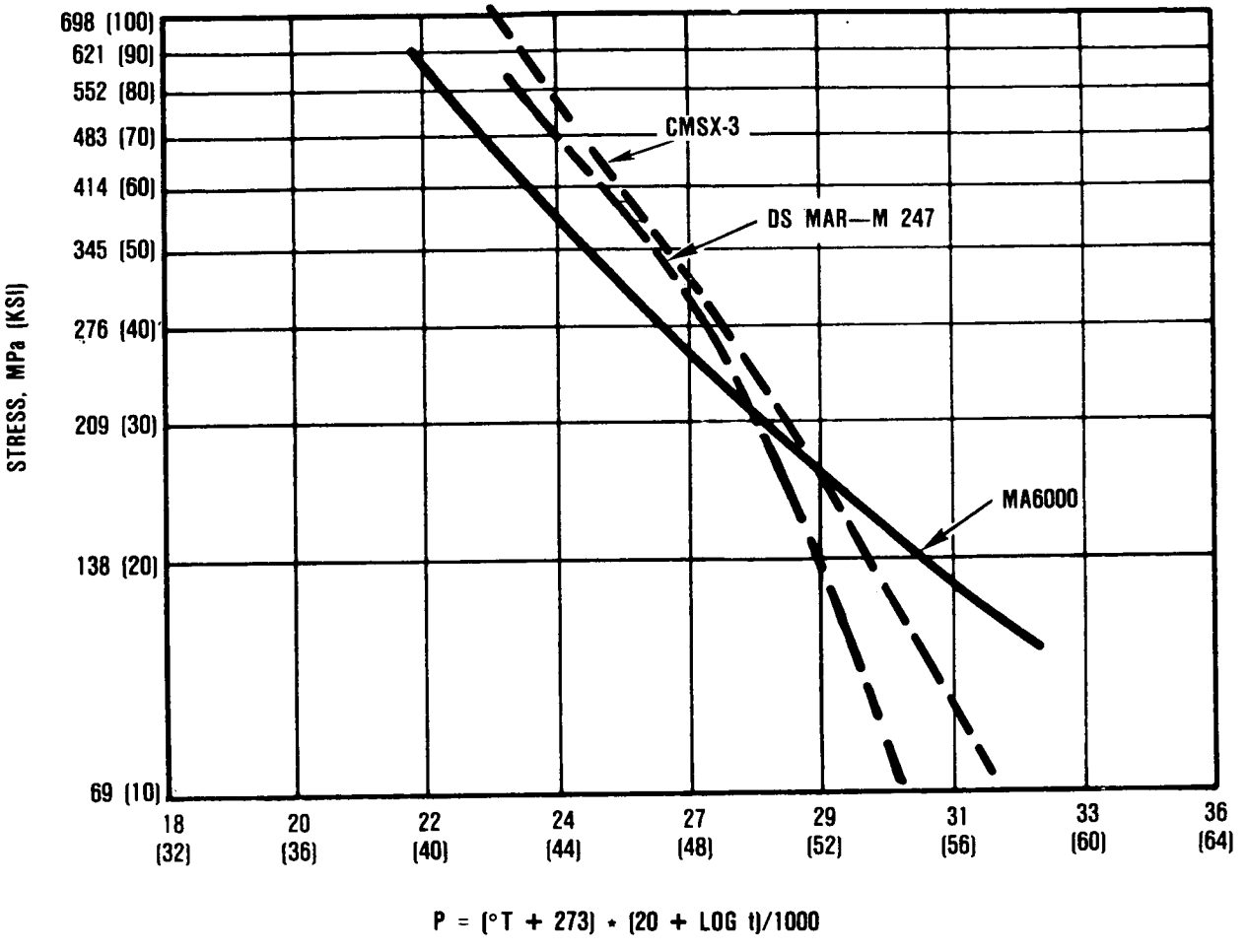

Figure 26. Stress-Rupture Data for MA6000 and DS MAR-M 247, Longitudinal Orientation.

TABLE 13. STRAIN-CONTROLLED LCF TEST RESULTS ON 0.025-INCH- - DIAMETER TEST SPECIMENS MACHINED FROM MA6000, LONGITUDINAL ORIENTATION, TEST AT 760C (1400F), A RATIO = ∞

Lot No. 1 Material			
Specimen Number	Total Strain Range, Percent	N_f Cycles	Remarks
6	1.60	154	
31	1.20	286	
73	1.00	806	
58	0.90	1,926	
28	0.80	2,473	
56	0.75	11,678	
39	0.70	--	Equipment malfunction
54	0.70	13,795	
60	0.65	43,017	Thread failure
36	0.60	53,000+	Test terminated
Lot No. 2 Material			
Specimen Number	Total Strain Range, percent	N_f Cycles	Remarks
197	1.40	286	Failed at radius
199	1.10	824	Failed at radius
221	0.95	1277	
223	0.85	1966	
228	0.79	3961	Failed at radius
234	0.73	9208	
235	0.71	4072	
256	0.69	6150	Failed at radius
261	0.76	3125	
263	0.67	5666	

A ratio = Alternating Stress/Mean Stress

Frequency = 0.33 Hz

TABLE 14. LOAD-CONTROLLED LCF TEST RESULTS ON 0.250-INCH-DIAMETER TEST SPECIMENS MACHINED FROM MA6000, TESTED AT 760 C (1400F), A RATIO = ∞

Lot No. 1 Material		
Specimen Number	Maximum Stress MPa (ksi)	N_f Cycles
5	1034 (150)	91
57	965 (140)	23
53	896 (130)	4,355
55	827 (120)	10,148
59	793 (115)	58,439
Lot No. 2 Material		
Specimen Number	Maximum Stress MPa (ksi)	N_f Cycles
196	1000 (145)	155
198	931 (135)	510
233	862 (125)	6,178
260	814 (118)	47,813
262	786 (114)	76,891

A Ratio = Alternating Stress/Mean Stress

Frequency = 1.0 Hz

TABLE 15. LCF TEST RESULTS ON 0.250-INCH-DIAMETER TEST SPECIMENS MACHINED FROM MA6000 (LOT NO. 2 MATERIAL) USING ECM METHODS SIMILAR TO METHODS USED TO PRODUCE BLADE SURFACES

Strain-Controlled					
Specimen Number	A Ratio	Temperature C (F)	Total Strain Range percent	N_f Cycles	Remarks
2A3	∞	760 (1400)	0.72	11,836	Failed out of gage section. Internal initiation
2A1	∞	760 (1400)	0.79	3125	Failed in gage
3B3	∞	760 (1400)	0.74	7307	Failed at radius - uniform section interface

Load-Controlled				
Specimen Number	A Ratio	Temperature C (F)	Maximum Stress MPa (ksi)	N_f Cycles
2A2	1.0	760 (1400)	128 (883)	2905
3A2	1.0	760 (1400)	119 (820)	9771
3A4	1.0	760 (1400)	123 (848)	17,660

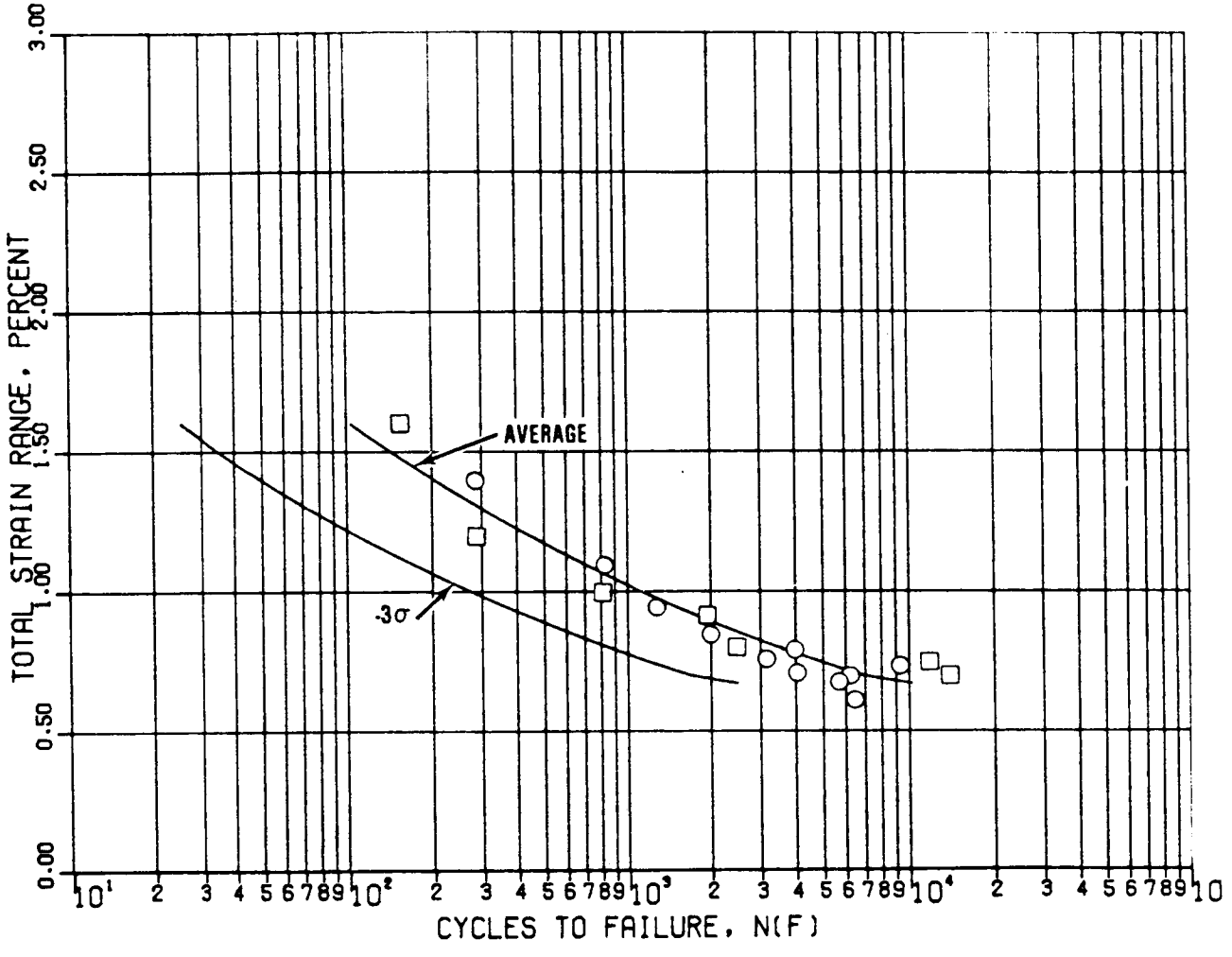

A = ∞
R = -1.0
K(T) = 1.0
FREQUENCY = 20 CPM
TEMPERATURE 760C (1400F)
NUMBER OF DATA POINTS = 17

□— LOT #1
○— LOT #2

Figure 27. Strain-Controlled Axial Low-Cycle Fatigue MA6000 Commercial Lots No. 1 and 2 Material, Longitudinal Orientation.

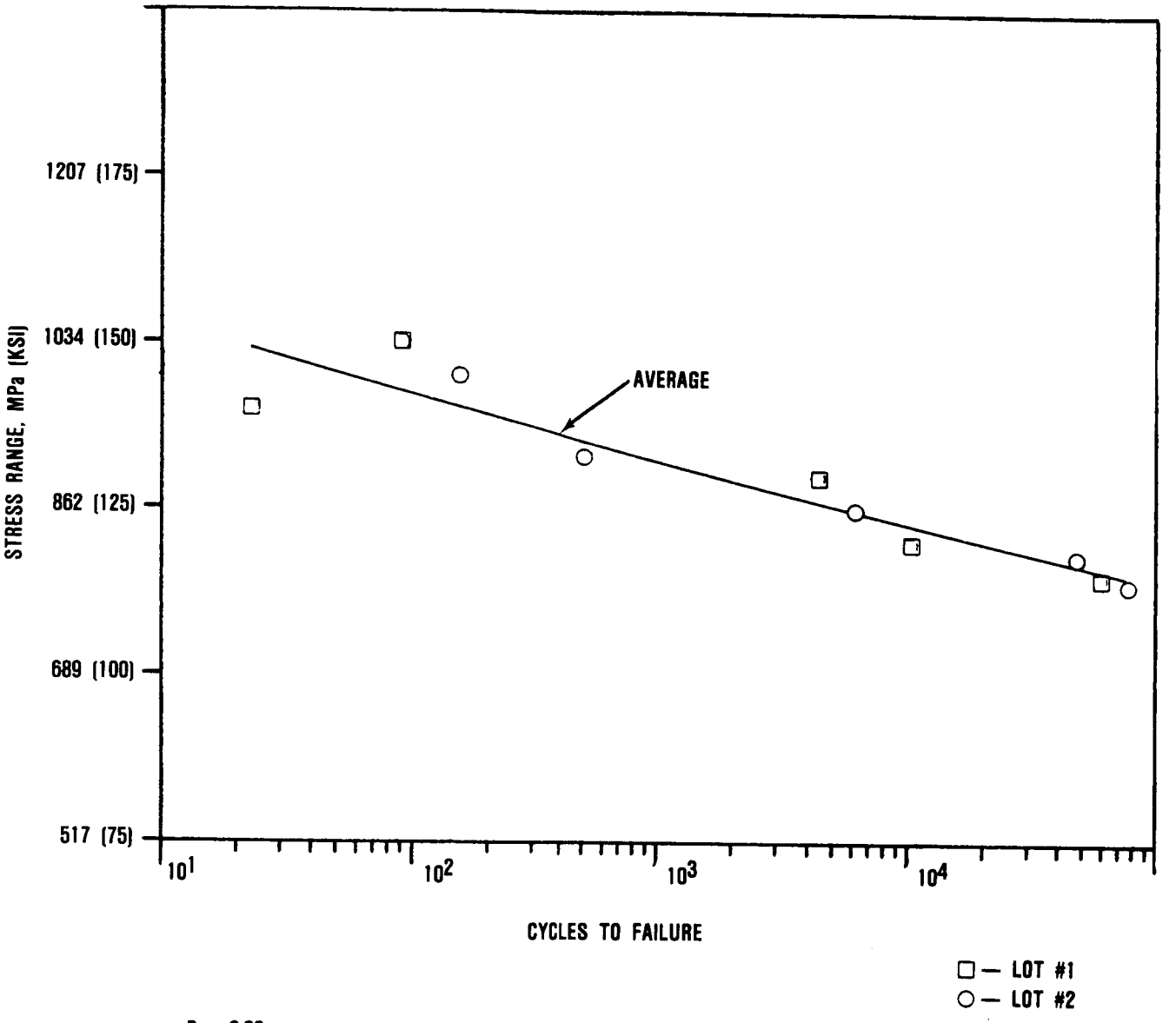

R = 0.00
K(T) = 1.00
FREQUENCY = 60 CPM
TEMPERATURE = 760C (1400F)
NUMBER OF DATA POINTS = 10
NUMBER OF RUNOUTS = 0

Figure 28. Load-Controlled Axial Low-Cycle Fatigue of MA6000 Commercial Lots No. 1 and 2, Longitudinal Orientation.

In general, these 760C (1400F) load- and strain-controlled tests compare very closely with data obtained from the conventionally prepared (by low stress grinding) test specimens. This finding is important, since no other definitive work has been conducted toward determining the LCF sensitivity of MA6000 to ECM-produced surfaces.

4.2.5 High-Cycle-Fatigue Testing

Axial-axial high-cycle-fatigue test results are given in Table 16. Optical 40X examination of the fractured surfaces of the failed 871C (1600F) HCF fatigue specimens showed all specimens to have internal failure initiation sites, with fatigue usually initiating as Stage I crystallographic fracture, and propagation as Stage II noncrystallographic fracture. Scanning electron microscopy (SEM) photos of the failed axial-axial high-cycle-fatigue specimens (Figure 29) show an internal Stage I origin surrounded by Stage II propagation.

Results of HCF tests of Lots No. 1 and 2 material at room temperature, 871C (1600F), and 982C (1800F) are presented in Table 17. The results show a slight improvement in fatigue life for Lot No. 2 versus Lot No. 1 with a 871C (1600F) runout stress of 538 MPa (78 ksi) versus 483 MPa (70 ksi) and an 982C (1800F) runout stress of 262 MPa (38 ksi) versus 228 MPa (33 ksi). The 871C (1600F) HCF data is presented in Figure 30 and compared to DS MAR-M 247 and CMSX-3 alloys.

4.3 Environmental Tests

Successful operation of MA6000 turbine blades depends on maintaining airfoil surface integrity under conditions of high temperature oxidation and intermediate temperature hot-corrosion (salt film accelerated oxidation). Consequently, burner rig testing was conducted to assess the environmental resistance of uncoated and over-

TABLE 16. MA6000 871C (1600F) HCF TEST RESULTS*

Specimen No.	σ_{ALT} MPa (ksi)	Cycles to Failure
614T-3	621 (90)	2.1×10^4
604T-10	483 (70)	1.97×10^5
604T-6	483 (70)	4.03×10^5
604T-5	448 (65)	7.51×10^4
604T-8	448 (65)	7.75×10^5
604T-4	414 (60)	3.56×10^6
604T-1	414 (60)	1.7×10^6
604T-8	379 (55)	10^7 Runout
604T-3	379 (55)	10^7 Runout
604M-7	379 (55)	1.7×10^6
604T-2	345 (50)	1.5×10^7 Runout
604M-6	276 (50)	10^7 Runout

*$A = \sigma_{ALT}/\sigma_{MEAN} = \infty$, $K_T = 1$, f = 60 cps

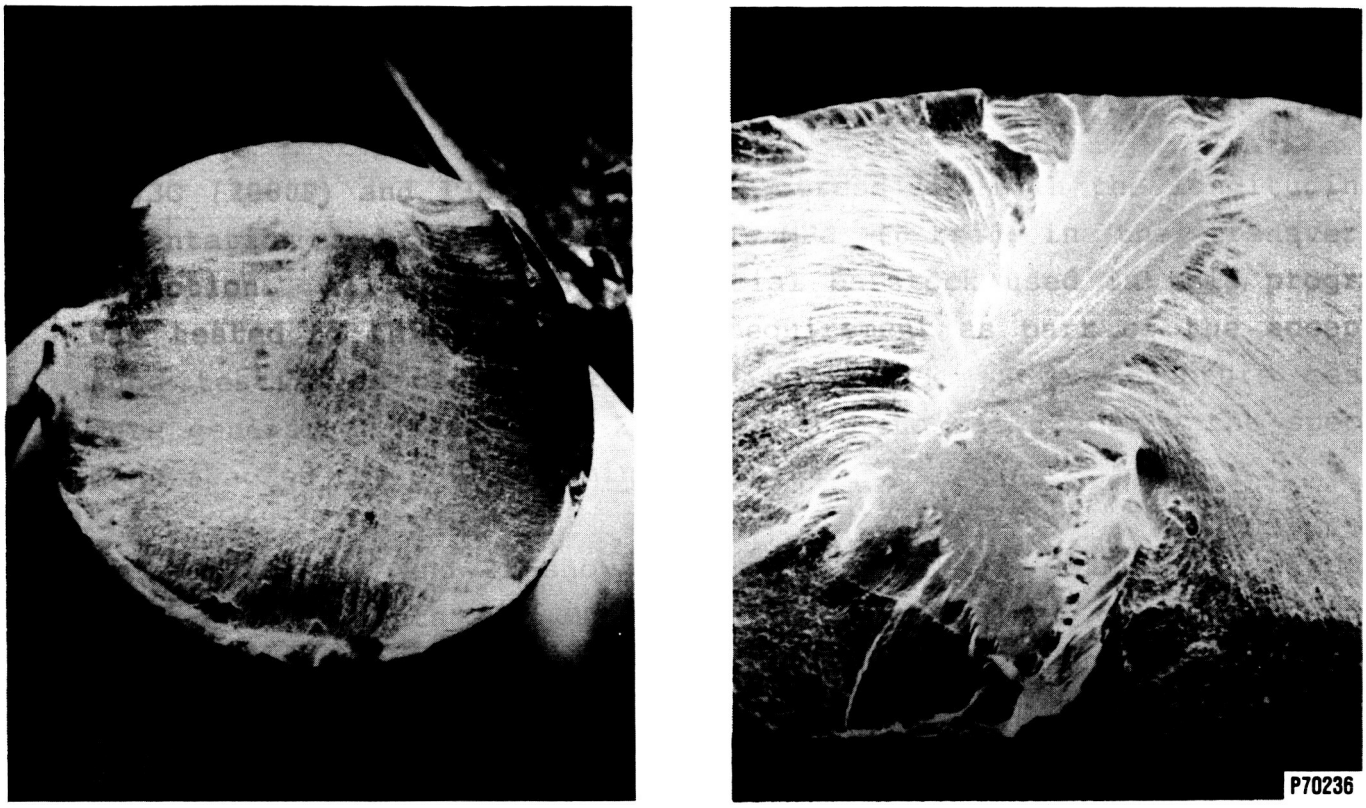

G5-000-46

Figure 29. SEM Photos of HCF Specimen 604T-5 Fracture Surface, Showing Internal Initiation Site and Small Stage I Type Fatigue Associated with Origin Surrounded by Stage II Type Fatigue.

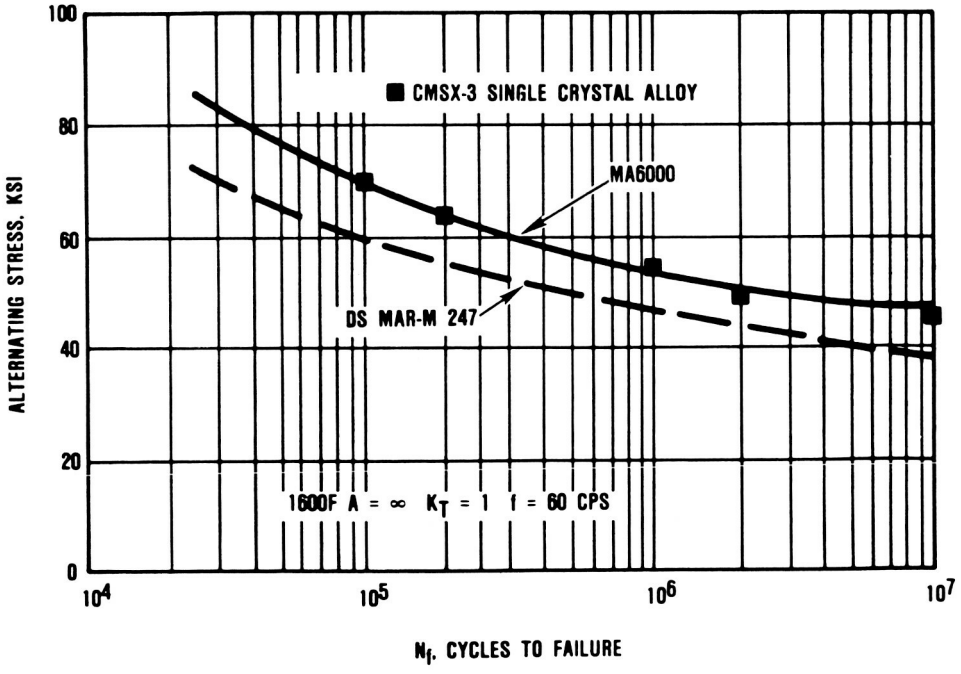

Figure 30. High-Cycle Fatigue Data for MA6000, DS MAR-M 247 and CMSX-3 at 1600F.

TABLE 17. HIGH-CYCLE-FATIGUE RESULTS FOR AXIAL-AXIAL TESTS OF UNCOATED 6.35 mm (0.250 INCH) DIAMETER SPECIMENS MACHINED FROM MA6000

Commercial Lot No. 1						
Specimen Number	A Ratio	Temperature C (F)	Stress MPa (ksi) Maximum	Alternating	Cycles to Failure	Remarks
3	∞	689 (100)	689 (100)	110,000		
63	∞	655 (95)	655 (95)	251,000		
65	∞	586 (85)	586 (85)	205,000		
67	∞	552 (80)	552 (80)	189,000		
69	∞	483 (70)	483 (70)	440,000		
38	∞	871 (1600)	483 (70)	483 (70)	140,000	
42	∞	871 (1600)	448 (65)	448 (65)	51,000	
46	∞	871 (1600)	414 (60)	414 (60)	538,000	
50	∞	871 (1600)	379 (55)	379 (55)	1,207,000	
83	∞	871 (1600)	365 (53)	365 (53)	1,650,000	
76	∞	871 (1600)	345 (50)	345 (50)	3,073,000	
64	∞	871 (1600)	345 (50)	345 (50)	8,338,000	
80	∞	871 (1600)	331 (48)	331 (48)	2,603,000	
73	∞	871 (1600)	310 (45)	310 (45)	10,000,000+	Runout - test terminated
68	∞	871 (1600)	310 (45)	310 (45)	10,000,000+	Runout - test terminated
82	0.95	871 (1600)	689 (100)	338 (49)	91,000	
70	0.95	871 (1600)	655 (95)	317 (46)	194,000	
66	0.95	871 (1600)	621 (90)	303 (44)	470,000	
40	0.95	871 (1600)	586 (85)	283 (41)	616,000	
44	0.95	871 (1600)	552 (80)	269 (39)	746,000	
48	0.95	871 (1600)	517 (75)	255 (37)	2,847,000	
84	0.95	871 (1600)	517 (75)	255 (37)	3,462,000	
78	0.95	871 (1600)	503 (73)	241 (35)	10,000,000+	Runout - test terminated
52	0.95	871 (1600)	483 (70)	234 (34)	10,000,000+	Runout - test terminated
74	0.95	871 (1600)	483 (70)	234 (34)	10,000,000+	Runout - test terminated
41	∞	982 (1800)	345 (50)	345 (50)	12,000	
43	∞	982 (1800)	310 (45)	310 (45)	11,000	
45	∞	982 (1800)	276 (40)	276 (40)	181,000	
81	∞	982 (1800)	262 (38)	262 (38)	8,150,000	
47	∞	982 (1800)	241 (35)	241 (35)	--	Equipment malfunction
49	∞	982 (1800)	241 (35)	241 (35)	2,319,000	
77	∞	982 (1800)	241 (35)	241 (35)	4,683,000	
79	∞	982 (1800)	228 (33)	228 (33)	10,000,000+	Runout - test terminated
51	∞	982 (1800)	207 (30)	207 (30)	10,000,000+	Runout - test terminated
75	∞	982 (1800)	207 (30)	207 (30)	10,000,000+	Runout - test terminated

A Ratio = Alternating Stress/Mean Stress

Frequency = 60 Hz

TABLE 17. HIGH-CYCLE-FATIGUE RESULTS FOR AXIAL-AXIAL TESTS OF UNCOATED 6.35 mm (0.250 INCH) DIAMETER SPECIMENS MACHINED FROM MA6000 (Contd)

Commercial Lot No. 2						
Specimen Number	A Ratio	Temperature C (F)	Stress MPa (ksi) Maximum	Alternating	Cycles to Failure	Remarks
264	∞	448 (65)	448 (65)	334,000		
266	∞	434 (63)	434 (60)	1,773,000		
236	∞	414 (60)	414 (60)	1,437,000		
240	∞	400 (58)	400 (50)	840,000		
238	∞	379 (55)	379 (55)	10,000,000+	Runout - test terminated	
237	∞	871 (1600)	517 (75)	517 (75)	59,000	
292	∞	871 (1600)	434 (63)	434 (63)	206,000	
265	∞	871 (1600)	400 (58)	400 (58)	95,000	
288	∞	871 (1600)	393 (57)	393 (57)	1,333,000	
276	∞	871 (1600)	372 (54)	372 (54)	248,000	
268	∞	871 (1600)	359 (52)	359 (52)	615,000	
294	∞	871 (1600)	352 (51)	352 (51)	3,734,000	
244	∞	871 (1600)	345 (50)	345 (50)	8,106,000	
248	∞	871 (1600)	338 (49)	338 (49)	3,574,000	
272	∞	871 (1600)	324 (47)	324 (47)	10,000,000+	Runout - test terminated
239	0.95	871 (1600)	710 (103)	345 (50)	149,000	
246	0.95	871 (1600)	676 (98)	331 (48)	209,000	
250	0.95	871 (1600)	641 (93)	310 (45)	441,000	
293	0.95	871 (1600)	621 (90)	303 (44)	1,020,000	
267	0.95	871 (1600)	606 (88)	296 (43)	1,232,000	
290	0.95	871 (1600)	586 (85)	283 (41)	1,378,000	
274	0.95	871 (1600)	572 (83)	276 (40)	5,319,000	
284	0.95	871 (1600)	552 (80)	269 (39)	710,000	
295	0.95	871 (1600)	545 (79)	269 (39)	1,887,000	
278	0.95	871 (1600)	538 (78)	262 (38)	10,000,000+	
273	∞	982 (1800)	345 (50)	345 (50)	585,400	
245	∞	982 (1800)	331 (48)	331 (48)	1,143,900	
291	∞	982 (1800)	324 (47)	324 (47)	48,000	
279	∞	982 (1800)	317 (46)	317 (46)	1,931,700	
275	∞	982 (1800)	310 (45)	310 (45)	1,211,800	
247	∞	982 (1800)	296 (43)	296 (43)	5,080,700	
289	∞	982 (1800)	290 (42)	290 (42)	4,511,800	
251	∞	982 (1800)	269 (39)	269 (39)	1,453,700	
277	∞	982 (1800)	262 (38)	262 (38)	10,081,900+	Runout*
249	∞	982 (1800)	255 (37)	255 (37)	10,920,800+	Runout

*Specimen 277 was broken after runout, while removing from the adapters.

A Ratio = Alternating Stress/Mean Stress

Frequency = 60 Hz

NiCrAlY and CoCrAlY overlay coatings were selected to protect the MA6000 alloy based on diffusional stability and environmental resistance requirements. Lower cost diffusion aluminide coatings, which are extensively used to protect conventional vacuum-cast superalloys, are not viable on oxide dispersion superalloys such as MA6000, i.e., formation of a diffusion aluminide coating results in extensive Kirkendahl and/or gas porosity (from interstitial nitrogen introduced during mechanical alloying) at the coating - ODS alloy interface region. Diffusionally stable overlay coatings can avoid this limitation. NiCrAlY coatings have the best oxidation resistance and diffusional stability on nickel base superalloys. CoCrAlY coatings are the most resistant coatings from a hot-corrosion standpoint. Commercial Ni-22.2Cr-10.9Al-0.4Y and Co-25.6Cr-89Al-0.2Y overlay coatings were selected for evaluation and applied by the electron beam evaporation - physical vapor deposition (EB-PVD) process by Temescal in Berkeley, California. Nominal coating thickness was 125μm (0.005 inch).

Uncoated and coated burner rig oxidation tests were conducted at 1093C (2000F) and 1149C (2100F), respectively. The 2000F tests results are provided in Table 18. They indicate that MA6000 has uncoated oxidation resistance that is superior to IN-792 and IN-738, but less than that of IN-713 and MAR-M 247. This result is primarily attributed to aluminum contents of the respective alloys, i.e.,

Material	Aluminum Content (Weight Percent)
IN-713	6.0
MAR-M 247	5.5
MA6000	4.5
IN-738	3.4
IN-792	3.1

TABLE 18. 1093C (2000F) OXIDATION BURNER RIG METALLOGRAPHIC RESULTS

Alloy	Time in Test (hr)	Max. Depth of Penetration m (Mils/Side)
MA6000	400	598 (23.9)
MA6000	400	555 (22.2)
IN-792	275	520 (20.8)
IN-738	275	570 (22.8)
IN-713	400	210 (8.4)
IN-713	400	182 (7.3)
MAR-M 247	400	305 (12.2)

High aluminum content superalloys, which form protective alumina scales, have superior uncoated oxidation resistance.

During high-temperature oxidation, aluminum and chromium diffuse to the surface from the adjacent alloy. Vacancies produced by extraction of aluminum and chromium atoms (to produce a protective oxide scale) and release of interstitially dissolved gases result in a porous diffusion affected layer of MA6000 adjacent to the surface (Figure 31)). Comparative data for IN-713 is also provided in this figure. It is obvious that the oxidation-affected layer in the MA6000 is significantly larger. Consequently, diffusionally stable oxidation resistant coatings are necessary to retain thin section mechanical properties of the MA6000 alloy.

To assess the viability of commercially available oxidation-resistant NiCrAlY and CoCrAlY overlay coatings, a cyclic oxidation test was conducted at 1149C (2100F). The coatings were applied to MA6000, MAR-M 247, and IN-792. This 1149C cyclic (60 minutes hot, 3 minutes forced-air cooled) burner rig testing was concluded after 502 hours with all specimens exhibiting substrate attack, which indicated failure. For each specimen, Table 19 gives the hours to failure, the original coating thicknesses, and the coating life in terms of hours per 25μm (mil) of coating. The results show that NiCrAlY coatings are definitely superior to CoCrAlY in high-temperature oxidation. The three alloys exhibited equivalent lives when coated with the same coating system. Figure 32 shows the burner rig specimens after testing.

Microstructural analysis indicated that both coatings improved the oxidation resistance and minimized (but did not eliminate) the formation of a porous diffusion-affected zone in the MA6000. Examination of the CoCrAlY-coated MA6000 specimen (adjacent to a failure location) indicated that the porous substrate layer was only about 50μm thick after 153 hours of exposure at 1149C (Figure 33). This

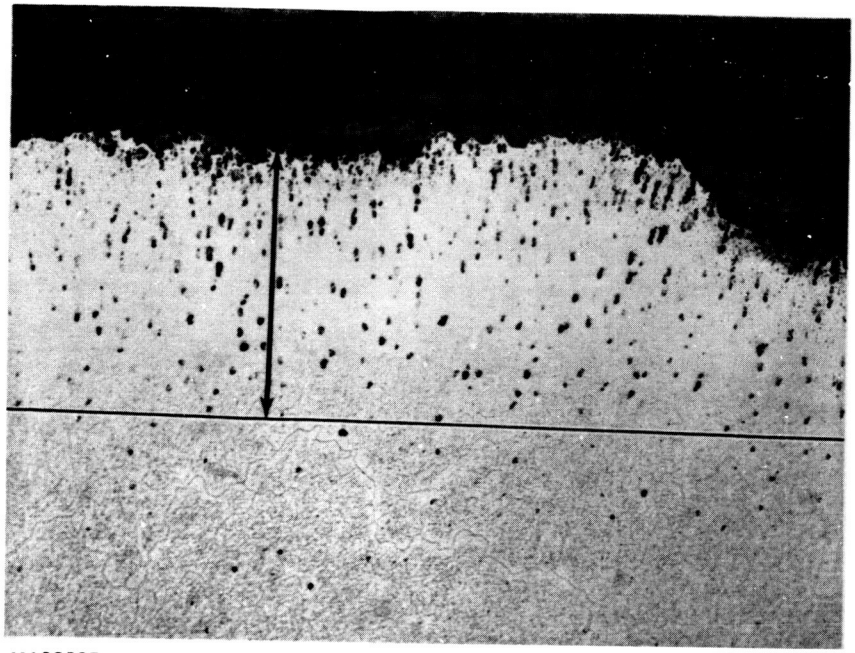

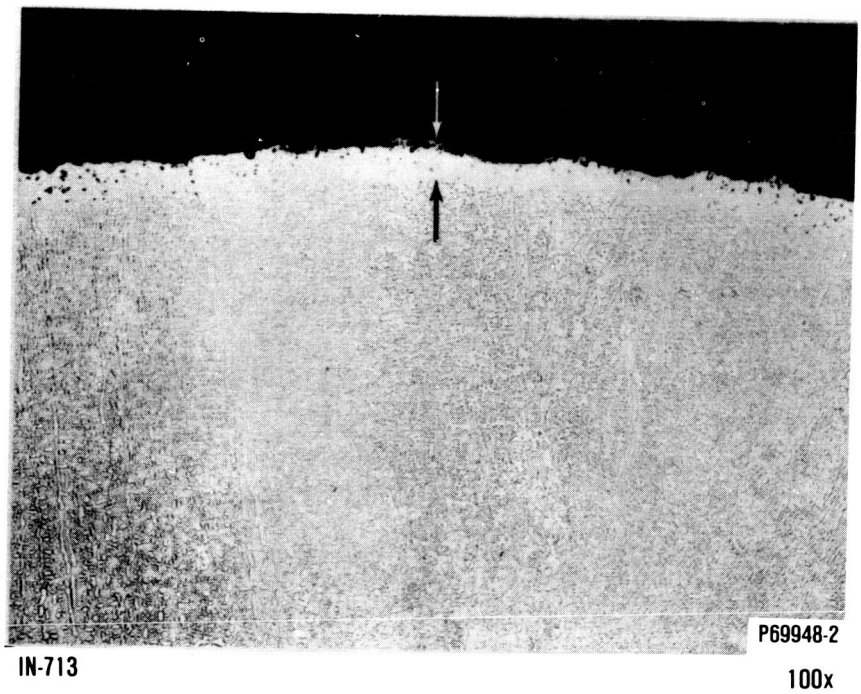

Figure 31. Microstructures of Transverse Section through the Hot Zone of MA6000 and IN-713 Burner Rig Specimens Showing Area Included in Depth of Penetration Measurements.

TABLE 19. OXIDATION BURNER RIG TESTING.

2100F Cyclic Oxidation (60 minutes hot - 3 minutes forced air-cooled)				
Alloy	Coating	Hours to Failure*	Coating Thickness m (mils)	Coating Life (Hours/25 μm)
MA6000	NiCrAlY	502	113 (4.5)	111
MA6000	CoCrAlY	153	143 (5.7)	26.8
MAR-M 247	NiCrAlY	502	103 (4.1)	122
MAR-M 247	CoCrAlY	204	163 (6.5)	31.4
IN-792	NiCrAlY	502	110 (4.4)	114
IN-792	CoCrAlY	129	130 (5.2)	24.8

*Failure is defined as the initiation of substrate attack.

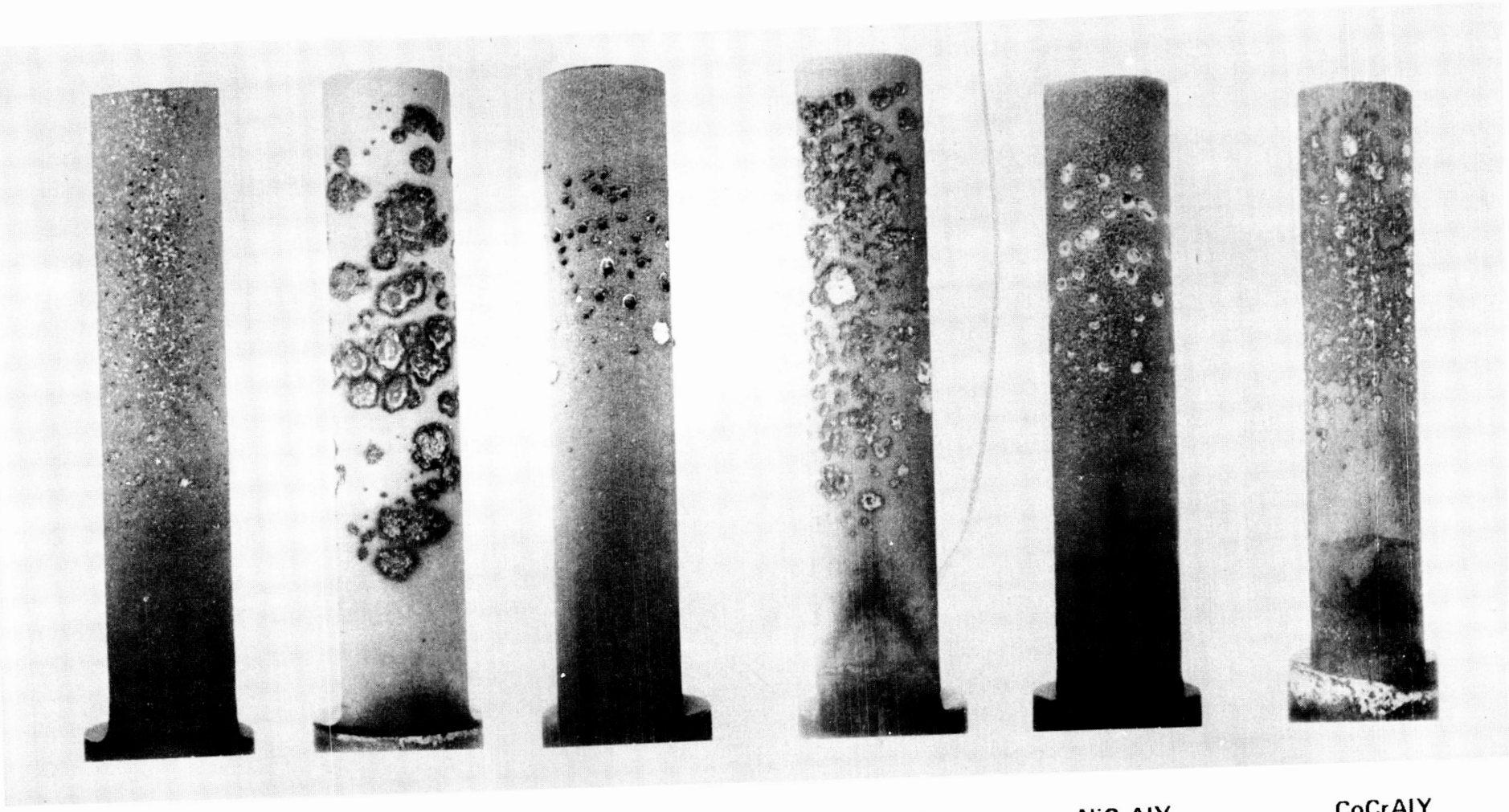

Figure 32. Oxidation Test Specimens at Failure Times Indicated. Test Conditions: 60 Minutes at 1149C (2100F) - 3 Minutes Forced Air-Cooled. (Mag: 2X)

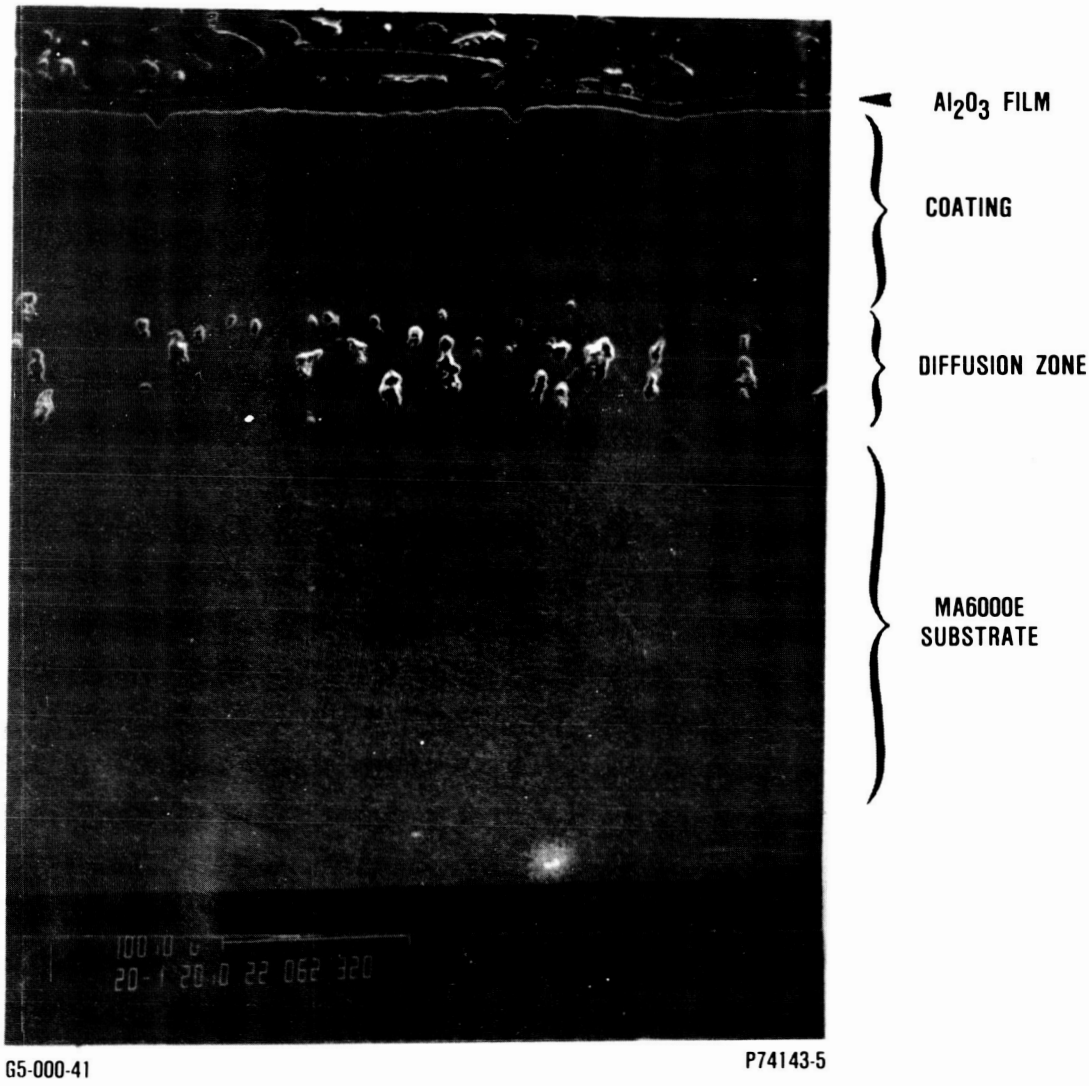

Figure 33. CoCrAlY/MA6000 Oxidation Specimen after 153 Hours of Testing, SEM Secondary Electron Image.

is an improvement over the 600μm-thick zone observed in the uncoated MA6000 tested at 1093C for 400 hours.

NiCrAlY coatings exhibited further improvements in both oxidation resistance and diffusional stability on the MA6000 alloy (Figure 34). The extent of the porous MA6000 layer adjacent to the coating interface was approximately 50μm-thick after 502 hours. Also, the porosity did not appear to be interconnected.

A localized pit failure in the NiCrAlY coating is shown in Figure 35, which shows that the protective alumina scale has reformed at the base of the pit. A slight increase in microporosity was observed in the MA6000 at the base of the oxide pit. Diffusion of aluminum from the MA6000 to reform the protective alumina scale is probably associated with the increase in microporosity.

Hot corrosion burner rig tests were conducted on MA6000, IN-792, and DS MAR-M 247 NiCrAlY and CoCrAlY EB-PVD coated specimens. At test conditions of cyclic temperatues (27 min at 927C/3 minutes forced air cool) and 20 ppm salt, after 475 hours of testing, only MA6000E/NiCrAlY and IN-792/NiCrAlY specimens failed. Test results are provided in Table 20. Figure 36 shows the specimens at the conclusion of the test. As anticipated, CoCrAlY was superior to NiCrAlY in a hot-corrosion environment.

Metallographic results confirmed the visual observations showing the CoCrAlY coating superior to NiCrAlY in a hot-corrosion environment. The CoCrAlY specimens showed little coating degradation with a high volume fraction of β(CoAl) still present in the coating. Examination of Co, Cr, and Al X-ray maps of the CoCrAlY/MA6000 specimen (Figure 37) showed extensive Co but little Cr diffusion into the substrate and a continuous Al_2O_3 film on the coating. As in the oxidation CoCrAlY coated specimen, substantial irregular void formation was observed in the diffusion-affected MA6000.

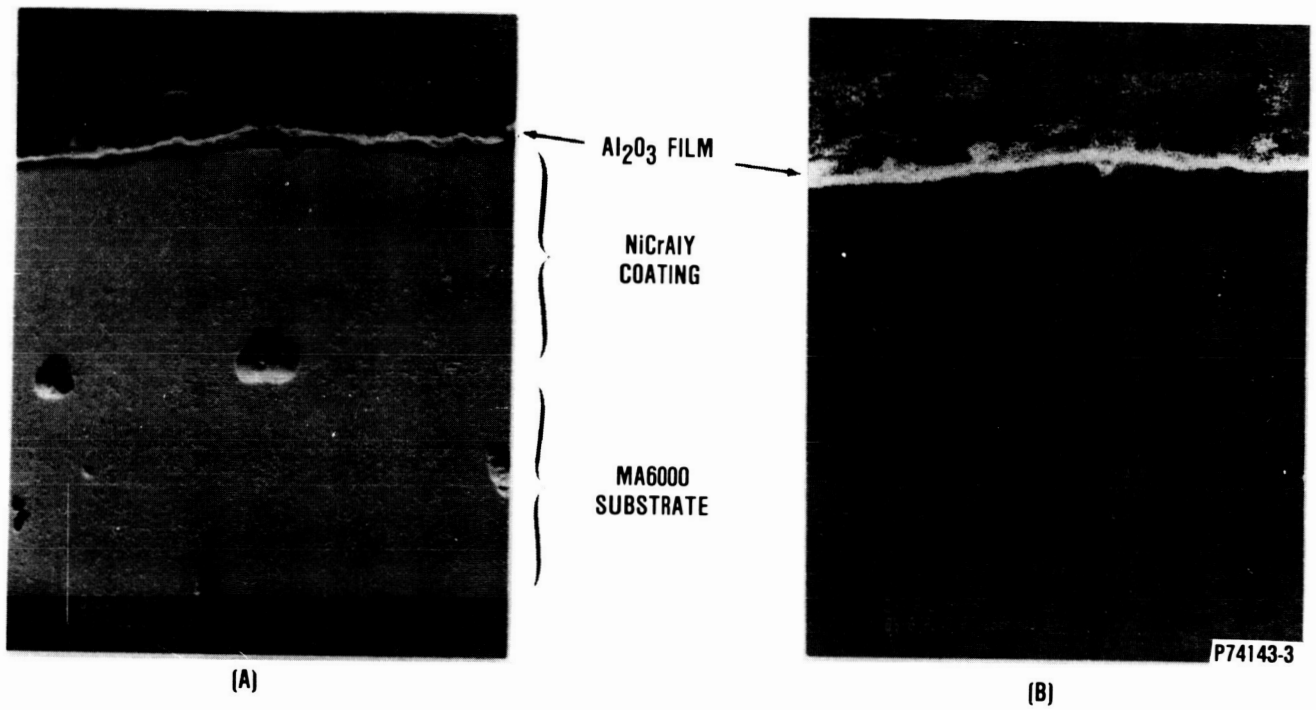

Figure 34. NiCrAlY/MA6000 Specimen after 502 Hours of Cyclic Oxidation Testing at 2100F. (A) SEM Secondary Electron Image, (B) Al X-Ray Map.

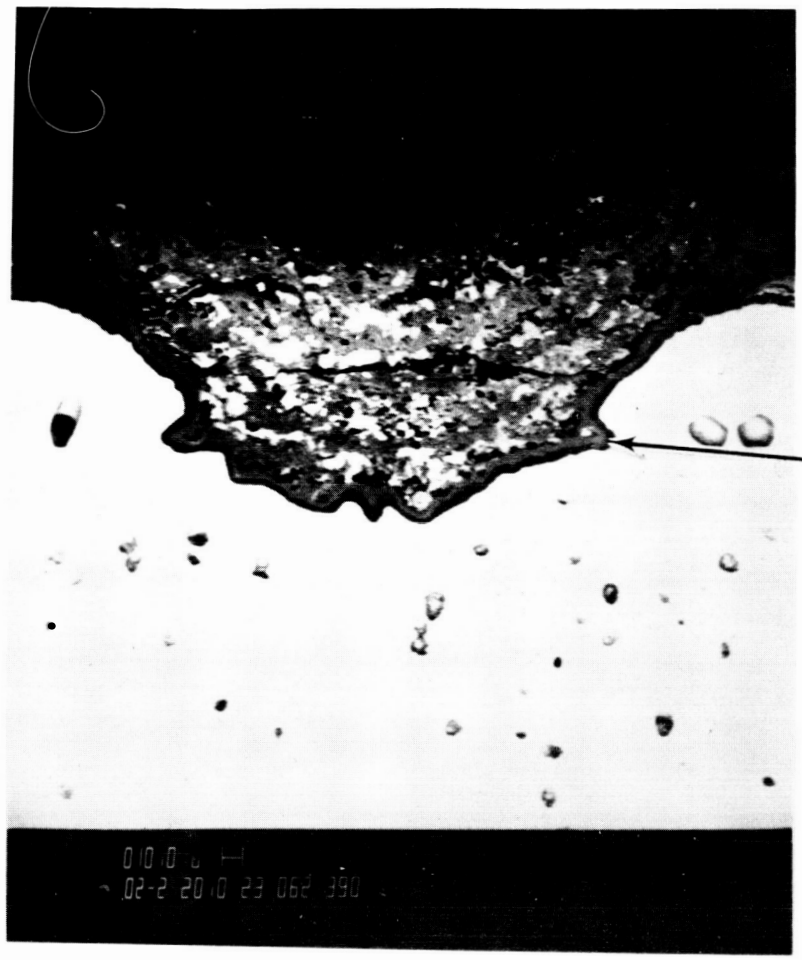

P74143-4

G5-000-52

Figure 35. NiCrAlY/MA6000 Oxidation Specimen after 502 Hours of Testing. Local Coating Failure Site Showing Reformation of Al_2O_3 Film.

TABLE 20. HOT-CORROSION BURNER RIG TEST RESULTS

927C (1700F) Cyclic Hot Corrosion (20 PPM SALT - 27 Min Hot - 3 Min Air-Cooled)		
Alloy	Coating	Time to Failure (hrs)
MA6000	NiCrAlY	475
MA6000	CoCrAlY	No Failure - 475*
MAR-M 247	NiCrAlY	No Failure - 475*
MAR-M 247	CoCrAlY	No Failure - 475*
IN-792	NiCrAlY	475
IN-792	CoCrAlY	No Failure - 475*
*Test Terminated After 475 Hours		

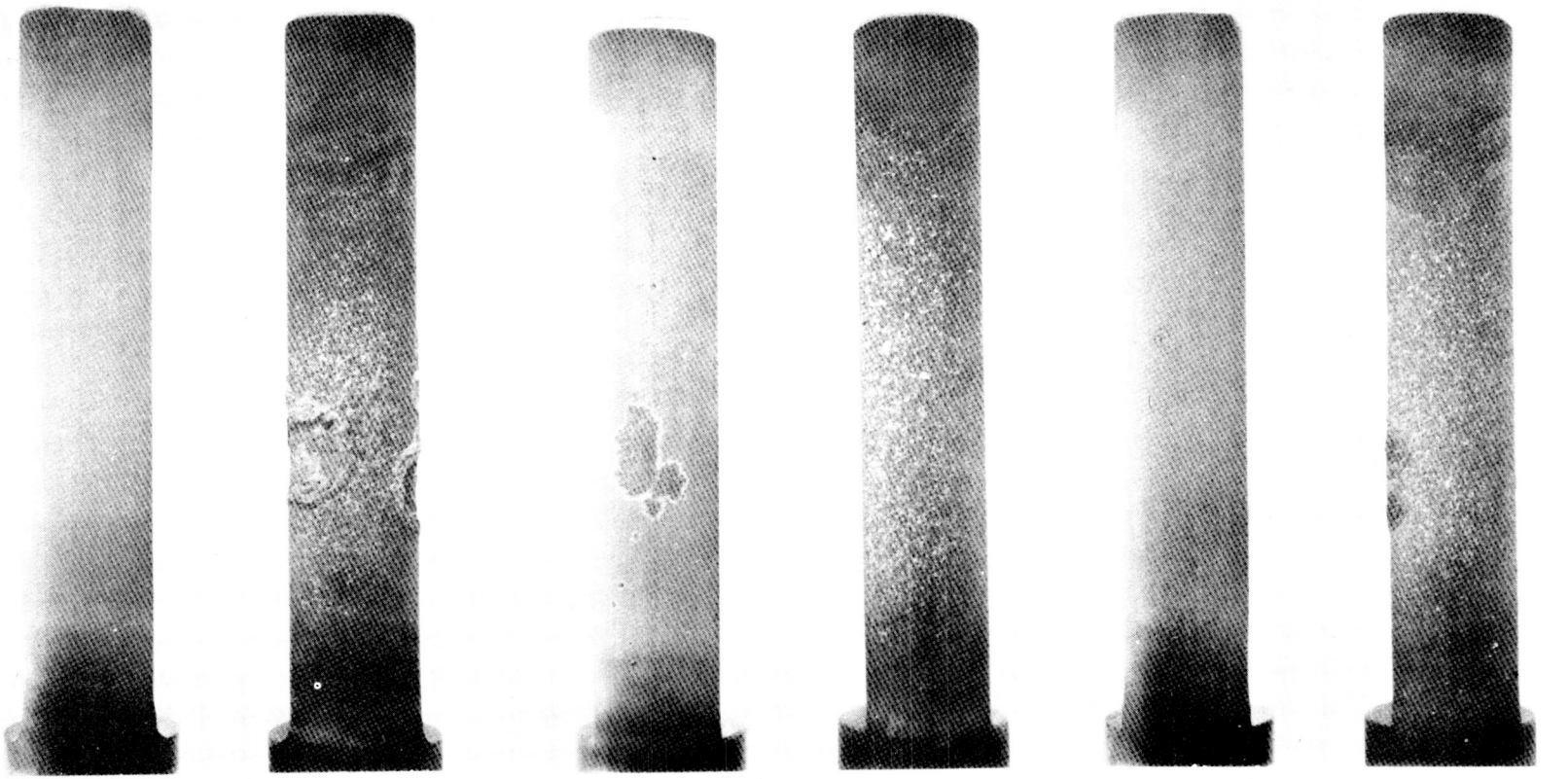

Figure 36. Hot Corrosion Specimen after 475 Hours of Cyclic Burner Rig Testing. Test Cycle: 27 Minutes at 927C -3 Minutes Force Air Cool, 20 ppm Salt. (Mag: 2X).

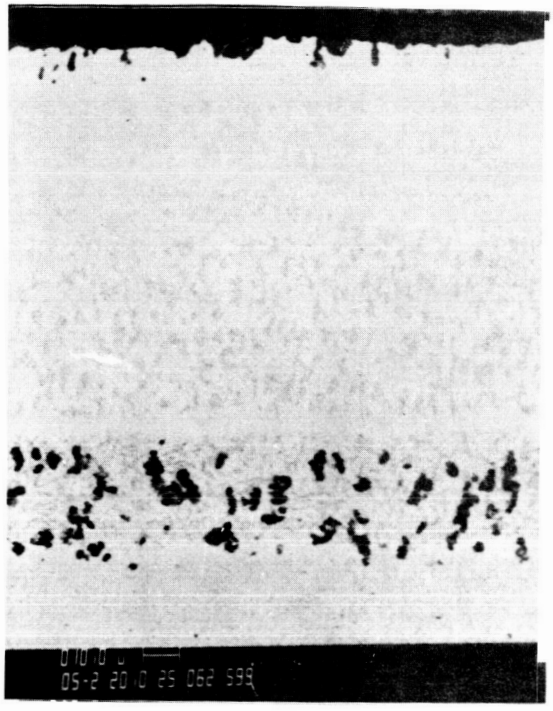

BSE IMAGE

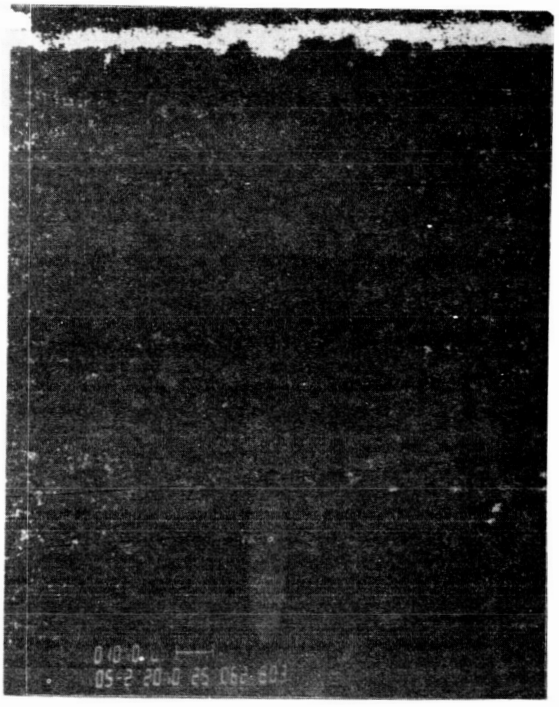

Al X-RAY MAP

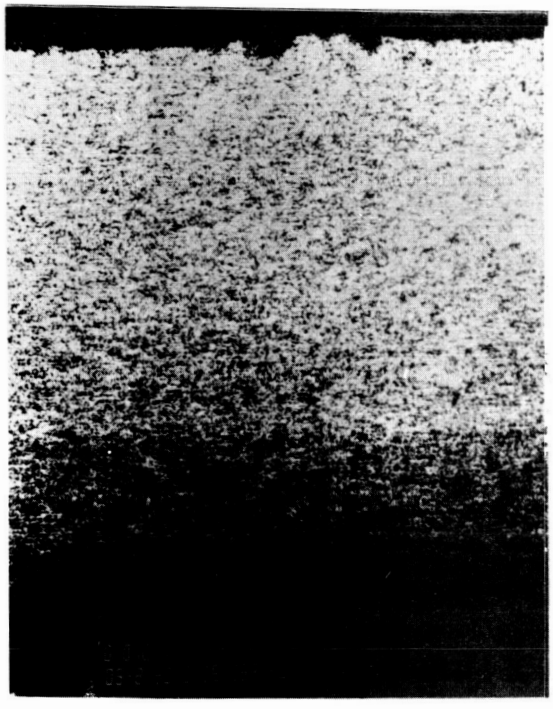

Co X-RAY MAP

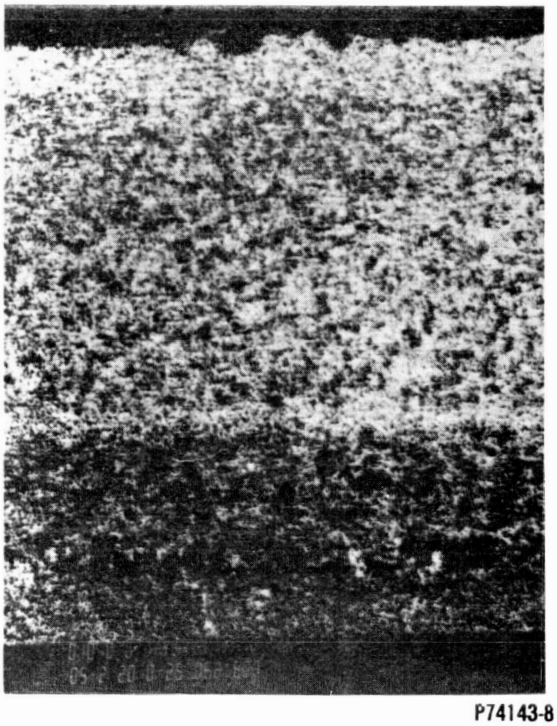

Cr X-RAY MAP

P74143-8

G5-000-44

Figure 37. CoCrAlY/MA6000 Hot Corrosion Specimen after 475 Hours of Hot-Corrosion Testing at 927C.

The NiCrAlY coating showed extensive degradation, including absence of the high Al beta phase. In localized areas, the coating was completely consumed. Examination of Cr and Al X-ray maps of the NiCrAlY/MA6000 specimen (Figure 38) shows a continuous Al_2O_3 and Cr_2O_3 film on the coating. Some void formation was observed at the coating/substrate interface. Unlike the NiCrAlY coating oxidation specimen, local coating failure did not heat itself by forming a protective Al_2O_3 film.

Based on these tests results, MA6000 can be effectively coated, provided that diffusional stability with the substrate is maintained. NiCrAlY coatings are recommended, based on oxidation resistance and diffusional stability considerations.

If hot corrosion conditions are anticipated, it is recommended that a CoCrAlY coating be applied on top of a thin NiCrAlY coating. This duplex coating will permit both diffusional stability and hot-corrosion resistance to be maintained.

4.4 Physical Properties

4.4.1 Thermal Expansion and Thermal Conductivity

The results of thermal expansion and thermal conductivity measurements of MA6000 are presented in Figures 39 and 40, and Tables 21 and 22. In general, the results are lower than those published by INCO.

Density measurements were also conducted by Southern Research on eight samples of Lot No. 2 material. The 0.292 lb/in^3 average density obtained from these samples compares very closely with the published INCO value.

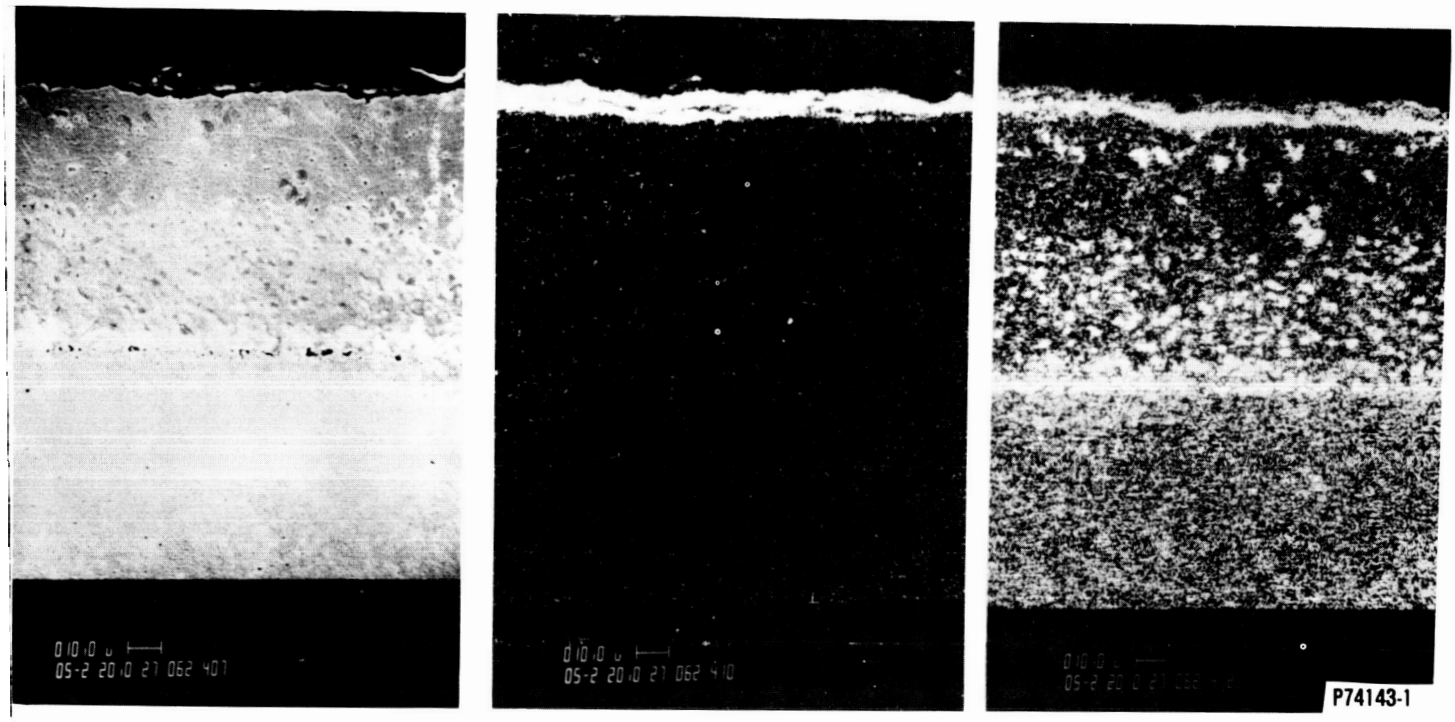

Figure 38. NiCrAlY/MA6000 Hot-Corrosion Specimen after 475 Hours of Hot Corrosion Testing at 927C.

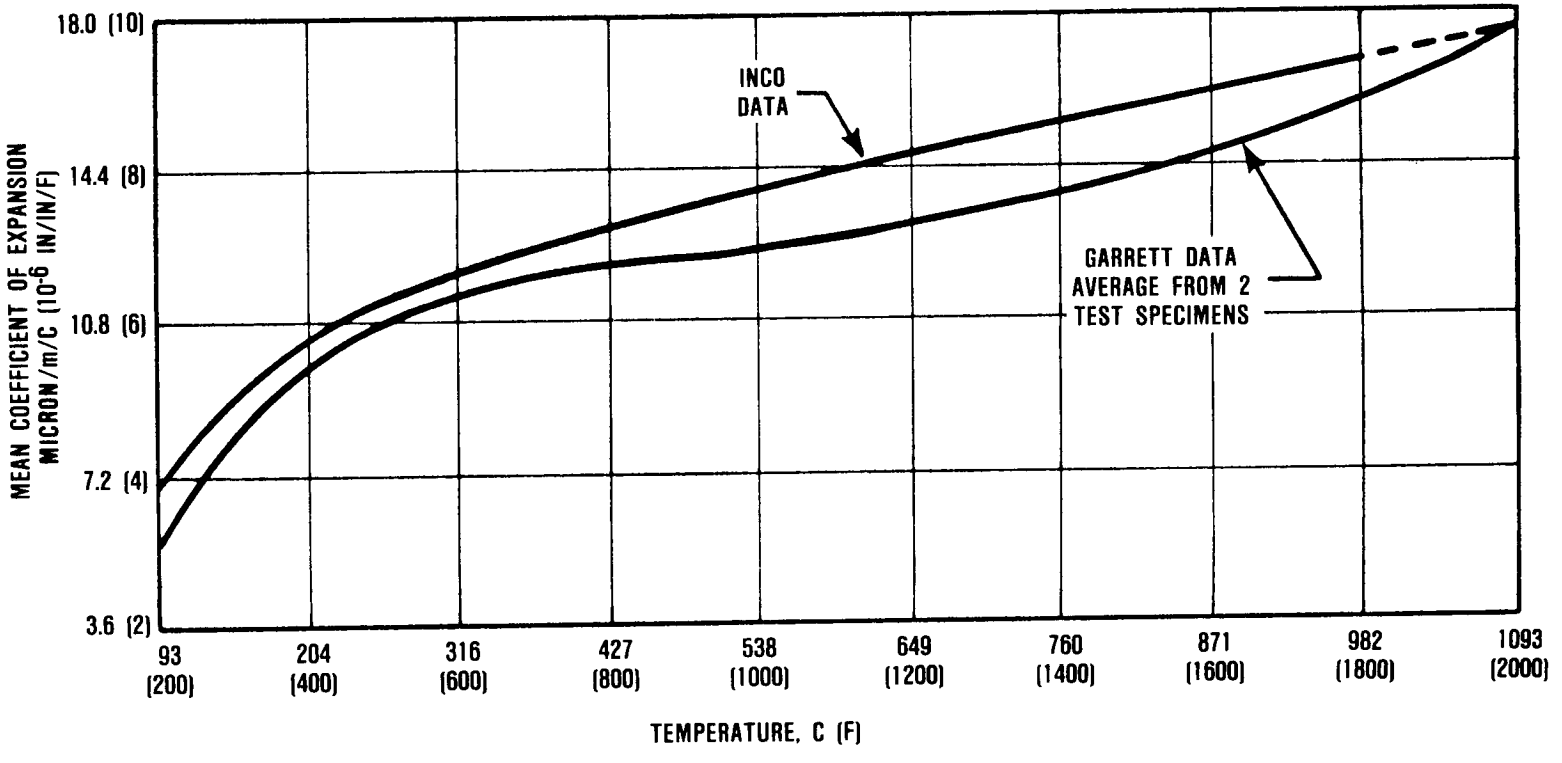

Figure 39. Mean Coefficient of Thermal Expansion of MA6000 from Commercial Lot No. 2 (Wiggin Produced Material) Compared with Published INCO Data. Garrett Data Obtained from Tests Conducted by Southern Research Institute.

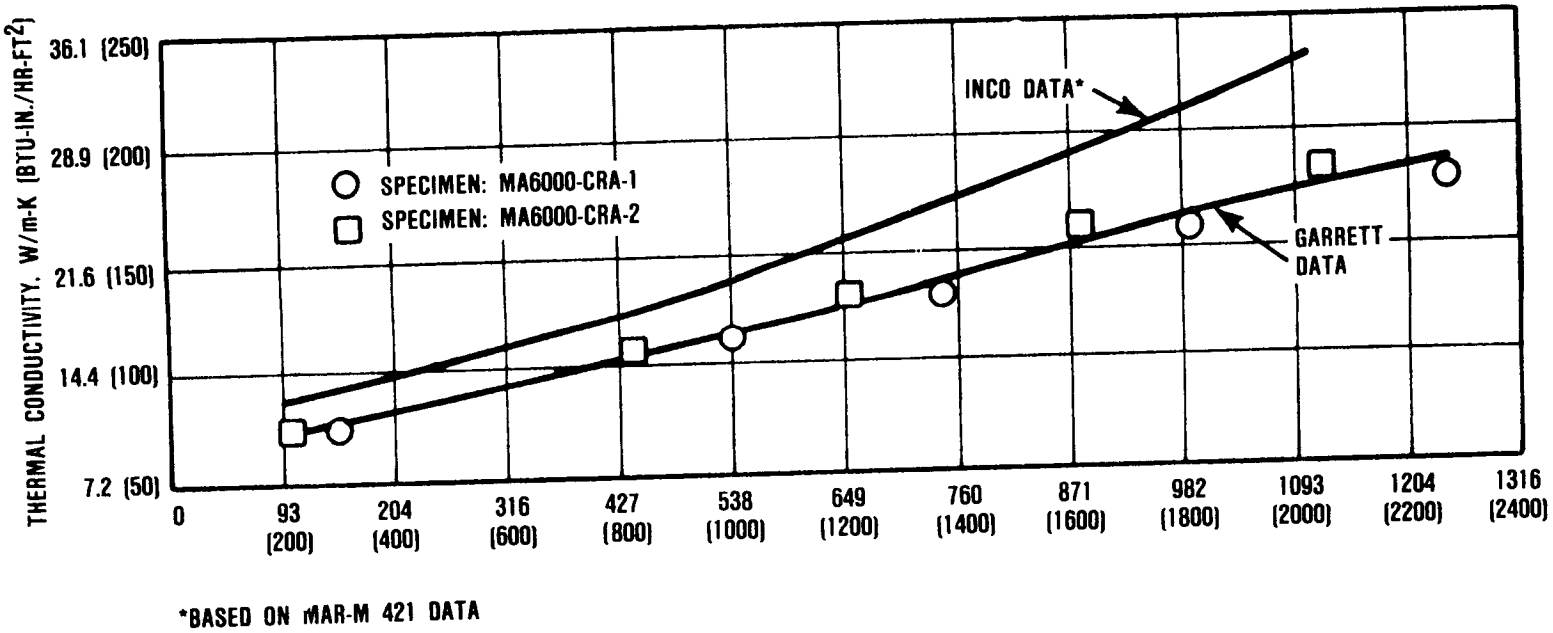

Figure 40. Thermal Conductivity of MA6000 Alloy from Commercial Lot No. 2 (Wiggin Produced Material) Compared with Published INCO Data. Garrett Data Obtained from Tests Conducted by Southern Research.

TABLE 21. COMPARISON OF THERMAL EXPANSION OF MA6000E ALLOY INCO MAP DATA VERSUS WIGGIN LOT NO. 2/SOUTHERN RESEARCH DATA.

Test Temperature F	Mean Coefficient of Expansion 10^{-6} In/In/F	
	INCO MAP	Garrett
70	-	-
200	3.82	3.00
400	5.65	5.50
600	6.58	6.33
800	7.19	6.63
1000	7.65	6.90
1200	8.03	7.23
1400	8.55	7.57
1600	8.89	8.25
1800	9.30*	8.89
2000	9.70*	9.60

*Extrapolated by INCO MAP. Data from INCO MAP Technical Bulletin "INCO MAP Mechanically Alloyed Products"

C-2

TABLE 22. COMPARISON OF THERMAL CONDUCTIVITY OF MA6000E ALLOY INCO MAP DATA VERSUS WIGGIN LOT NO. 2/SOUTHERN RESEARCH DATA.

Test Temperature F	Thermal Conductivity Btu-In/Hr-Ft^2-F	
	INCO MAP	Garrett
200	85*	75
400	95*	82
600	105	92
800	121	107
1000	137	111
1200	154	132
1400	170	139
1600	187	150
1800	207	163
2000	229	174
2200	--	182

*Extrapolated by INCO MAP, based on MAR-M 421 Data.

4.4.2 Elastic Modulus

The results of dynamic modulus testing of Wiggin-produced commercial material are presented in Table 23 with the INCO plotted map data in Figure 41.

4.5 Materials Specification

As part of the contractual task of the progam, a Materials Specification was prepared with input from INCO and reviewed/approved by the NASA Project 4 Manager. The specification essentially defines the technical and quality requirements for MA6000 barstock suitable for turbine vane and blade application. Garrett Specification No. EMS554AD is attached as Appendix A of this report.

Chemical composition conforming to established limits, material heat treat condition, and mechanical property minimums are defined. Macrostructural as well as microstructural control is established from typical commercial production lot received from INCO Alloys International (Wiggin Alloys) during the program. Aggregately, these parameters evolved from the technical effort conducted in this Project 4, and primarily supported the blade design and manufacturing activity.

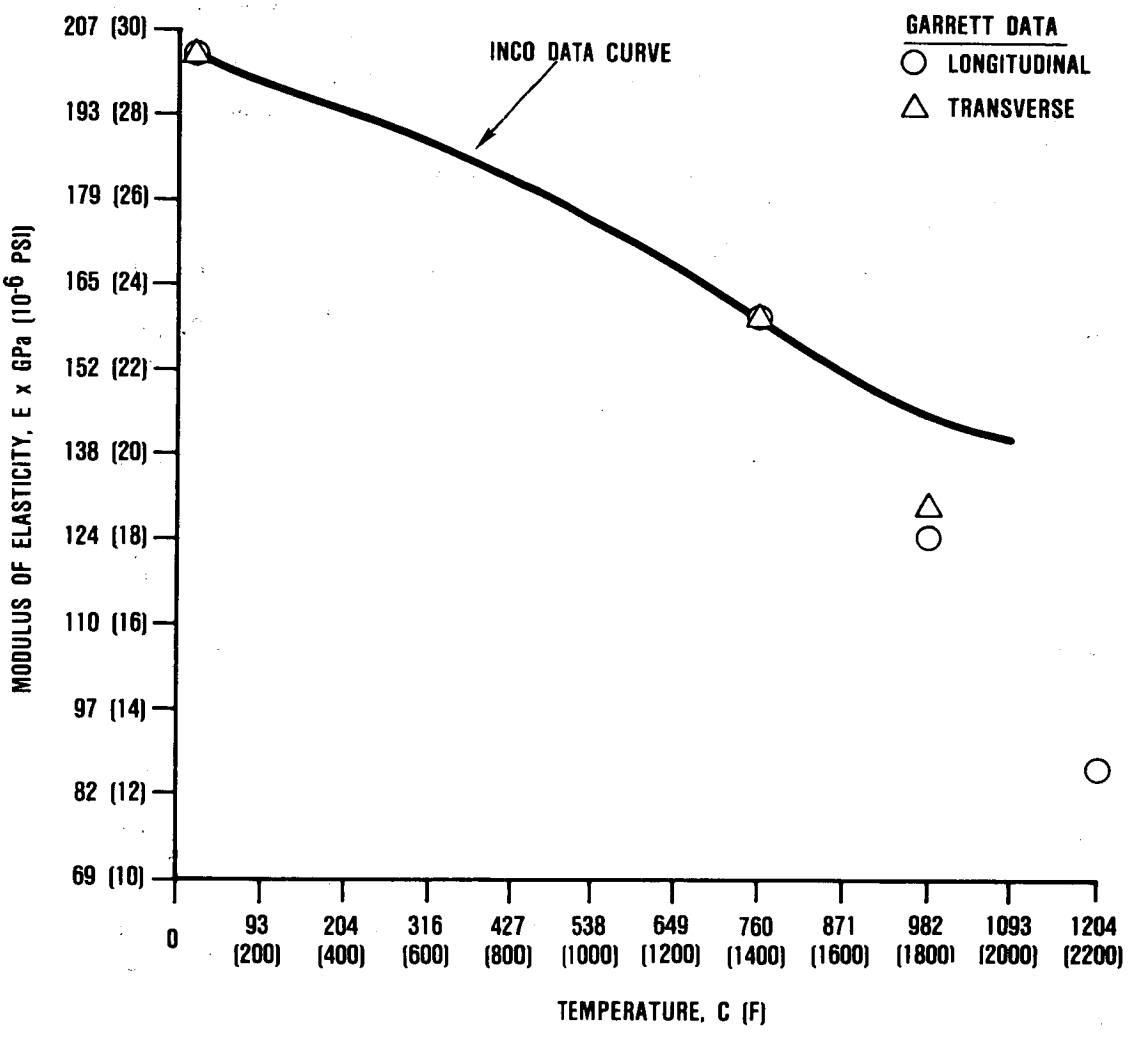

Figure 41. Dynamic Modulus of Elasticity of MA6000. Testing Conducted by Dr. C.B. Gilpen of California State University. Specimen Configuration: 0.15 min (0.06 inch) Diameter by 6.35 mm (2.5 inch) long.

TABLE 23. MODULUS OF ELASTICITY OF MA6000.

	Garrett Data		INCO Map Data*
	Modulus Elasticity, E x 10^{-6} psi (GPa)		
Temperature F	Longitudinal	Transverse	
70	(29.3/28.9) 0.202/0.199	(30.0/28.8) 0.207/0.199	(29.4) 0.203
200			(28.8) 0.199
400			(28.1) 0.194
600			(27.2) 0.188
800			(26.5) 0.183
1000			(25.4) 0.175
1200			(24.4) 0.168
1400	(24.4/22.5) 0.168/0.155	(23.5/23.3) 0.162/0.161	(23.2) 0.160
1600			(21.9) 0.151
1800	(18.0/18.1) 0.124/0.125	(18.7/18.9) 0.129/0.130	(21.0) 0.145
2000			(20.4) 0.141
2200	(12.6/12.7) 0.087/0.088	--/--	

*Estimated values; data are for MAR-M Alloy 421

SECTION V

5.0 BLADE MANUFACTURING PROCESS SELECTION

The manufacturing processes to be used in producing HP turbine blades from MA6000 barstock were identified by GTEC during this phase of the project. The gamma-prime strengthening mechanism in MA6000 makes this alloy more difficult to machine than prior ODS nickel alloys. Therefore, experimentation was required to determine which machining process was the most cost-effective for producing turbine blades from MA6000. Machining methods studied include electrical discharge machining (EDM), electrochemical machining (ECM), milling, and grinding.

EDM techniques to produce the blade airfoil yielded an unacceptably rough surface finish due to the recast layer generated. Substantial hand-finishing was needed to meet surface finish quality requirements. Thus, early in the program, EDM did not appear to be a viable manufacturing method.

Airfoil ECM trials were conducted at TRW's Marsch Ecomatic facility with existing tooling for a similar blade configuration. The chordal width was snagged to produce an airfoil similar to those used by GTEC. Together with MA6000, Udimet 700 and Greek Ascoloy were concurrently ECM'd to compare the response of the two materials. Results indicated that MA6000 behaved similarly to Udimet 700 and Greek Ascoloy in all aspects including ease of machining and surface quality. Surface finish measurements of the airfoils conducted at GTEC show an average surface finish of 8 rms, with most having better than 16 rms without any additional mechanical or hand polishing. This exceeds current turbine airfoil specifications. Metallographic examination of the blades confirmed the airfoil to be free of pits or other preferential attacks that might be harmful to the blade in engine service.

Conventional grinding was initially selected to generate the root form of each blade with existing tooling and machining parameters at the TRW Harrisburg facility. No difficulty was experienced in grinding the firtree serration. This technique was incorporated into the blade manufacturing process.

Prototype blades produced by this airfoil/root combined machining technique from MA6000 barstock are shown in Figure 42.

A limited cold and warm forming technique evaluation was conducted to determine the possibility of achieving better material use since considerable material waste results from having to ECM an airfoil from a rectangular block. Forming trials were conducted at the Schurman Machinery Co., Ltd., Ontario, Canada with less than optimum results. The material cracked when subjected to hot or cold forming, probably because it should have been in the annealed, not the recrystallized condition. Another apparent problem with the material, centerline cracks, detracted from optimum soundness. TRW thought that further work should be done with hot forming, using material in the annealed condition. However, the forging approach was considered beyond the context of this program, and no further activity was attempted.

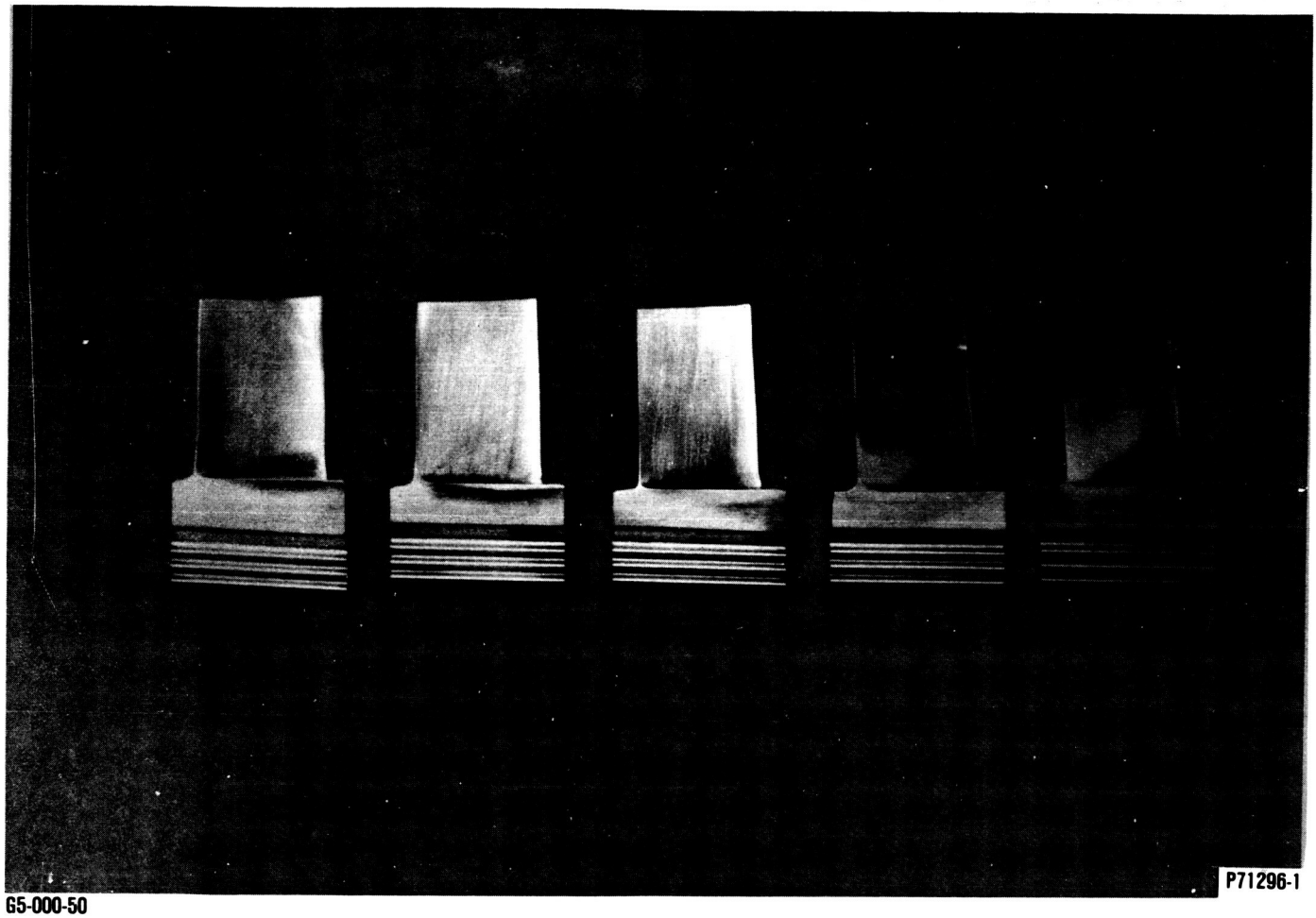

Figure 42. Five MA6000 Blades Manufactured at TRW. Airfoils Produced by ECM (Three Airfoils on Right Received Final Airfoil Grinding), Firtree Produced by Conventional Root Grinding.

SECTION VI

6.0 BLADE DESIGN SCOPE

6.1 Aerodynamic Design

The design requirement of low blade stress for MA6000 material calls for a high taper ratio blade configuration. Figure 43 presents the initially specified and the finally achieved area ratio distributions. The initial requirement called for an overall area ratio of approximately 6.25 to 1. During the course of the design, other mechanical constraints on leading and trailing edge inflections and flair angles led to the final overall area ratio of 7.1 to 1. Based on two-dimensional blade-to-blade flow solutions and boundary layer analyses, no performance penalty was identified for the new high-taper-ratio blade design when compared to the previous blade design.

6.1.1 Vector Diagram

The vector diagram used for the new blade design is the same as that used for the MAR-M 247 DS final blade design documented in the project completion report for MATE Project 1 (NASA CR-159464).

6.1.2 Blade Geometry

Five stream surface design sections were initially used to define the blade: at the hub, 10 percent, 40 percent, 70 percent, and tip streamlines. The exit radii of these streamlines correspond to the radii of the cylindrical design sections used for the previous blade design. A sixth design section between the 70 percent and the tip streamlines was added in one of the final iterations with the mechanical design group in an effort to smooth the blade stack and eliminate an apparent inflection in the blade shape. Blade

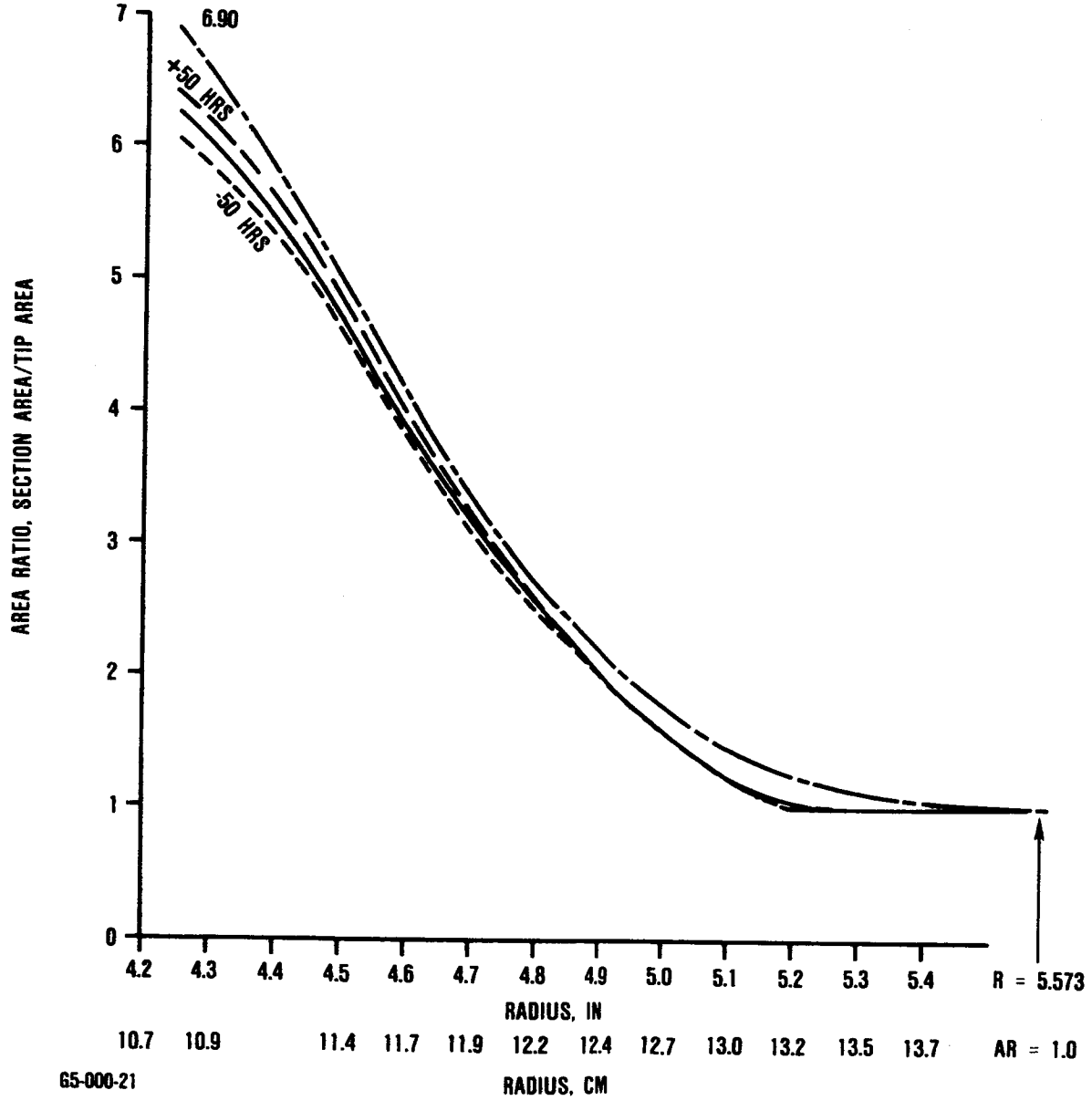

Figure 43. TFE731-5 HP Turbine Blade Area Distribution.

geometry data for the final six design sections are presented in Table 24. The six design sections are shown in Figures 44 through 49, and a blade stack is shown in Figure 50.

The increased area ratio relative to the previous design was achieved primarily through changes in axial chord, increasing from 0.962 inch to 1.19742 inch at the hub and decreasing from 0.645 inch to 0.57371 inch at the tip. Maximum thickness and leading edge radius also were increased at the hub and decreased at the tip, but these have less of an influence on section area than the axial chord does.

Preliminary iterations with the mechanical group were based on a section center of gravity, and stack in the final iteration, the blade lean and tilt relative to a center of gravity stack was included. A linear distribution of lean and tilt from hub to tip was used, with the tip lean of 0.010 inch in the direction of rotation and the tip tilt of 0.125 inch toward the trailing edge.

6.1.3 Rotor Blade Loading

Critical velocity ratio distributions versus normalized axial distance for the original five design sections are presented in Figures 51 through 55. Because the sixth design section was added only to smooth the blade geometry and was based on curve-fitting the input parameters for the original five design sections, loadings were not generated for this section. The velocity distributions for the sections near the hub reflect the reduced level of loading and the increased blockage because of the increased axial chord and maximum thickness, and exhibit some deceleration near the trailing edge on the suction surface. The tip section velocity distribution shows a higher level of loading due to the decreased axial chord, but only a slight diffusion on the suction surface near the trailing edge.

TABLE 24. FINAL BLADE DESIGN GEOMETRY.

Inlet Radius	4.300	4.422	4.779	5.140	5.342	5.538
Exit Radius	4.242	4.424	4.872	5.244	5.425	5.573
Leading Edge Radius	0.04617	0.04617	0.03274	0.01590	0.01590	0.01590
Trailing Edge Radius	0.017	0.017	0.0115	0.010	0.010	0.010
Leading Edge Half-Wedge Angle	10.0	10.0	9.0	9.0	8.805	8.0
Trailing Edge Half-Wedge Angle	8.5	8.5	6.6	4.5	4.5	4.5
Throat Angle	-50.32801	-49.50314	-48.65181	-47.38432	-47.65	-48.31996
Throat Width	0.21065	0.22801	0.27837	0.31649	0.325	0.32923
Axial Chord	1.19742	1.070	0.79516	0.64058	0.59486	0.57371
Inlet Mean Camber Angle	33.534	31.201	33.901	38.898	37.93	36.483
Exit Mean Camber Angle	-57.32801	-56.50314	-57.05181	-57.88432	-58.370	-58.81996
Maximum Thickness	0.22054	0.204	0.11039	0.060802	0.052	0.0479
Suction Surface Turning Downstream of Throat	15.5	15.5	15.0	15.0	15.22	15.0

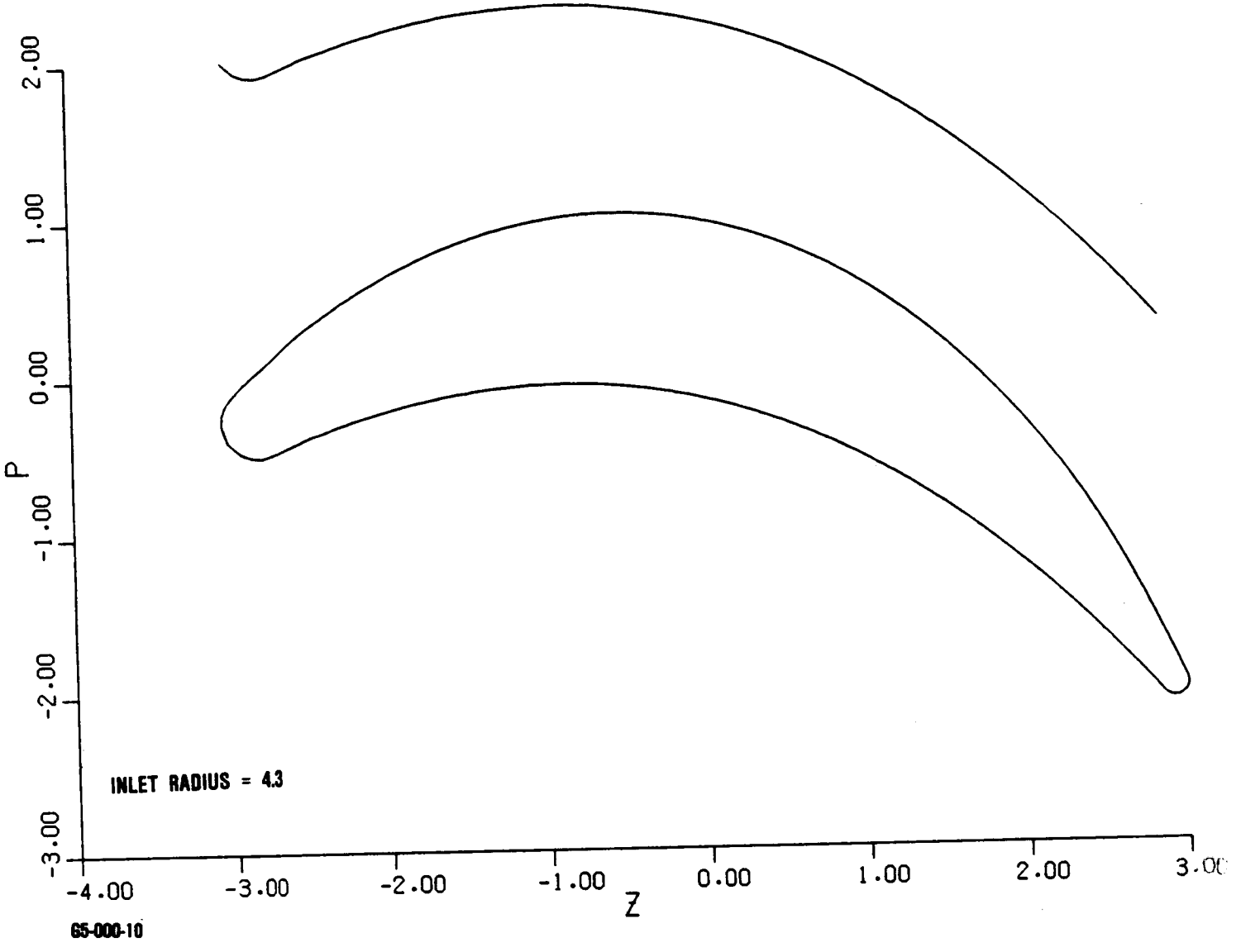

Figure 44. MATE TFE731 HP Turbine Blade Design Section 1.

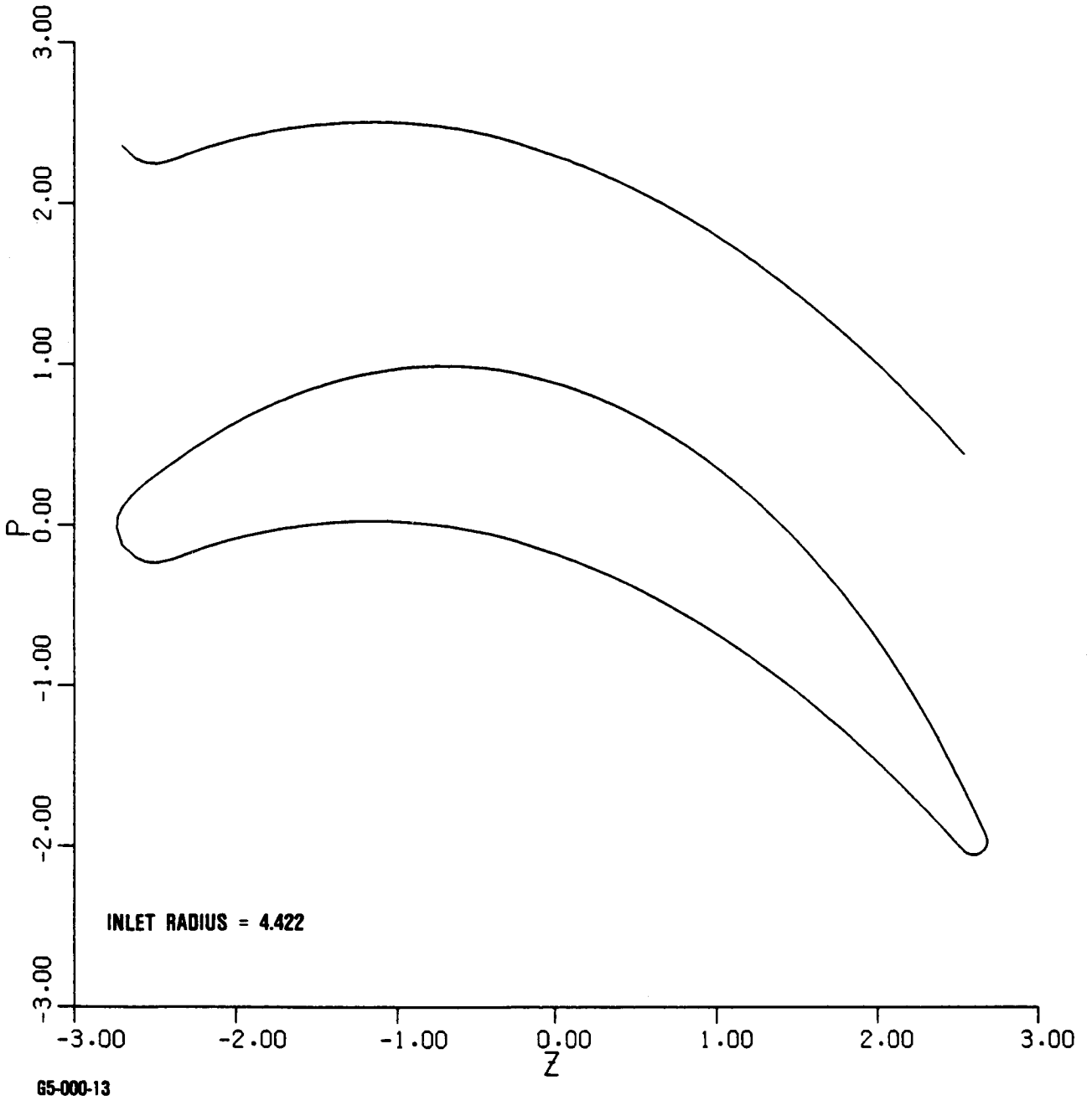

Figure 45. MATE TFE731 HP Turbine Blade Design Section 2.

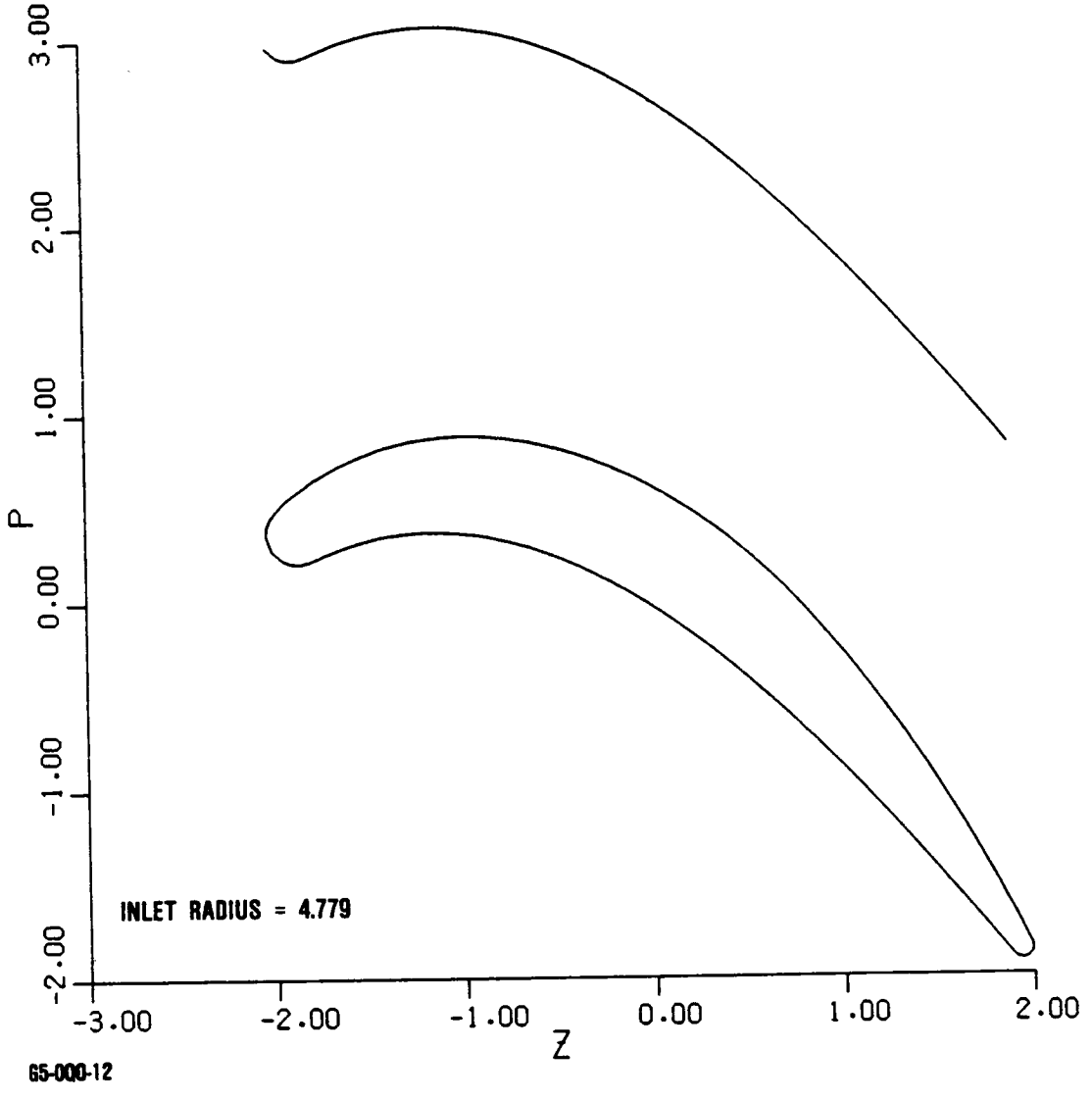

Figure 46. MATE TFE731 HP Turbine Blade Design Section 3.

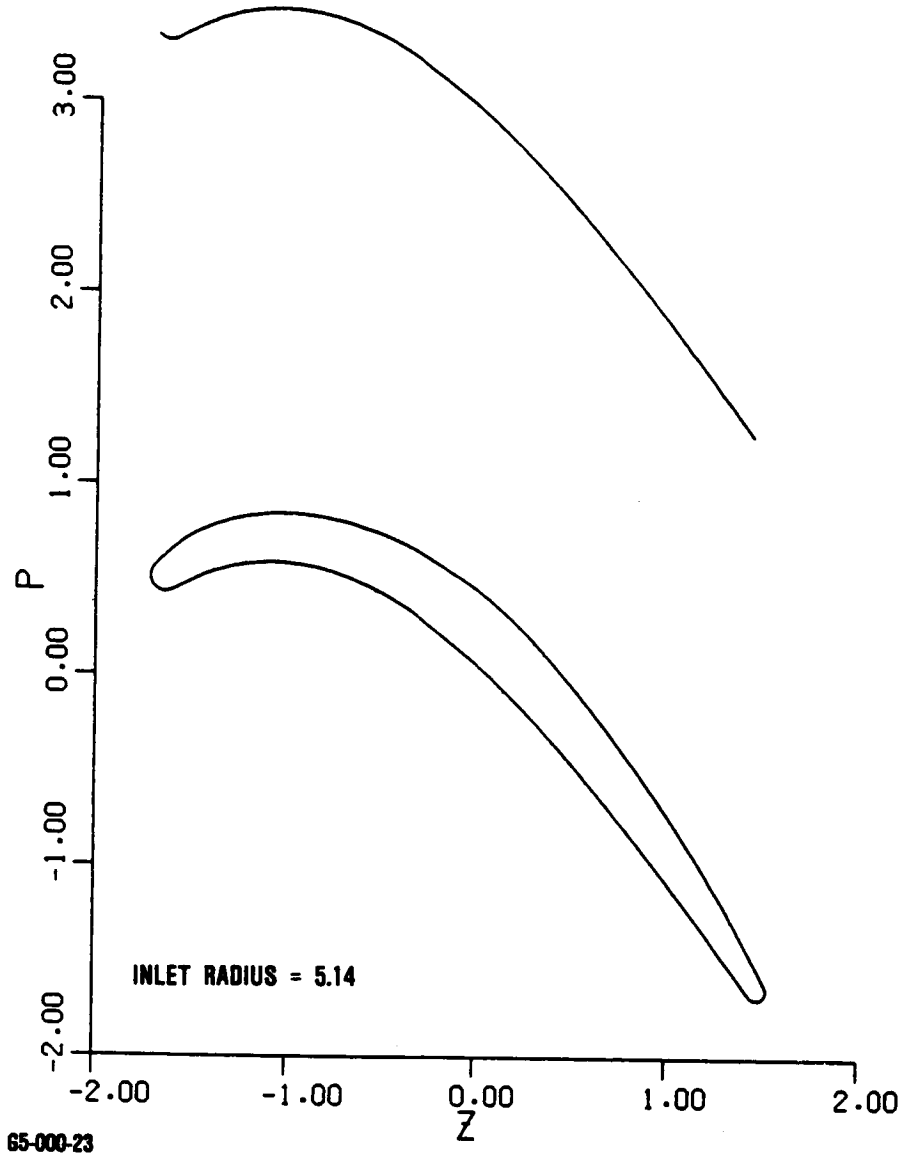

Figure 47. MATE TFE731 HP Turbine Blade Design Section 4.

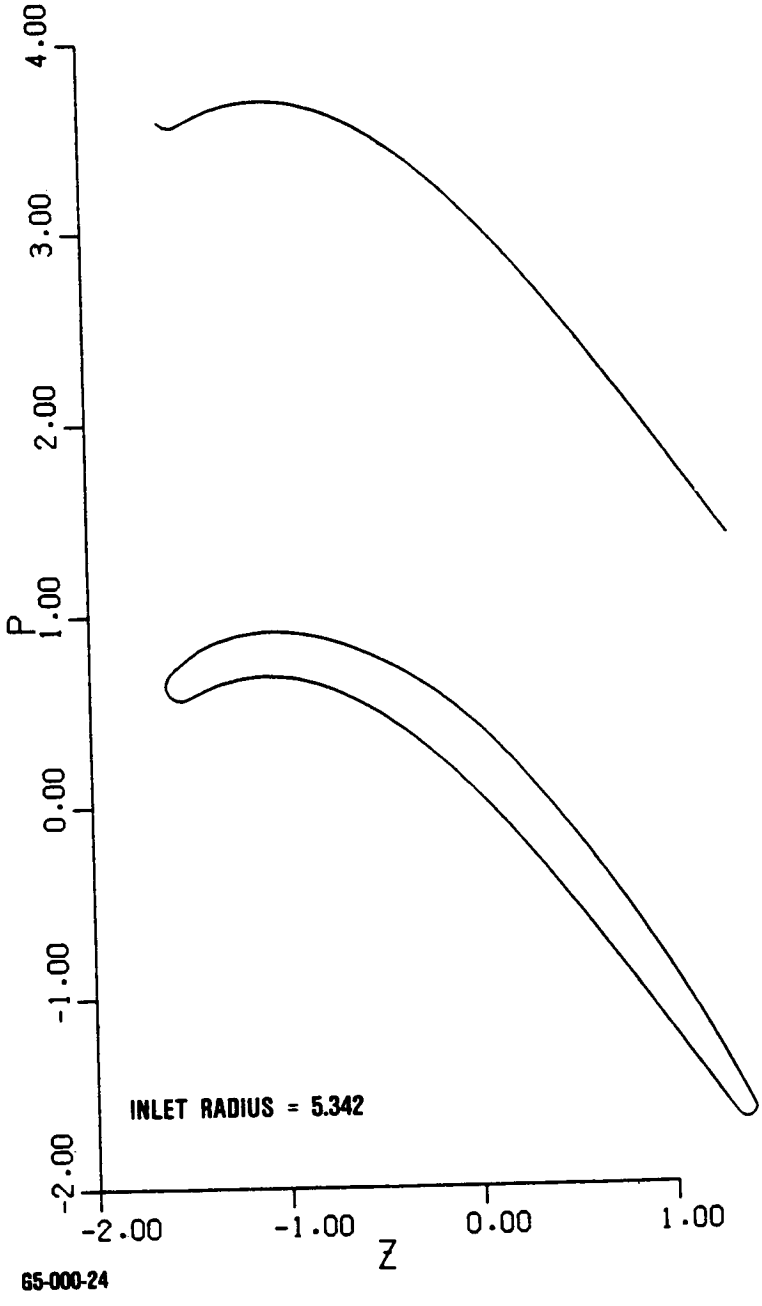

Figure 48. MATE TFE731 HP Turbine Blade Design Section 5.

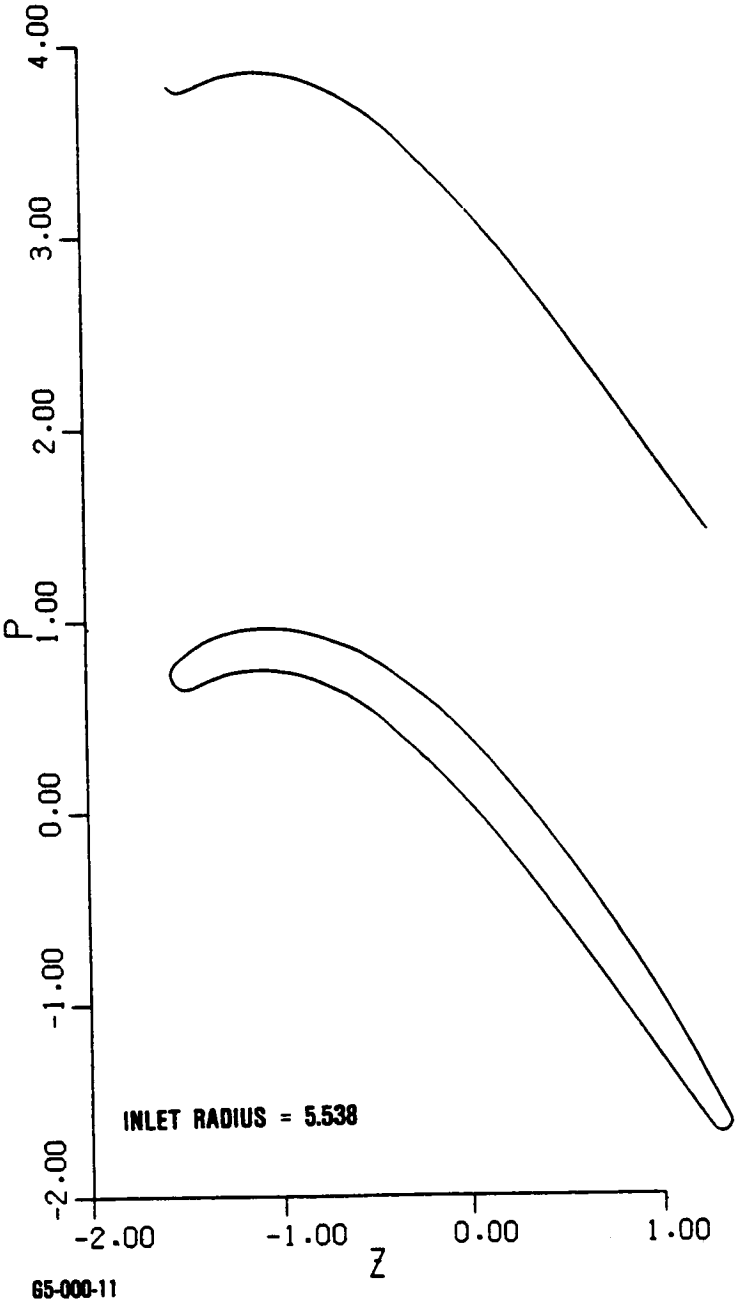

Figure 49. MATE TFE731 HP Turbine Blade Design Section 6.

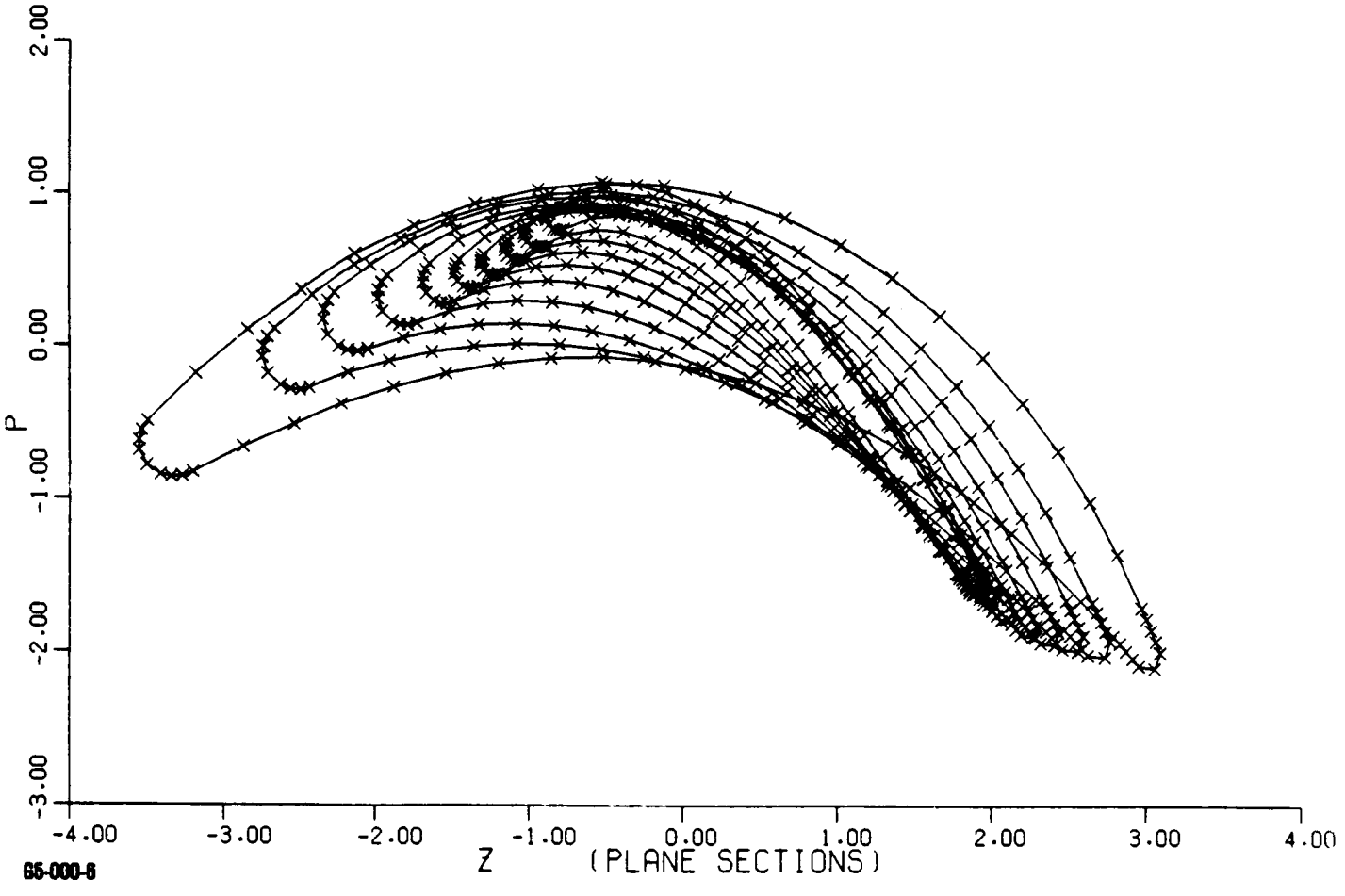

Figure 50. MATE TFE731 HP Turbine Blade Stack.

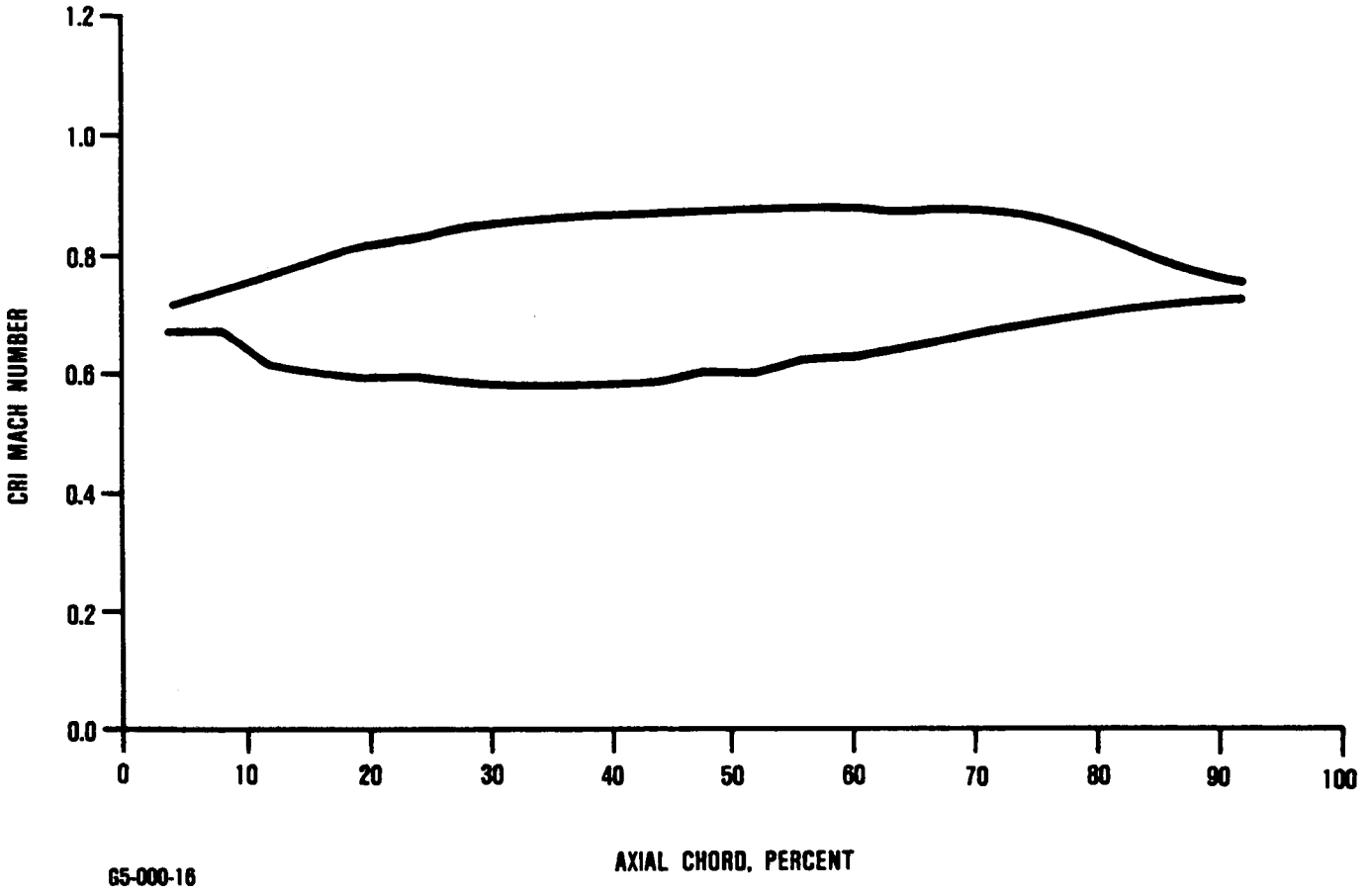

Figure 51. TFE731 MATE HP Turbine Blade RIN = 4.30.

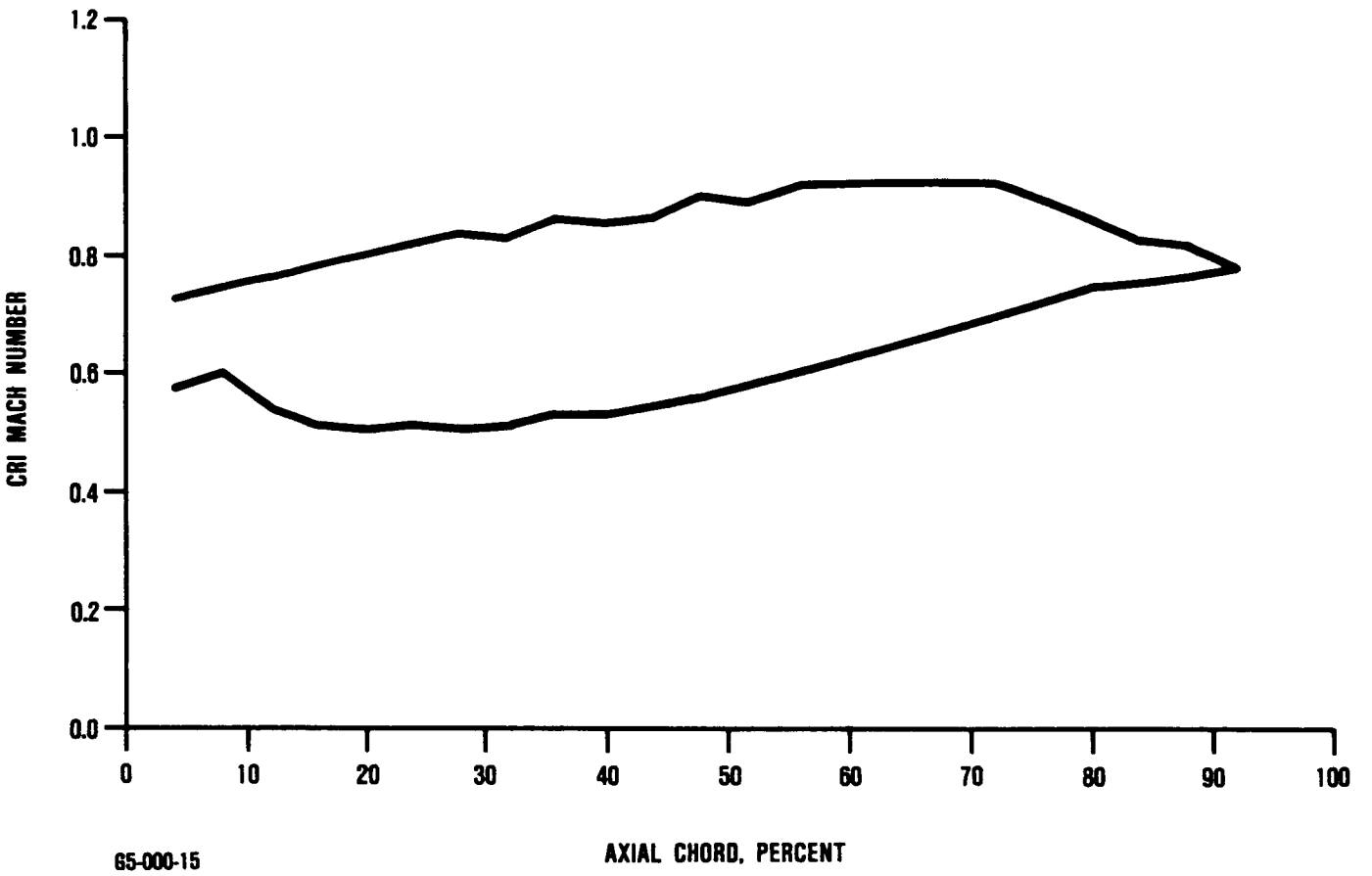

Figure 52. TFE731 MATE HP Turbine Blade RIN = 4.222.

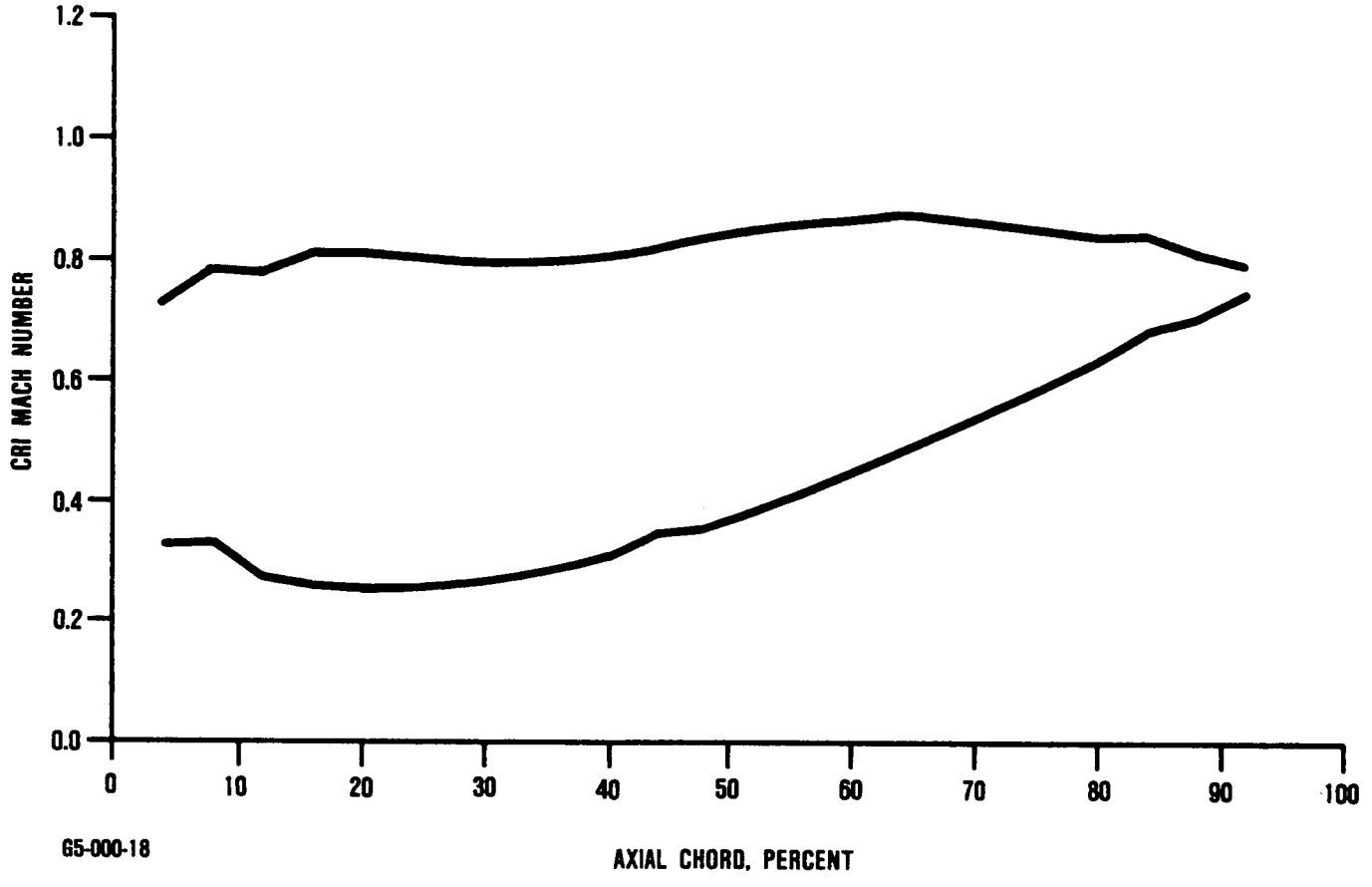

Figure 53. TFE731 MATE HP Turbine Blade RIN = 4.779.

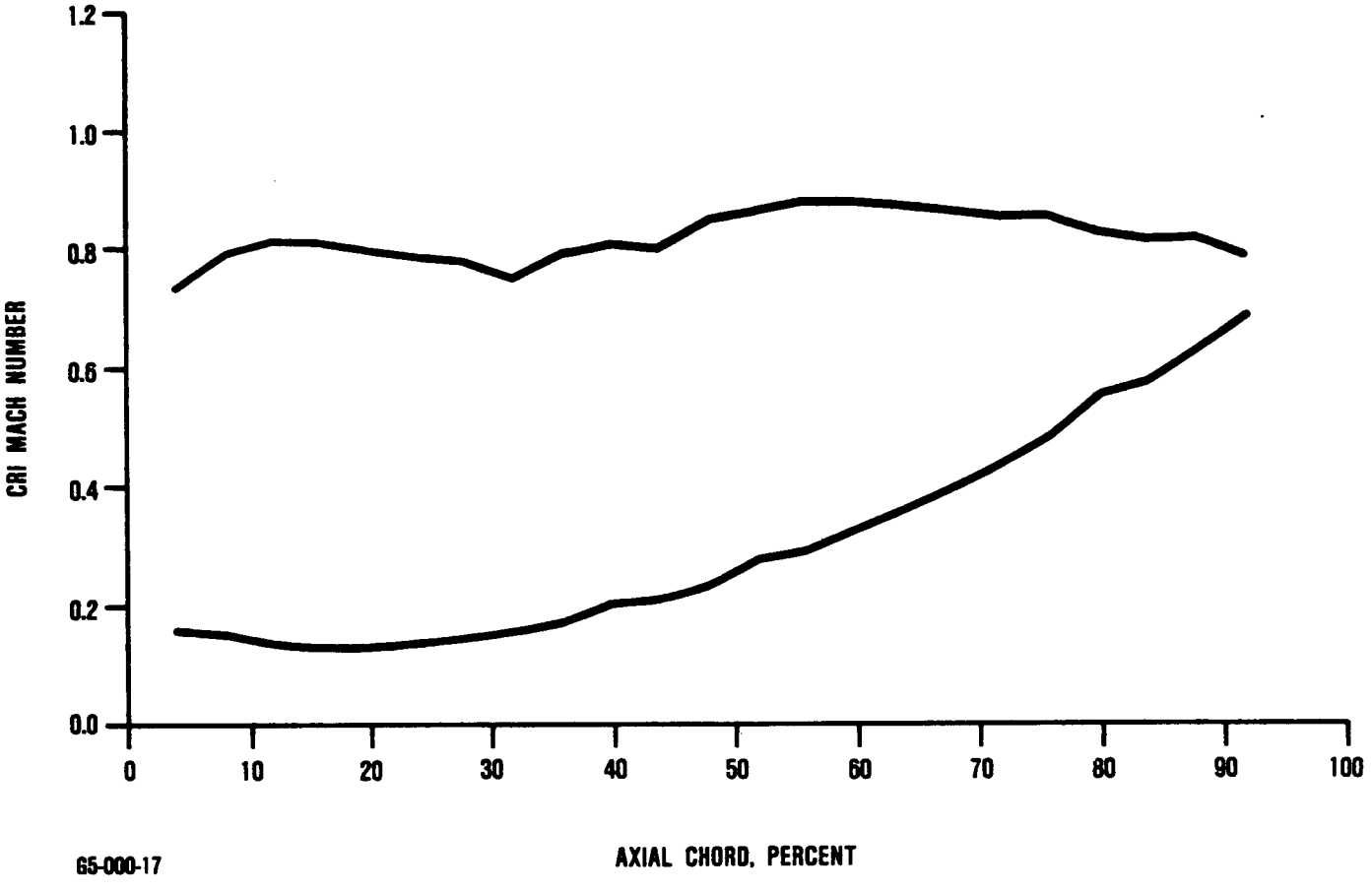

Figure 54. TFE731 MATE HP Turbine Blade RIN = 5.140.

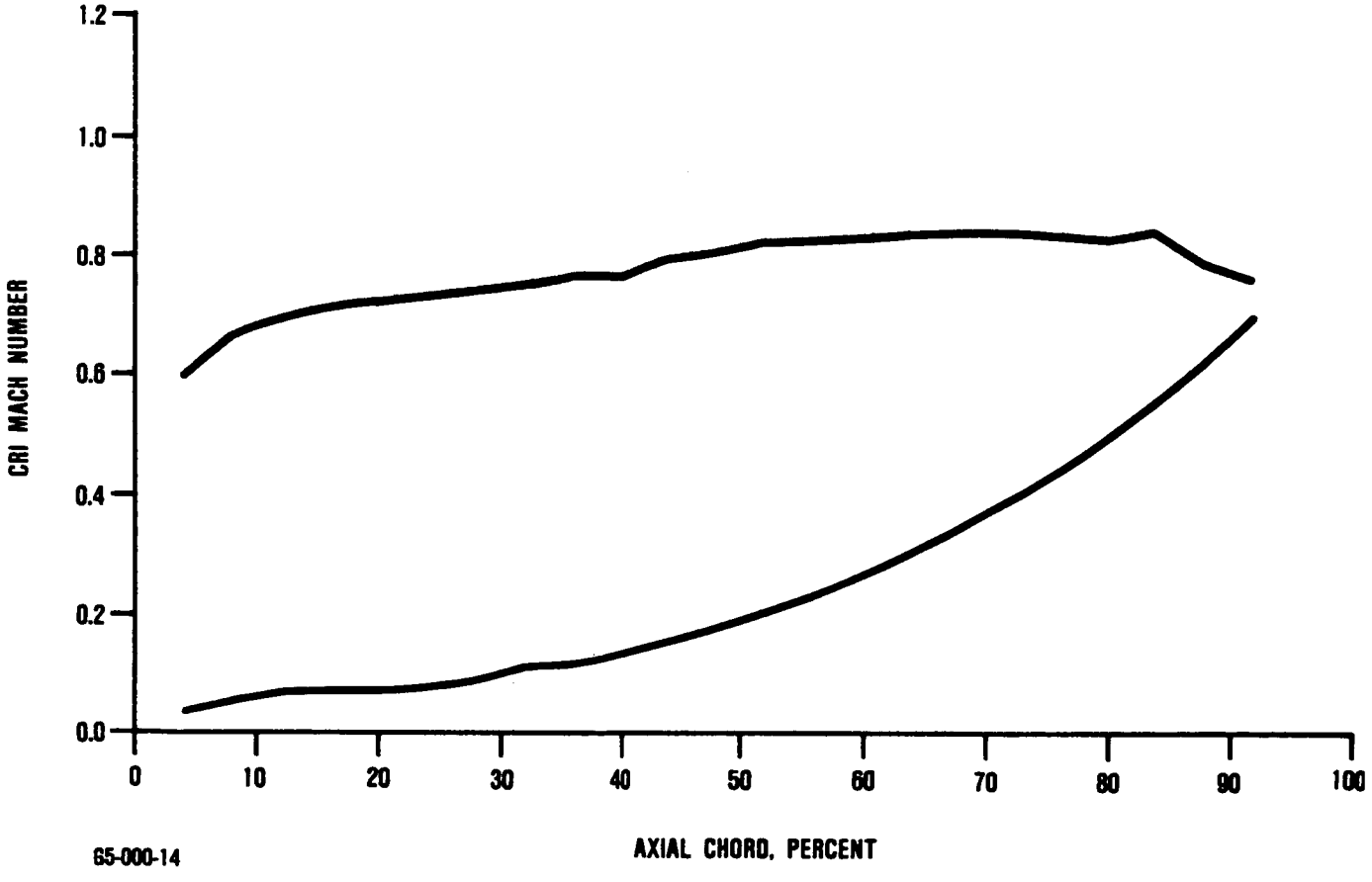

Figure 55. TFE731 MATE HP Turbine Blade RIN = 5.538.

Boundary layer analyses for the new blade design and the previous blade design were conducted and compared. Results of the Trukenbrodt calculation indicated no separation on any of the sections of the new design. Based on the boundary layer calculation results, pressure loss calculations were made for the new and the previous designs. Results agreed to within 0.1 percent, leading to the conclusion that no detectable performance penalty was associated with the higher taper ratio design.

6.2 Mechanical Design

After several iterations, the MA6000 blade airfoil was designed with acceptable aerodynamics and area ratio of 7.1. Because the MATE airfoil taper ratio is higher and its blade count is lower than that of its MAR-M 247 counterpart, a longer blade firtree length was required. The HP turbine disk was therefore redesigned for the airfoil. In addition, the LP nozzle and the HP stator vanes were slightly altered to allow for effective integration of the MATE rotor into the engine.

To ensure successful completion of the engine test, the following analyses were performed:

- Thermal and Stress Analysis
- Blade Life Analysis

6.2.1 Thermal and Stress Analysis

As part of design analysis, a 2-D thermal model of the MATE HP rotor was constructed. The thermal boundary conditions for this model were obtained from the secondary flow model of the TFE731-3B turbofan engine, which was modified to account for the MATE replacement hardware.

This secondary flow model included the low pressure section of the engine as well as the high pressure section. Flow resistances of interest in the HP section of the model are listed below:

(1) HP forward 3-tooth stepped lab seal with 0.0077-inch clearance

(2) HP forward 3-tooth straight lab seal with 0.0067-inch clearance

(3) Eight 1/8-inch holes in the HP forward seal plate

(4) HP aft 3-tooth stepped lab seal with 0.009 inch clearance

(5) Bath tub seals under the HP blade platform

(6) Nickel graphite seal for the HP attachment

The resulting secondary flows in percent of core flow were subsequently determined.

Using these flows, the HP disk thermal boundary conditions (gas temperatures and heat transfer coefficients) were calculated. Figures 56 through 60 show the thermal mesh model, the boundary gas temperatures, the heat transfer coefficients, and the rotor gas profile and metal temperature distribution, respectively.

Airfoil and attachment stresses were analyzed using 2-D and 3-D finite-element models. The airfoil stresses were calculated by using the 3-D finite-element model shown in Figure 61. The root of the airfoil was given a zero displacement boundary condition. This model predicted maximum effective stresses of 35 ksi for the suction surface and 23 ksi for the pressure surface (Figure 61). Note that the imposed boundary conditions at the root may distort the stresses in the lower 10 percent of the airfoil. However, the stresses in the rest of the airfoil should not be affected.

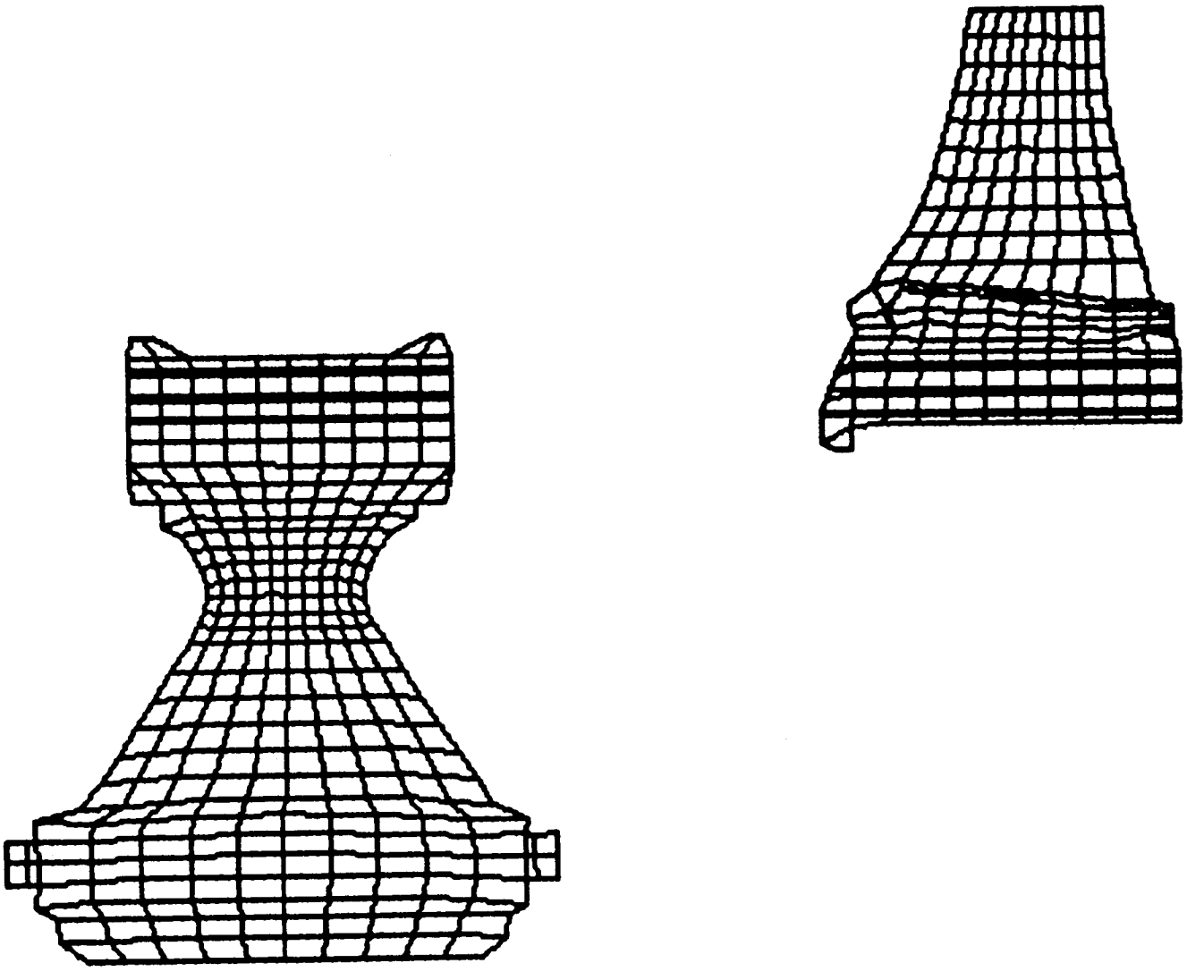

Figure 56. Thermal Mesh Model Of NASA MATE HP Rotor.

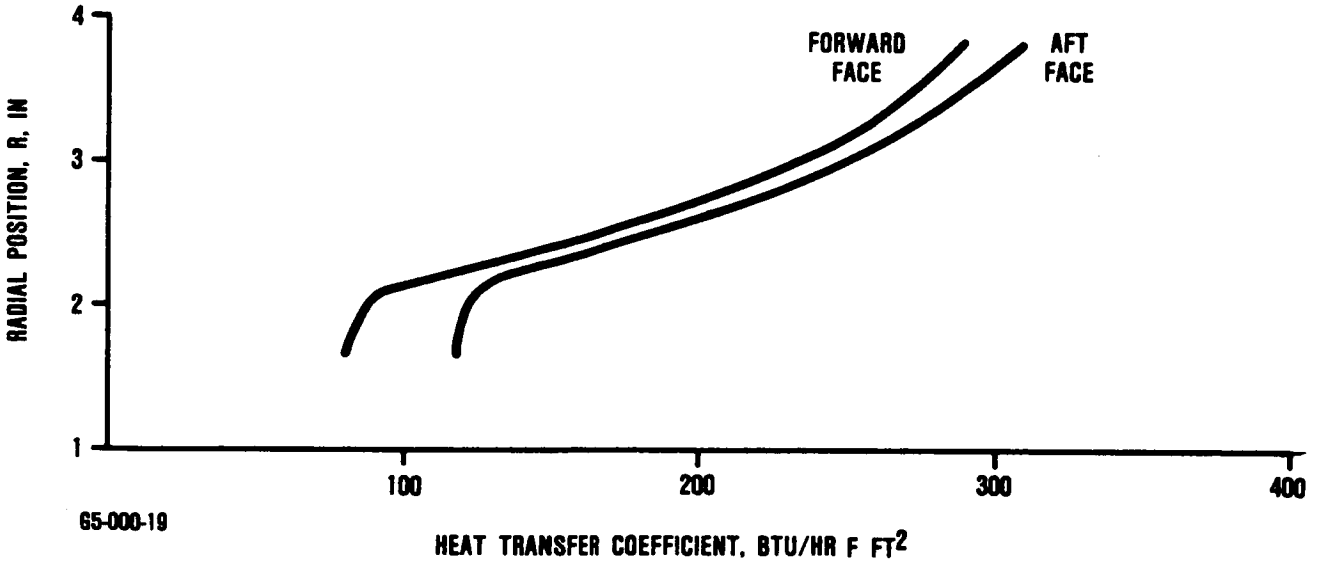

Figure 57. Disk-Face Heat Transfer Coefficient Versus Radii.

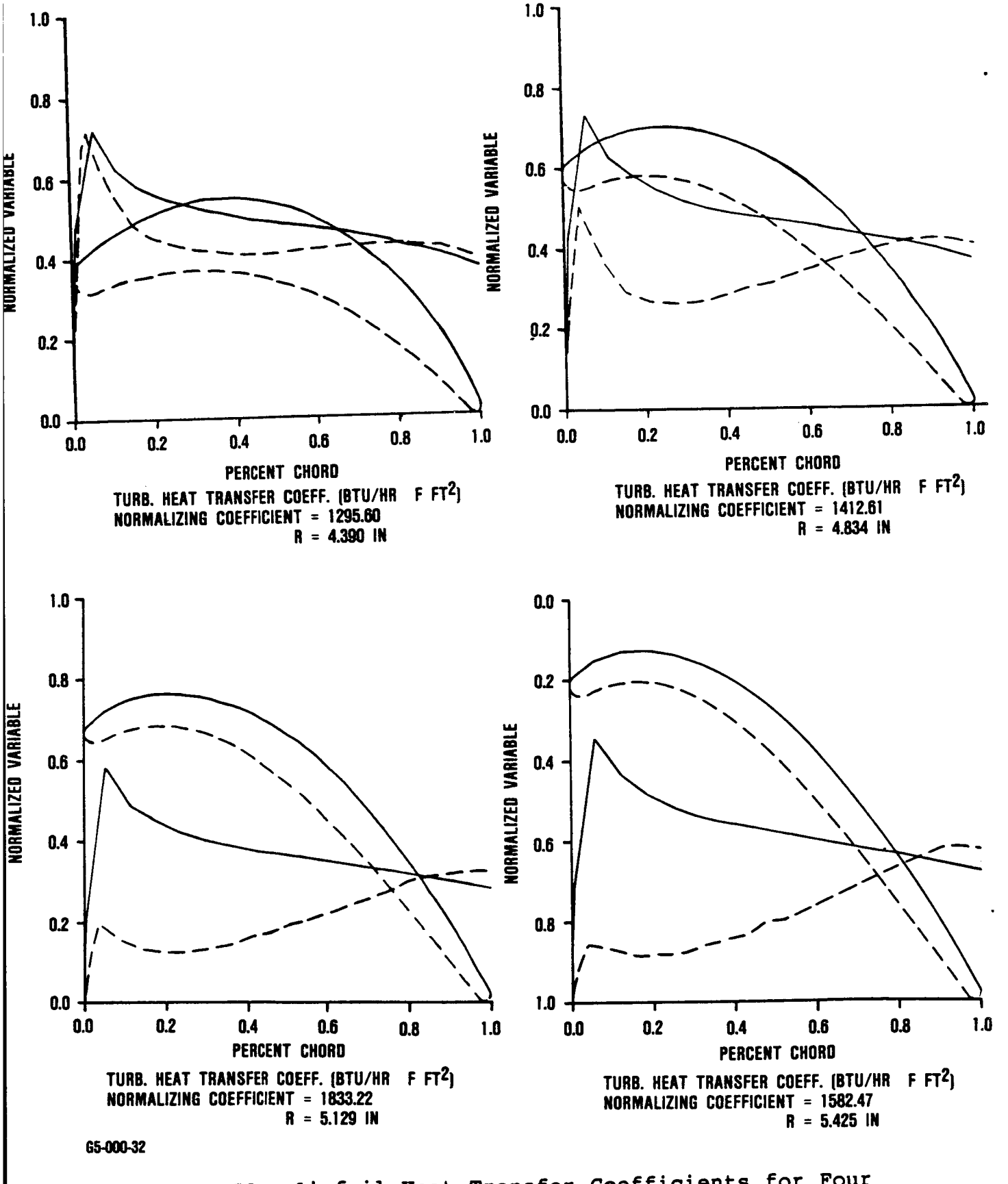

Figure 58. Airfoil Heat Transfer Coefficients for Four Radial Sections.

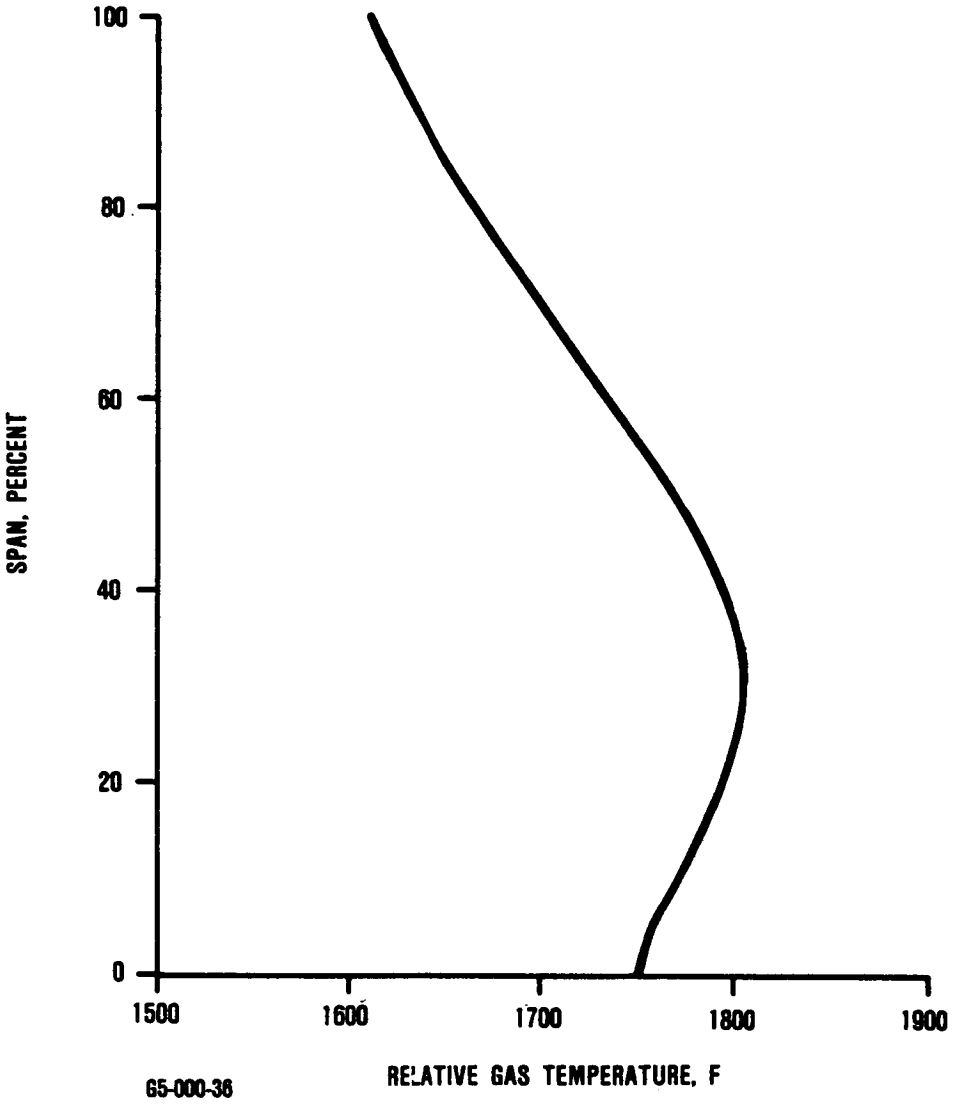

Figure 59. Flow Path Relative Gas Temperatures Profile at Sea Level Static, T_5 = 1635F.

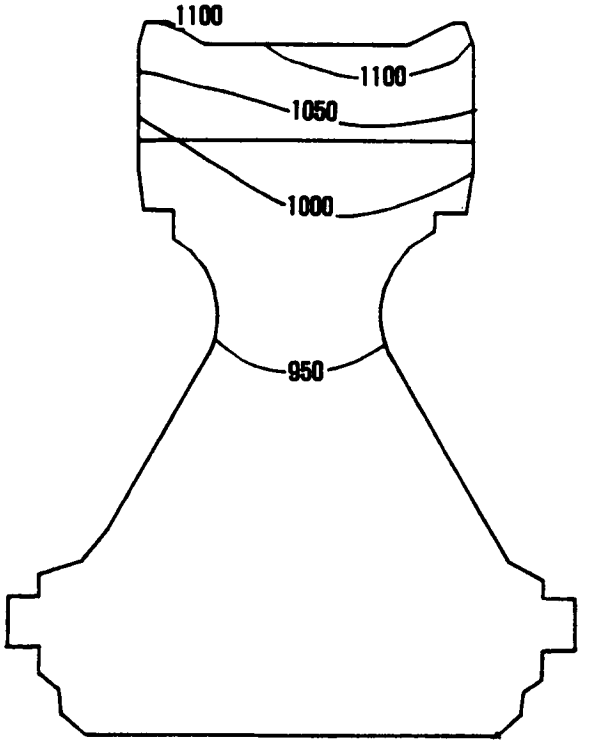

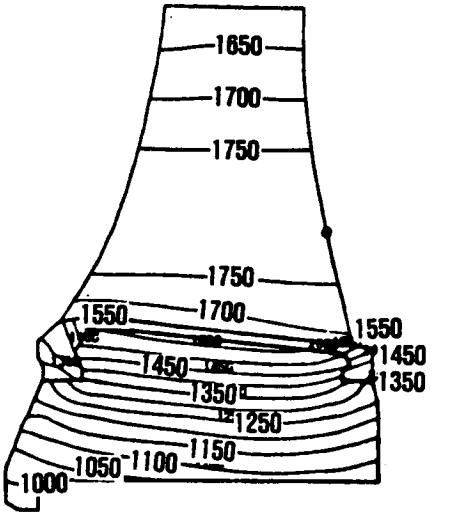

SEA LEVEL STATIC, MAXIMUM POWER CONDITION

Figure 60. NASA MATE HP Rotor Temperature Distribution.

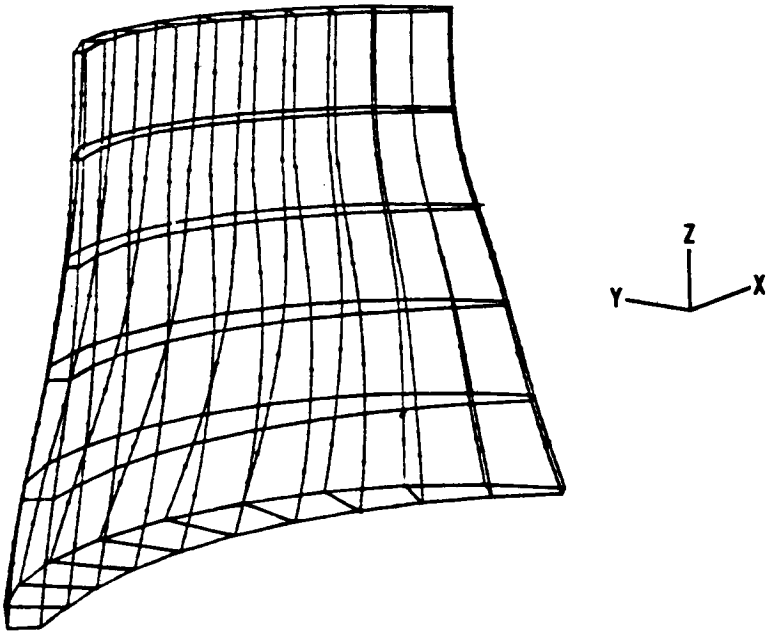

3-D MODEL OF THE MA6000 BLADE AIRFOIL

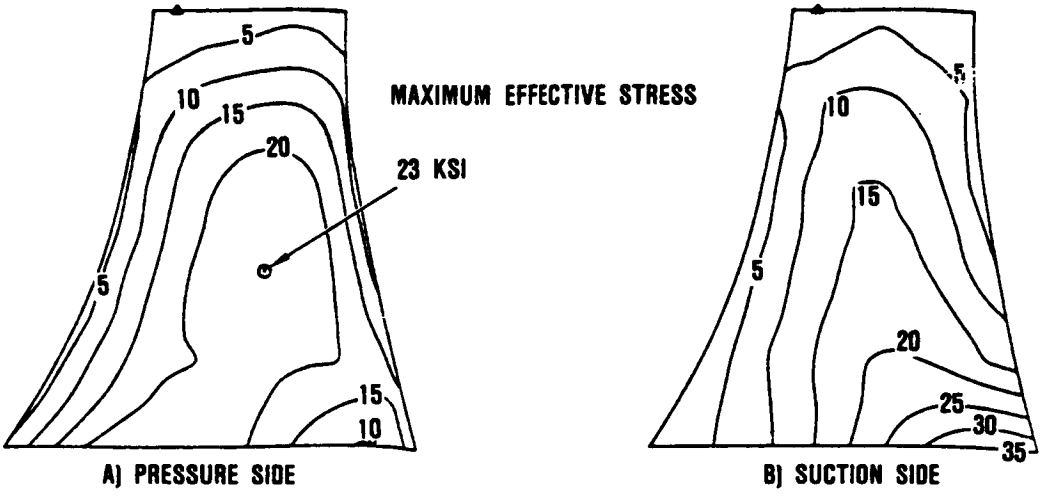

65-000-34

Figure 61. 3-D Finite Element Model and Effective Stress Distribution for the Blade Airfoil.

For the attachment region, the 2-D finite-element model shown in Figure 62 was constructed. The airfoil, platform, and shank loads were calculated by stacking several radial sections of the blade and using a beam model (Figure 63). The forces at the blade shank section that are shown in Figure 64 were applied to the 2-D attachment model, and maximum principal stresses of 131.7 ksi in the disk post and 100.6 ksi in the blade firtree were predicted. For this analysis, the temperature distribution from the 2-D rotor thermal analysis was used. Plots of the temperature and the maximum principal stress distribution are provided in Figures 65 and 66, respectively.

6.2.2 Blade and Attachment Life Analysis

A detailed blade life analysis was performed, based on the planned NASA/MATE 200-hour test mission, which consists of four 50-hour cycles (Figures 67 through 70). Operating conditions for each cycle point were specified in terms of engine turbine inlet temperature, T_4; compressor exit temperature, T_3; and speed of high pressure spool, N; from the performance analysis for this engine. These parameters are normalized by the corresponding design values (sea level static, max power) and are presented in Table 25. Using the normalized values, the airfoil and the attachment stresses and temperatures were scaled, and the local stress rupture damage due to each point was determined. The results of the damage analysis, which are shown in Table 26, indicate that the critical section of the blade airfoil (30 percent span) is the life-limiting location. At this location, approximately 25 percent of the stress-rupture life of the blade is consumed during one 200-hour test cycle given that the maximum operating is sea level static, T_4 = 1930F.

The low-cycle fatigue life of the blade and the disk attachment were also calculated based on σ_{max} at steady-state conditions to be in excess of 10^4 0-max-0 cycles. This easily satisfies the approximate 50 0-max-0 and 200 idle-max-idle cycles required by the test.

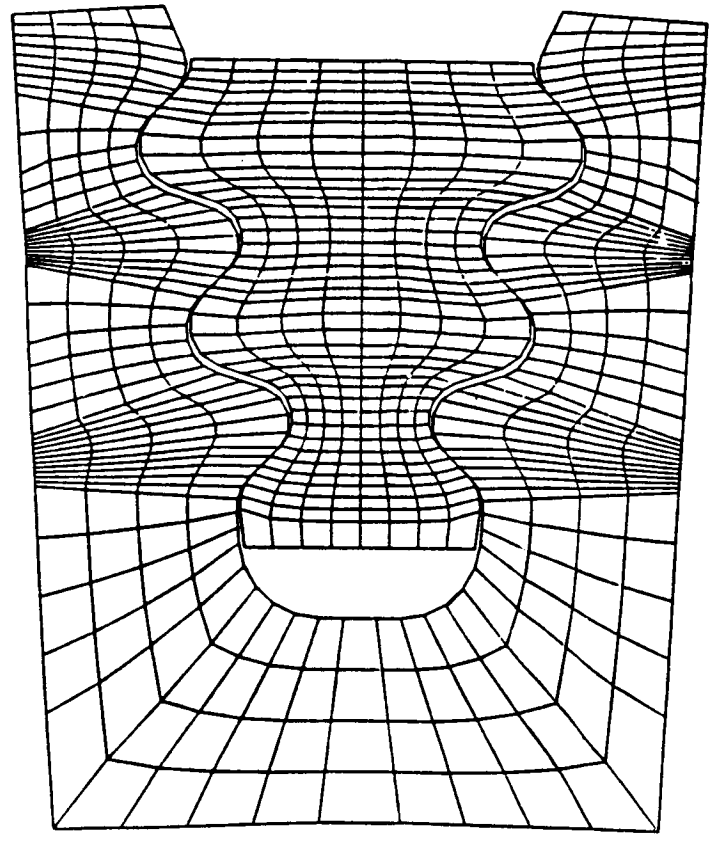

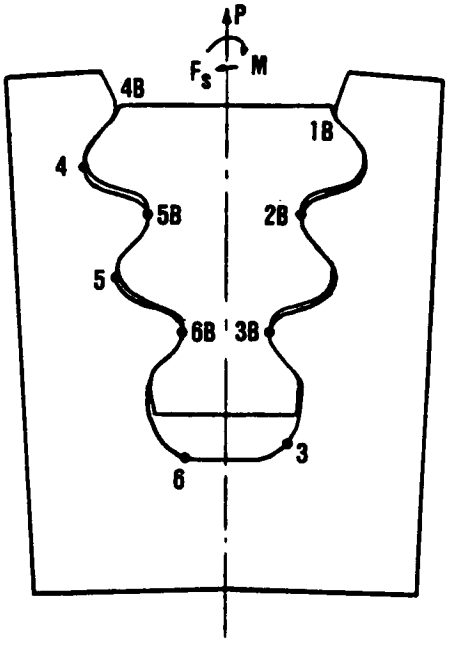

BLADE ATTACHMENT SCHEMATIC

P: RADIAL PULL
M: BENDING MOMENT
F_s: SHEAR FORCE

Figure 62. 2-D Mesh Model of the NASA/MATE HP Rotor Attachment.

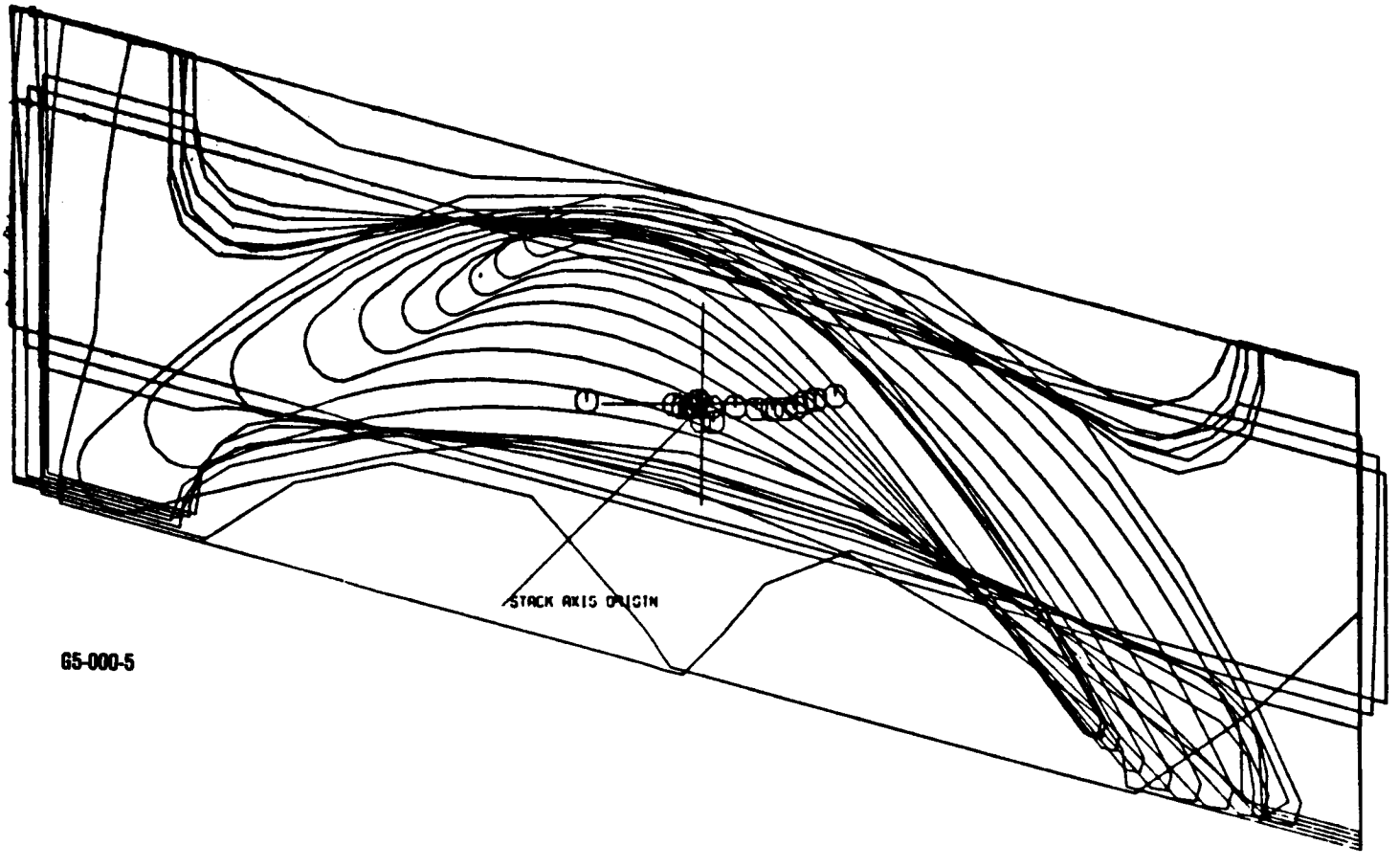

Figure 63. Beam Analysis of the Manufactured MA6000 Blade.

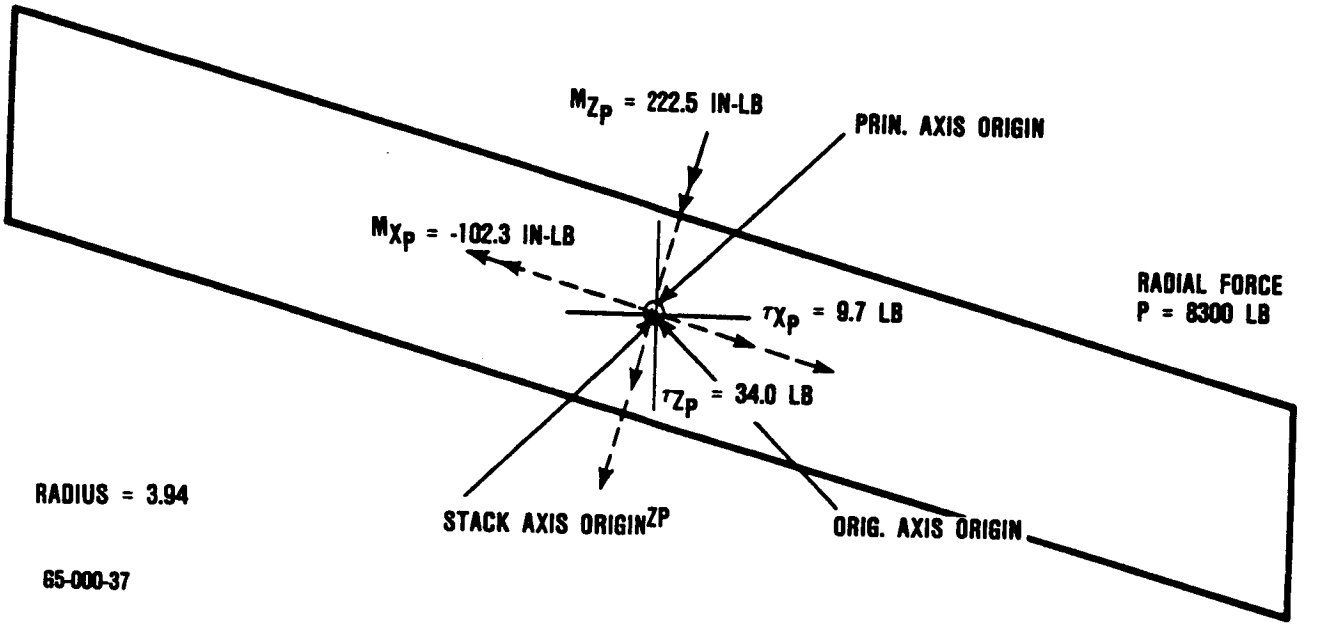

Figure 64. Beam Model Resulting Blade Forces and Moments at the Bottom Section of the Shank.

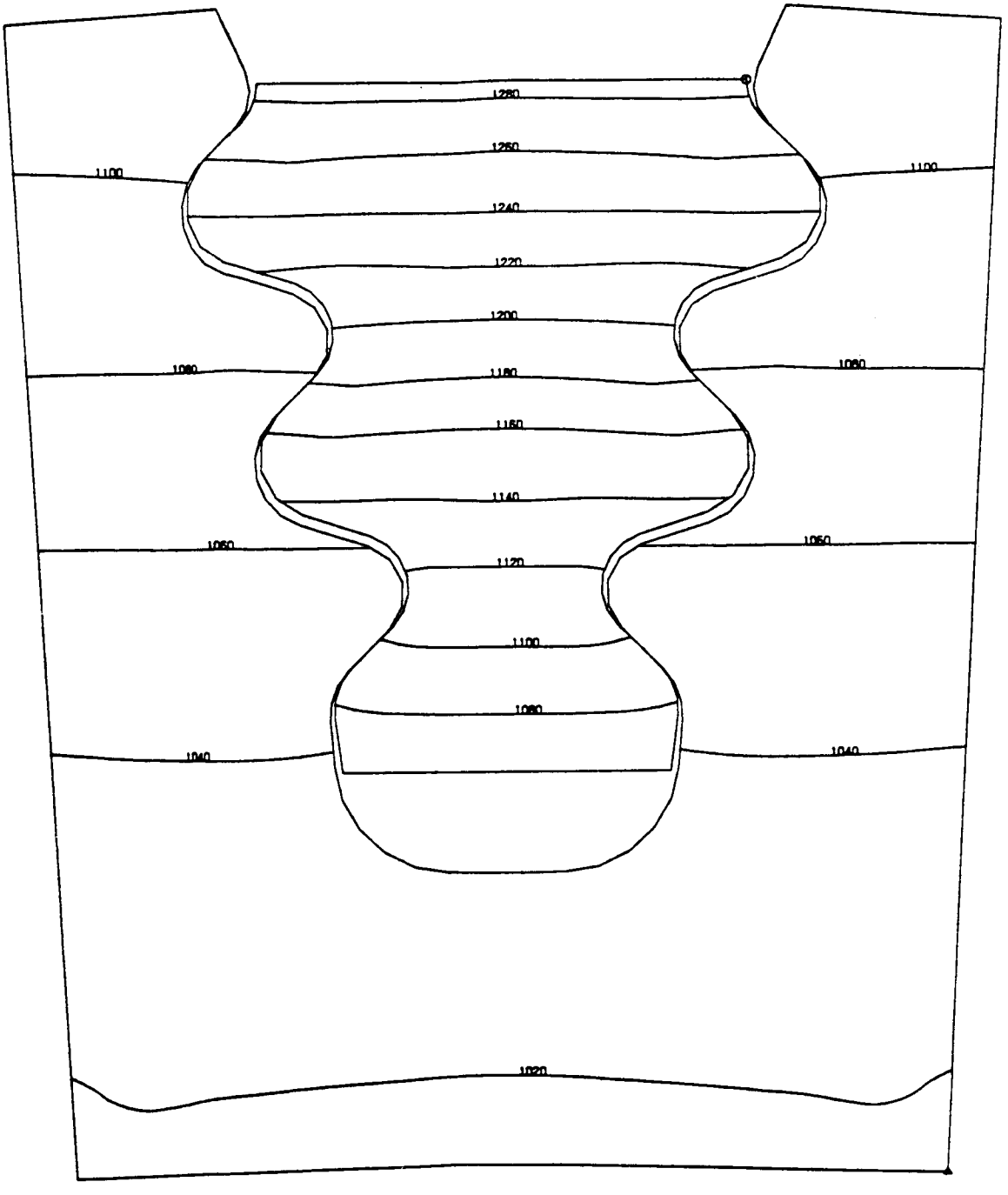

Figure 65. Plot of Temperature Distribution for the Blade Attachment.

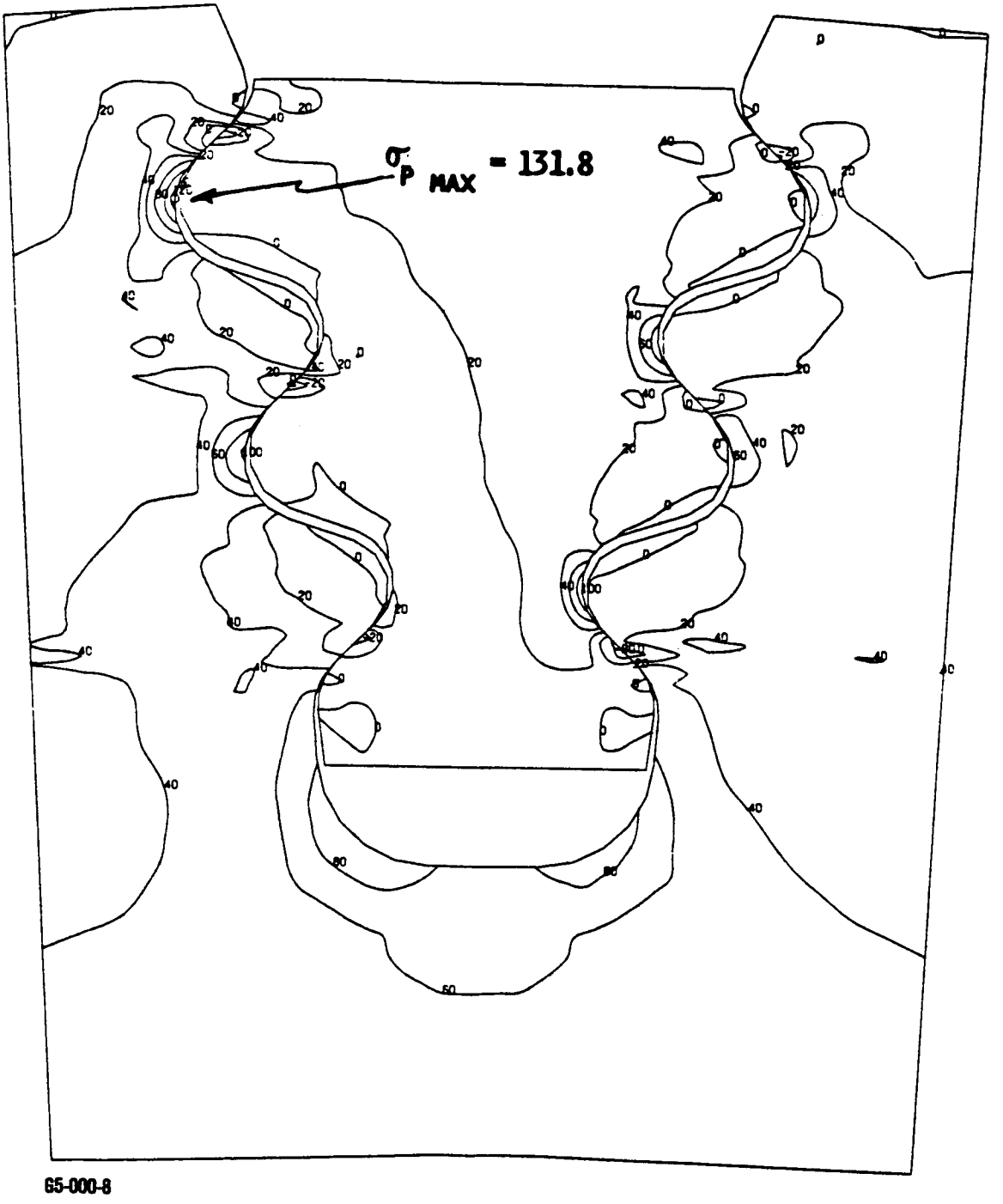

Figure 66. Plot of Principal Stress Distribution for the Blade Attachment.

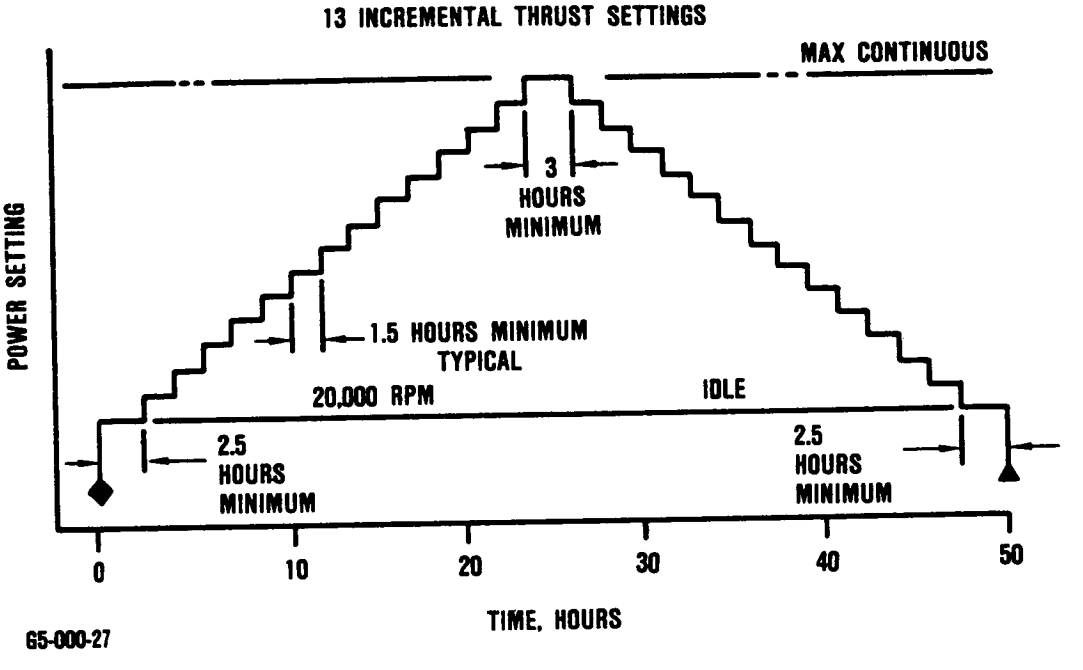

Figure 67. First 50-Hour Test - High-Cycle-Fatigue Evaluation.

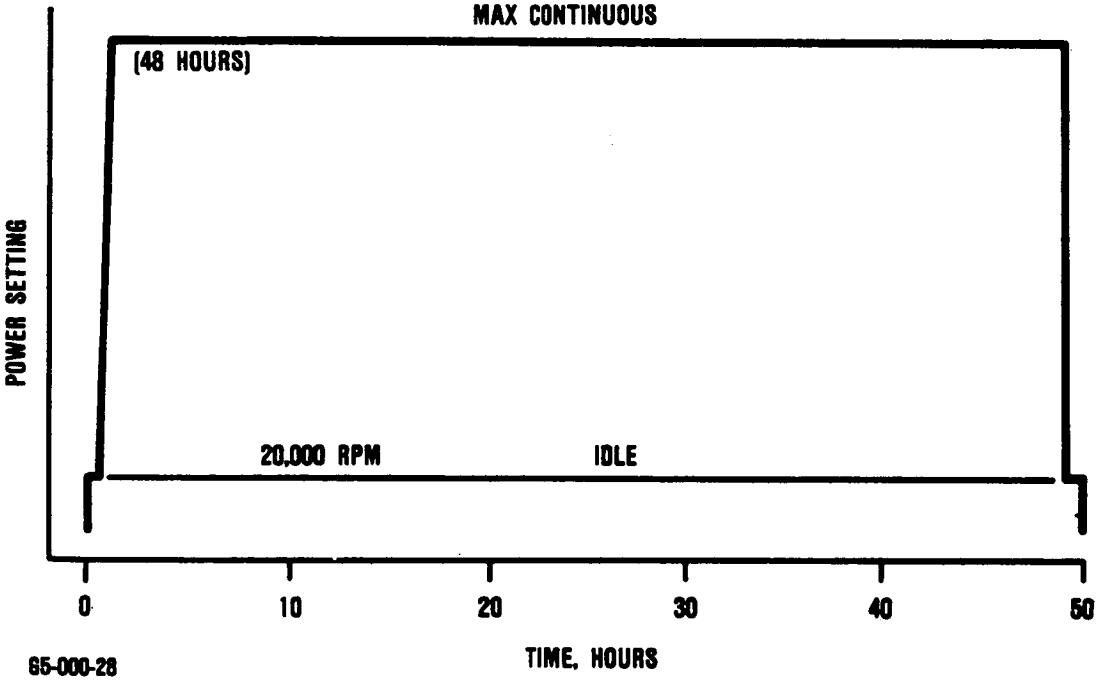

Figure 68. Second 50-Hour Test - Stress-Rupture Evaluation.

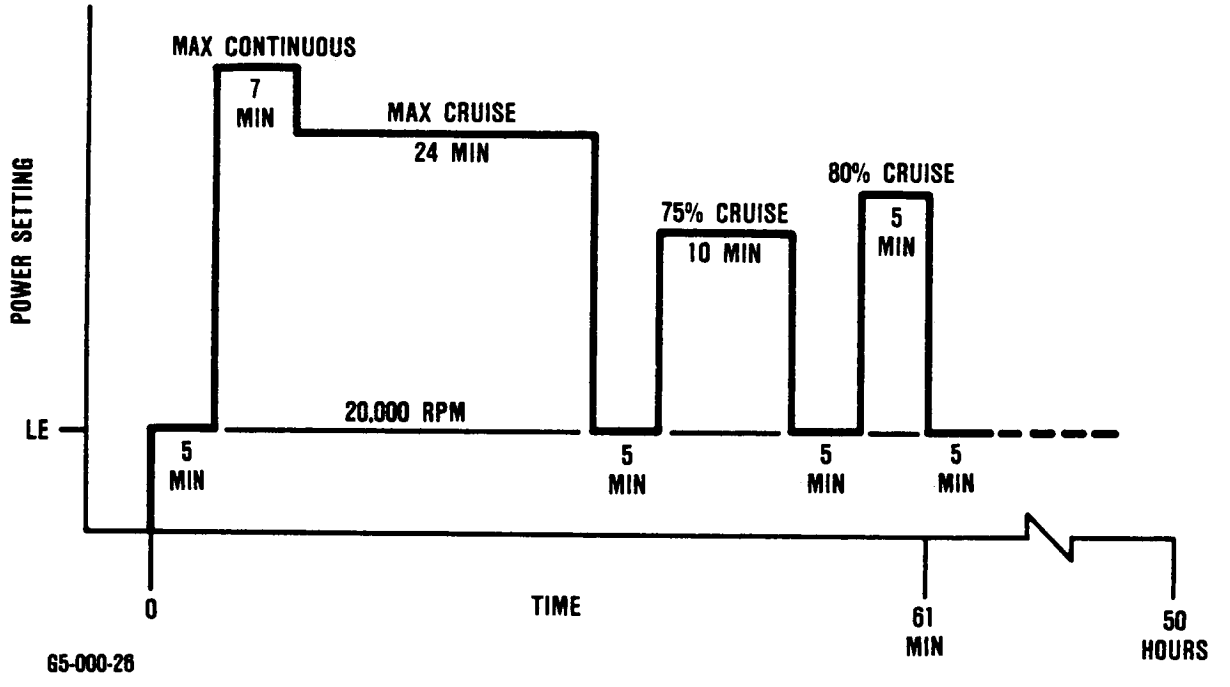

Figure 69. Cycle C: Third 50-Hour Test, Simulated Commuter Aircraft Mission.

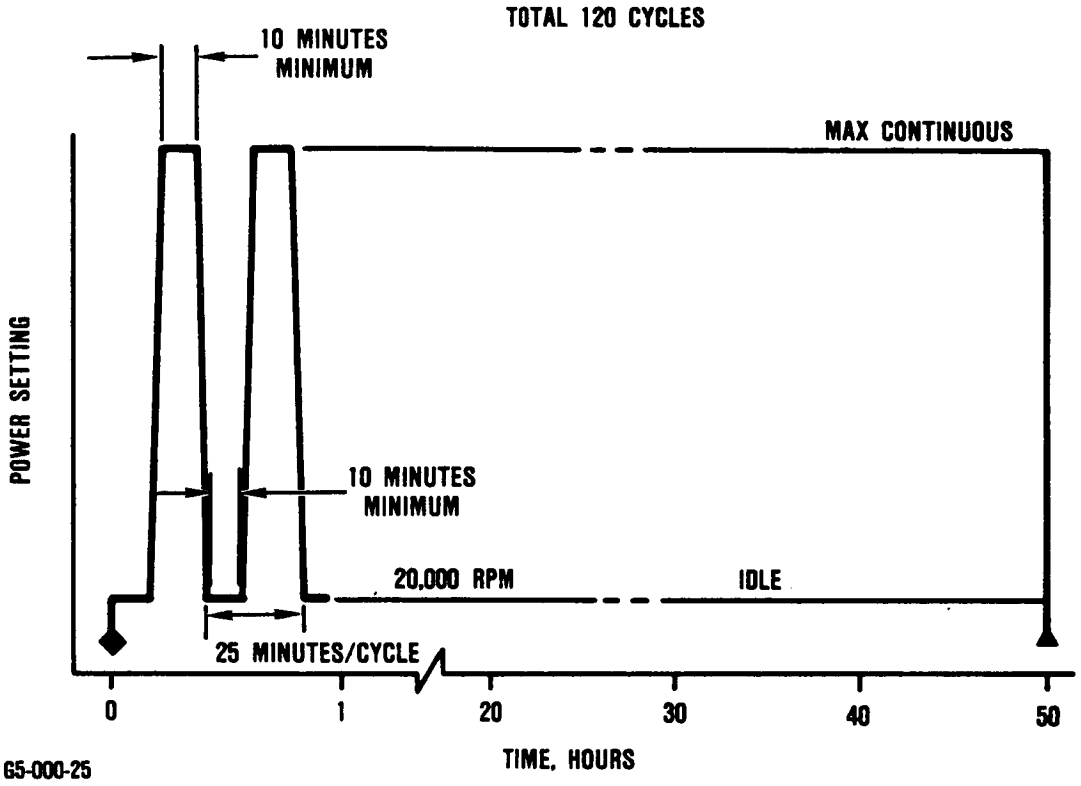

Figure 70. Fourth 50-Hour Test - Low-Cycle-Fatigue Evaluation (Normal Accels and Decels Required).

TABLE 25. NORMALIZED SPEED AND TEMPERATURE FOR EACH OPERATING POINT

Condition	N_2/N_{Design} rpm/rpm	$T_4/T_{4\ Design}$ $^oR/^oR$	$T_3/T_{3\ Design}$ $^oR/^oR$
Max Power (Design)	1.0	1.0	1.0
Max Continuous	0.999	0.997	0.990
Max Cruise	0.988	0.976	0.972
80% Cruise	0.959	0.923	0.919
75% Cruise	0.952	0.910	0.904
Idle	0.673	0.628	0.579
Step down 1	0.989	0.978	0.974
Step down 2	0.980	0.960	0.956
Step down 3	0.969	0.941	0.938
Step down 4	0.959	0.923	0.919
Step down 5	0.948	0.904	0.897
Step down 6	0.936	0.883	0.874
Step down 7	0.921	0.860	0.847
Step down 8	0.905	0.836	0.819
Step down 9	0.888	0.812	0.789
Step down 10	0.865	0.788	0.756
Step down 11	0.842	0.761	0.720
Step down 12	0.807	0.728	0.681
Step down 13	0.755	0.680	0.634

TABLE 26. STRESS-RUPTURE DAMAGE FRACTION

Cycle	Airfoil 30 Percent Span	Blade Firtree Top Lobe ($\times 10^{-3}$)	Blade Firtree Middle Lobe ($\times 10^{-6}$)	Blade Firtree Bottom Lobe ($\times 10^{-9}$)	Disk Firtree Top Lobe (10^{-3})	Disk Firtree Middle Lobe (10^{-4})	Disk Firtree Bottom Lobe (10^{-4})
A High-Cycle Fatigue	0.0015	0.011	0.028	0.044	0.048	0.070	0.017
B Stress-Rupture	0.140	0.13	0.36	0.63	0.56	0.85	0.21
C Low-Cycle Fatigue	0.026	0.019	0.046	0.069	0.085	0.13	0.030
D Simulated Commuter Aircraft	0.072	0.055	0.14	0.23	0.25	0.34	0.081
Total	0.253	0.21	0.57	0.97	0.92	1.4	0.34

Comparison of the rupture life of the MA6000 blade with that of the CMSX-3 single crystal blade at T_4 = 1930F and 29700 rpm indicates that the MA6000 blade has 44 percent longer life than the single crystal blade.

SECTION VII

7.0 COMPONENT MANUFACTURE

The object of this part of Project 4 was to manufacture and quantify at least three complete sets of MA6000 blades and one set of all required components for testing these blades.

Studies conducted earlier (Section V - Blade Manufacturing Process Selection) established the optimum fabrication technique for the MA6000 blades. ECM of the blade airfoil and shank plus conventional grinding of the root firtree section were identified as the fabrication steps in the production of the blades required for component and engine testing.

All heats for each individual lot received from INCO (Wiggins) in this program are summarized in Table 27. To provide traceability of each blade manufactured, every bar from each heat/lot combination was divided into sections representing a blade blank and identified as shown in Figure 71. The first integer represents the lot number, the second set represents the heat number, the third set is an extrusion bar number, and the letter represents a sequential blade blank identification from the beginning to the end of that particular extrusion lot. Thus, in Figure 71:

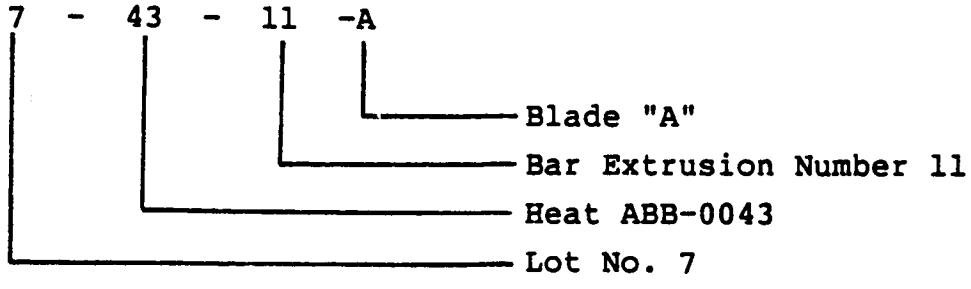

TABLE 27. LIST OF HEATS USED IN THE PROJECT 4 PROGRAM.

Lot Number	Heat Number
1	ZG-0077
2	ABB-0040
3	ABB-0040
4	ABB-0040
5	ABB-0041
6	ABB-0041
7	ABB-0041 ABB-0043
8	ABB-0046 BBB-0068

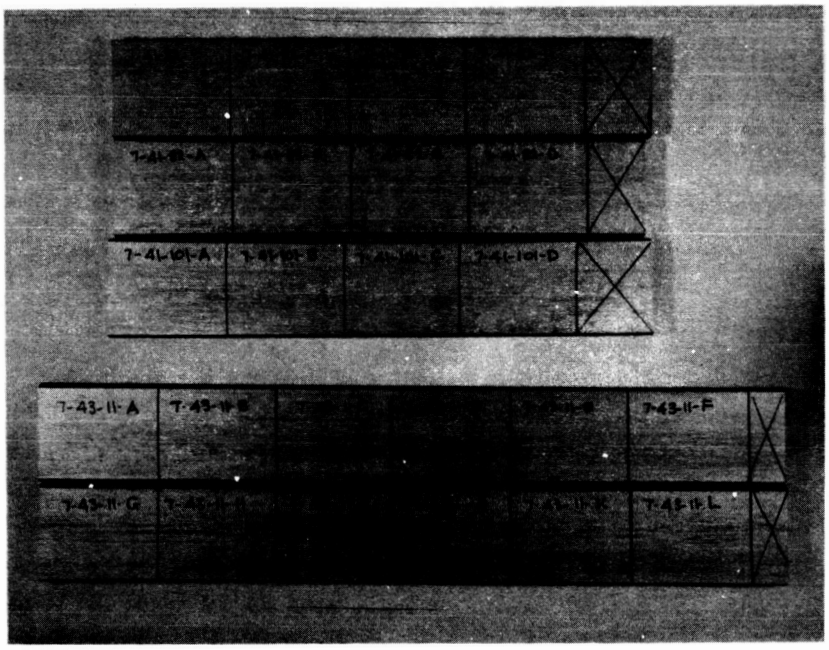

Figure 71. MA6000 Bar Identification.

A total of 168 blades were manufactured in this program, 56 of which were the interim design used during the component testing. Figure 72 shows the assembled blades and disk. The results of this testing led to the conclusion that the interim design was acceptable as the final design. Two sets of blades (112) were then ordered for the engine test. During the machining operation at the vendor, the blade shank was erroneously ECM'd with a tangential shift of 0.06 inch (average) with respect to the airfoil. Because all of the 112 blades in process were machined with this error and MA6000 bar stock was scarce, a 2-D model of the firtree was constructed to evaluate the blade and attachment life with and without the machining error. Three cases were evaluated.

- Blade as designed
- Blade as manufactured with machining error
- Blade with firtree shifted 0.025 inch toward mismachined shank

The latter case was evaluated to determine if the firtree should be repositioned when grinding in the next operation. Calculated firtree lives for all three cases were in excess of the cycles projected for the engine test. Therefore, the firtree was not repositioned and the mismachined blades were finished with the firtree as designed. For details of this analysis see Appendix A.

Because the mismatched blades were no longer exactly like the blades evaluated in the high rotor rig, it was considered a slight possibility that the vibration results of the high rotor rig test were not applicable to the mismanufactured blade. Therefore, it was recommended that the high rotor rig blades be used in the engine test. Sixty of the "best" mismachined blades were identified as substitute blades for the engine test and completed. Thus, a total of 116 blades were purchased, 56 properly machined as designed, and 60 with mismatched shanks but otherwise per the design. The mismatched blades are interchangeable with the "as-designed" blades.

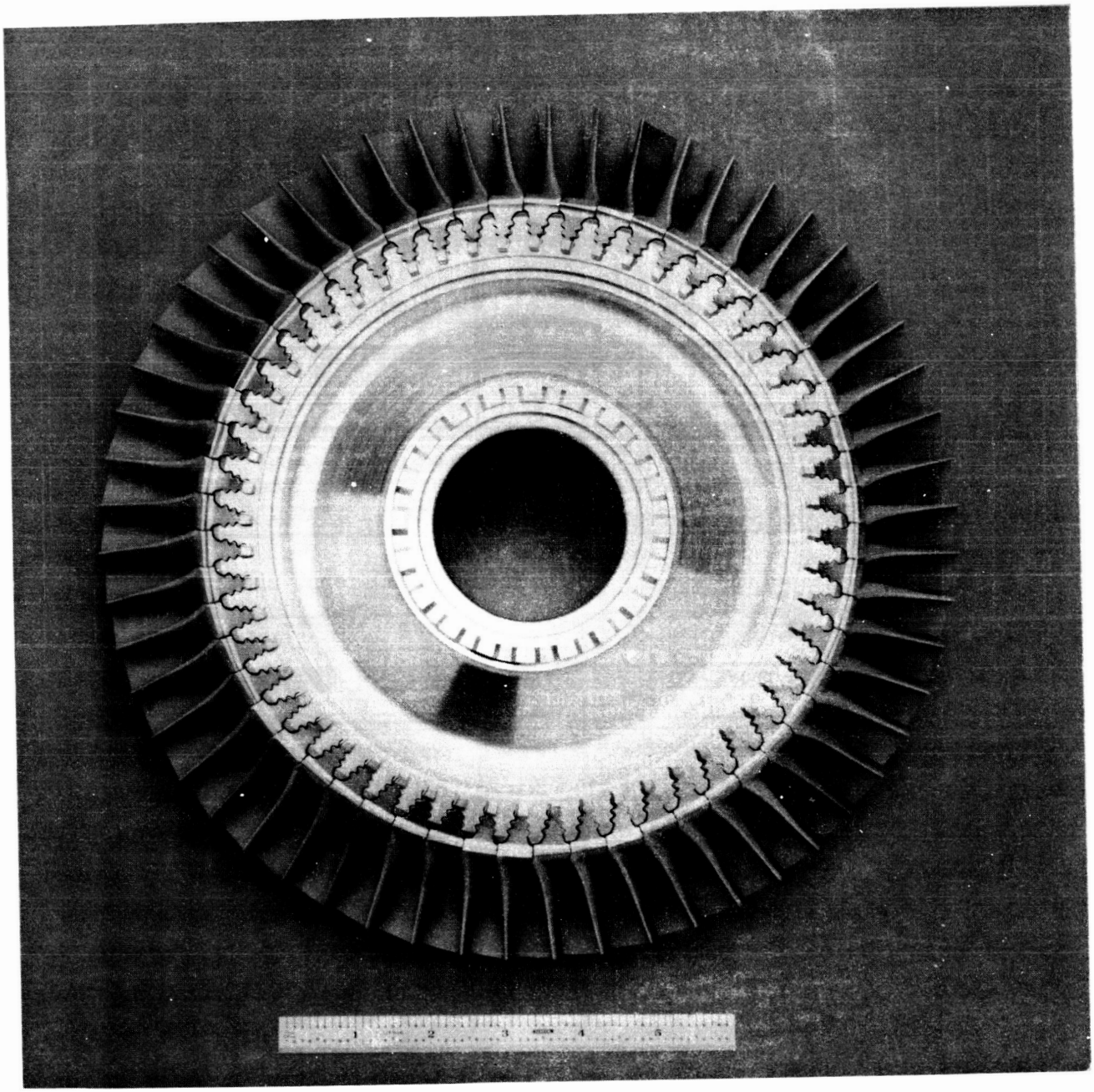

Figure 72. Assembled Interim Blades and Disk for High-Rotor-Rig Testing.

SECTION VIII

8.0 COMPONENT TESTING

To ensure successful completion of the engine test of the MA6000 TFE731 high pressure turbine blades, various component tests were conducted:

1. Vibration Tests
2. Whirlpit Test
3. High-Rotor-Rig Test

8.1 Vibration Tests

Vibration in turbine blades causes alternating stresses that affect the blade's high-cycle-fatigue life. Therefore, maximum alternating strains must be determined prior to engine testing. Alternating strains can be minimized by avoiding excitation sources at resonant frequencies.

Holography and shaker tests of strain-gaged blades were conducted to determine the frequency, mode shapes, and blade critical strain locations. Results of this test were compared to holography prediction and frequencies were in agreement. Holographic mode shapes and predicted natural frequencies for the first four modes at room temperature are shown in Figure 73.

The shaker test consisted of strip gages mounted on the leading edge, tip, and trailing edge of the blade (Figure 74). The blade was clamped at the shank and was vibrated with gradually increasing shaker frequency. At each gage location, the shaker frequency and strain were recorded. The blade resonance condition, defined by a sharp increase in strain amplitude, and mode frequency and maximum strain location were determined. Figure 75 shows a sample recorded resonant condition of one blade.

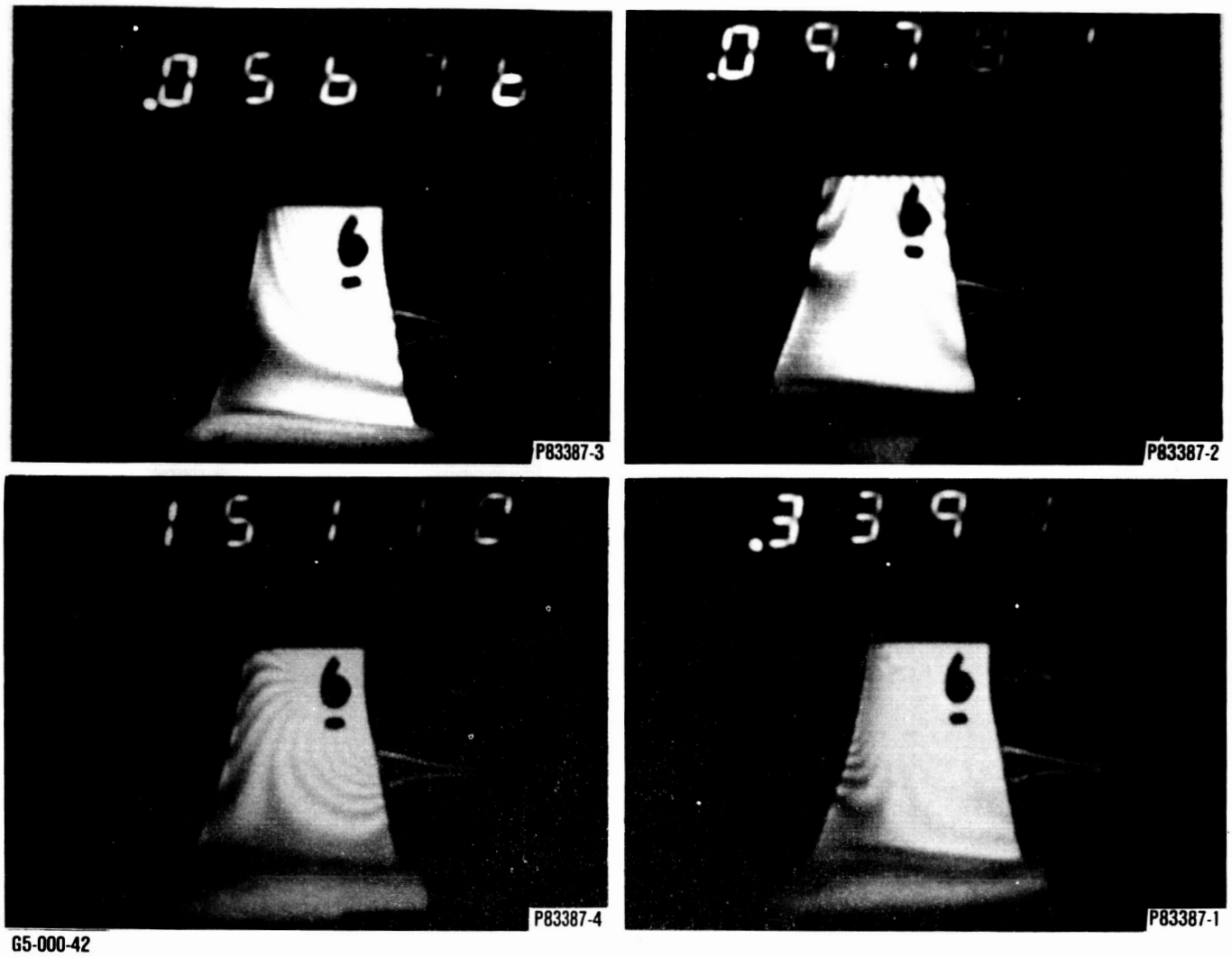

Figure 73. Holography Results for NASA/MATE MA6000 Blade.

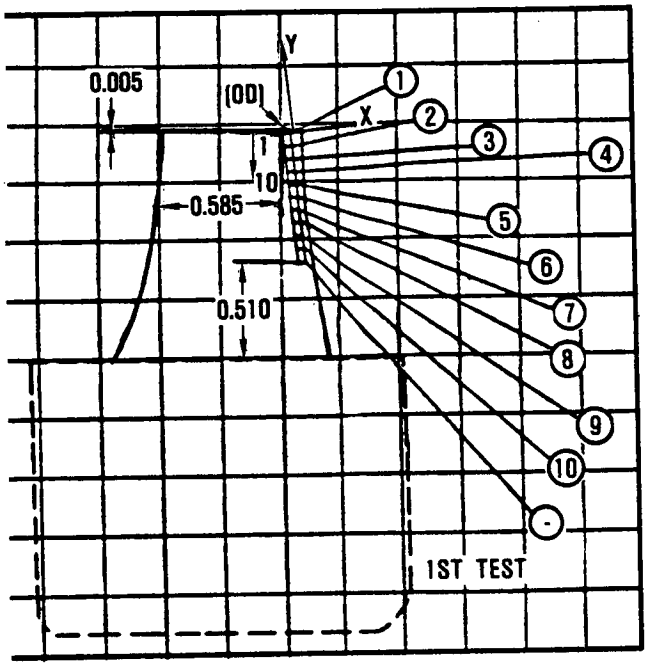

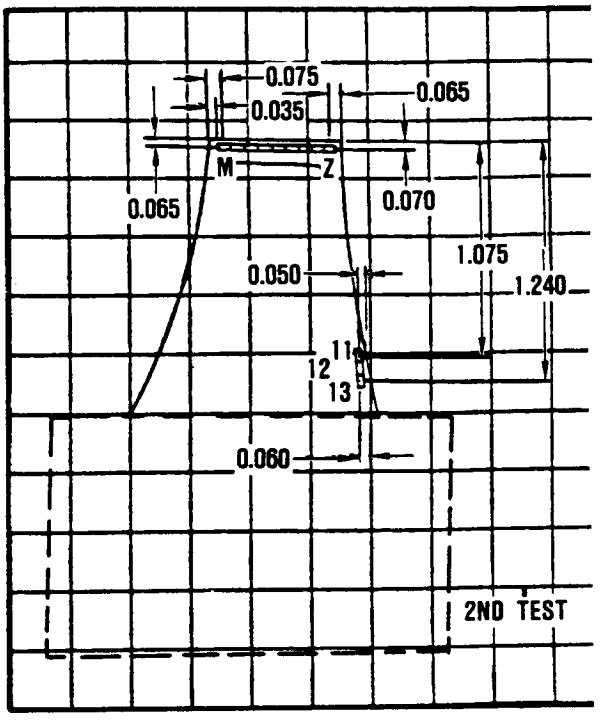

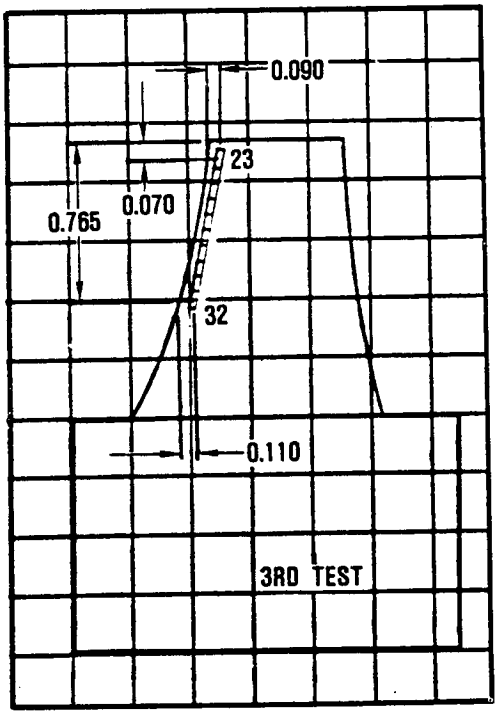

G5-000-31

Figure 74. Location of Strain Gages for the First, Second, and Third Shaker Tests.

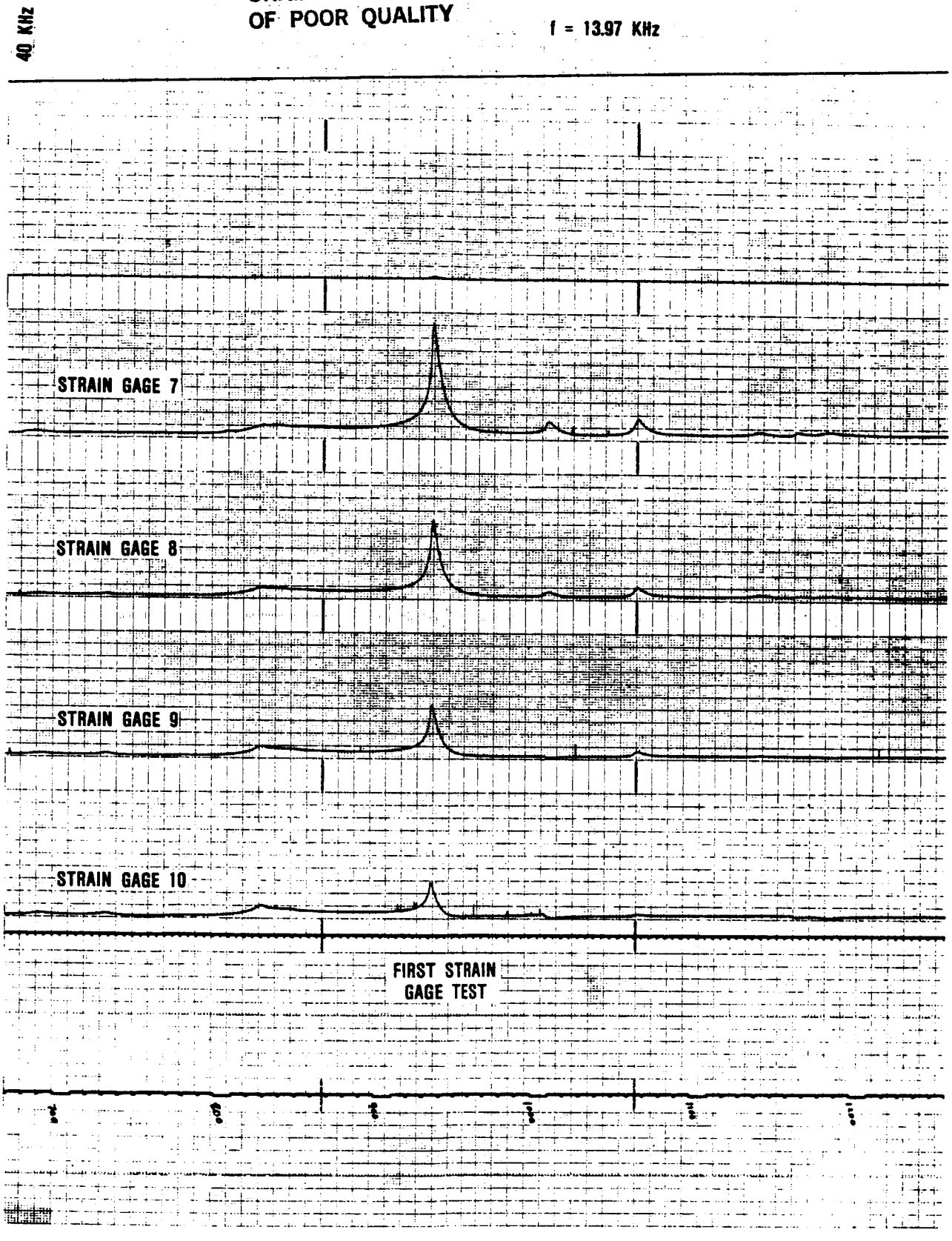

Figure 75. A Sample Resonant Condition Recorded from the Shaker Test.

Since recorded strain during the shaker tests is a variable that depends on the amplitude of the forcing function (shaker) and the degree of damping, actual engine strains could be quite different. However, the critical locations will be similar.

8.2 Whirlpit Test

The structural integrity of the MA6000 blade airfoil and its firtree attachment was verified by a whirlpit test. Four MA6000 blades were whirlpit-tested in a 17-4 stainless steel test disk at a speed equivalent to the maximum operating speed (31,100 rpm). The whirlpit test rotor assembly is shown in Figure 76. Zyglo penetrant inspections and measurements of key locations were taken prior to and upon completion of the test. No indications of incipient failure or critical distortion were found.

8.3 High-Rotor-Rig Test

A high-rotor-rig test was conducted to evaluate MA6000 airfoil vibratory strains under engine conditions. Figures 77 and 78 show the locations of strain gages used in this test. The HFN-063 type gages were positioned at locations where maximum vibratory stress was indicated by the holographic and strip-gage tests and engine experience. Four strain gages were attached to the disk: two measuring radial strains and two measuring circumferential strains.

At typical turbine exhaust temperature, the rotor was run up to 102 percent rated speed. The maximum indicated disk strain was a circumferential strain of 60με p-p (microstrain, peak to peak) at frequencies of 11280 to 11320 Hz. At 57 percent and 84 to 94 percent rated speed, blade excitations were noted. All blade excitations with amplitudes greater than 100με p-p are summarized on the experimental Campbell diagram shown in Figure 79. The maximum allowable amplitude was 750με p-p. The strongest blade excitation

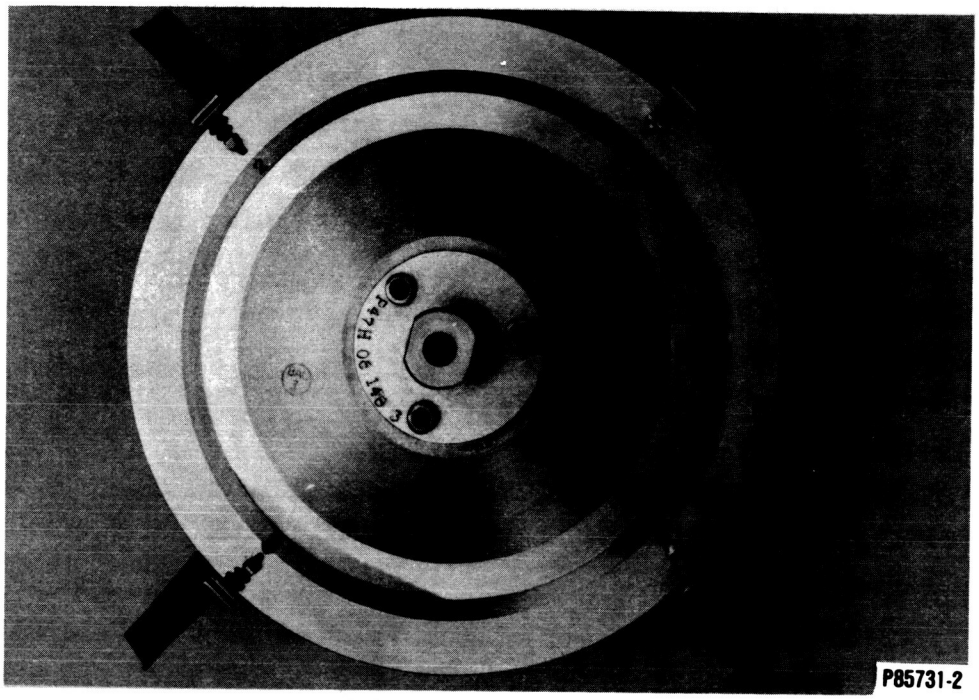

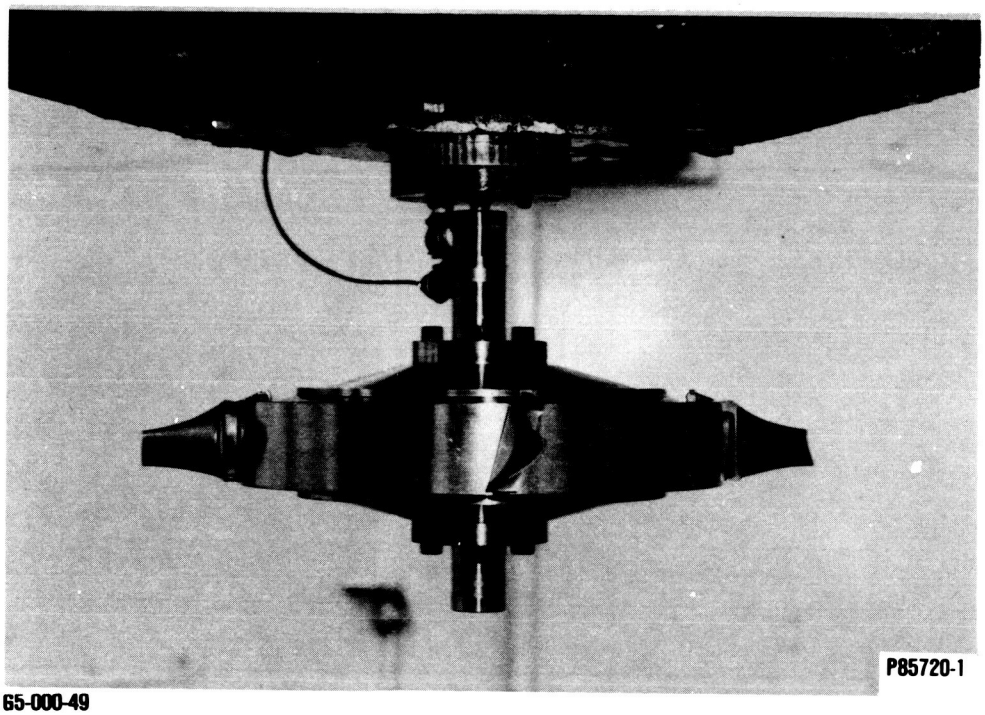

65-000-49

Figure 76. NASA/MATE MA6000 Blade Whirlpit Test Rotor Assembly.

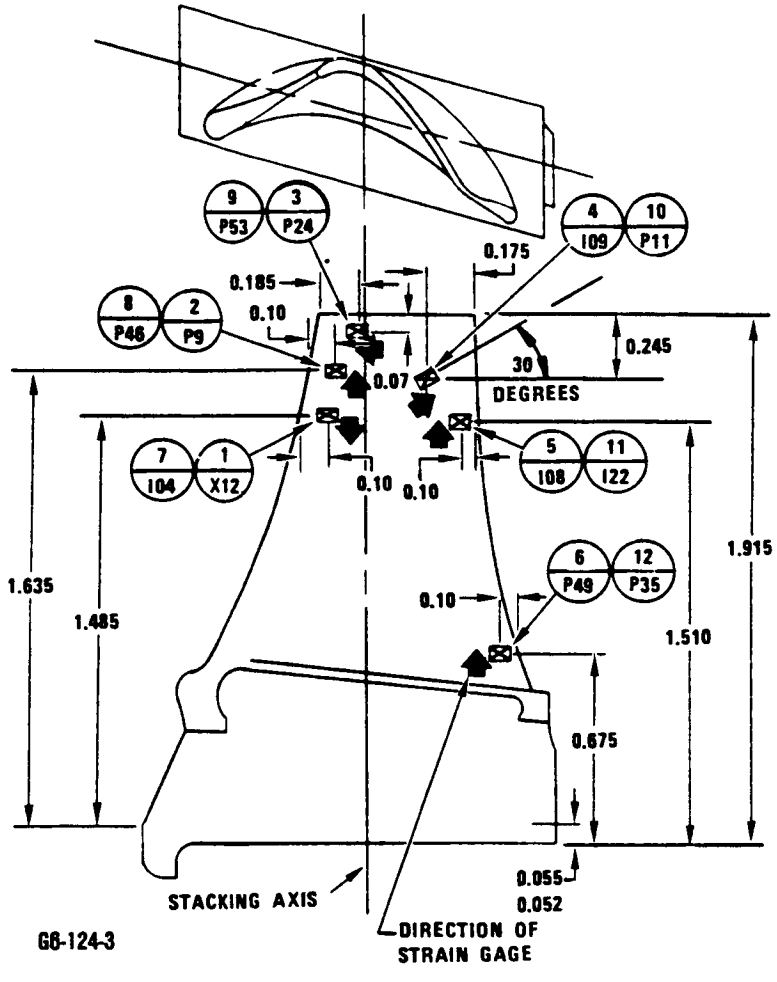

STRAIN GAGE INSTALLATION:

- ALL GAGES TO BE INSTALLED ON PRESSURE SIDE SURFACE
- ONE GAGE ONLY PER BLADE
- DYNAMIC HIGH TEMPERATURE STRAIN GAGE TO BE USED
- TWO BLADES FOR EACH STRAIN GAGE LOCATION

Figure 77. MA6000 Turbine Blade Strain Gage Locations for Whirlpit Test.

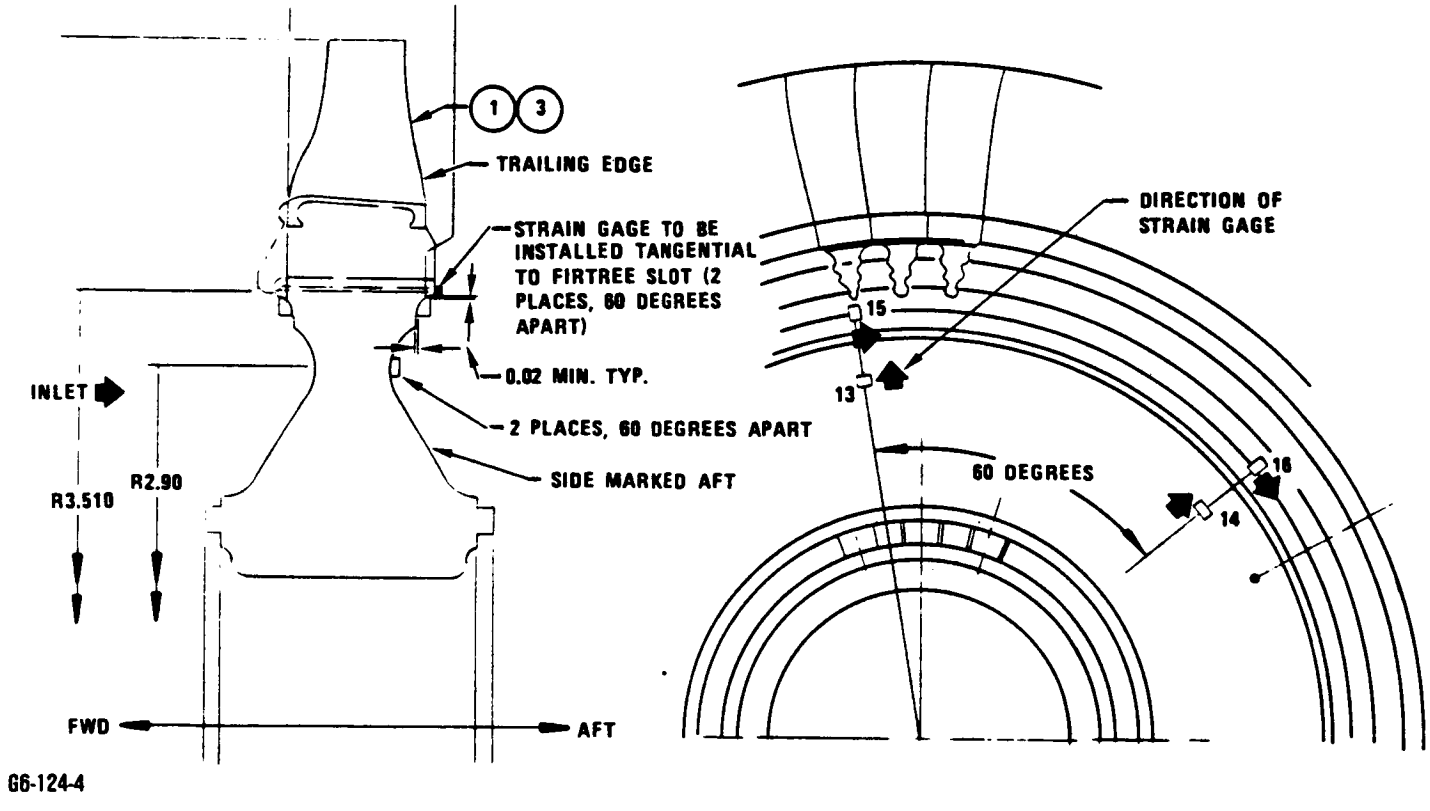

Figure 78. Strain Gage Location on NASA/MATE Disk for Whirlpit Test.

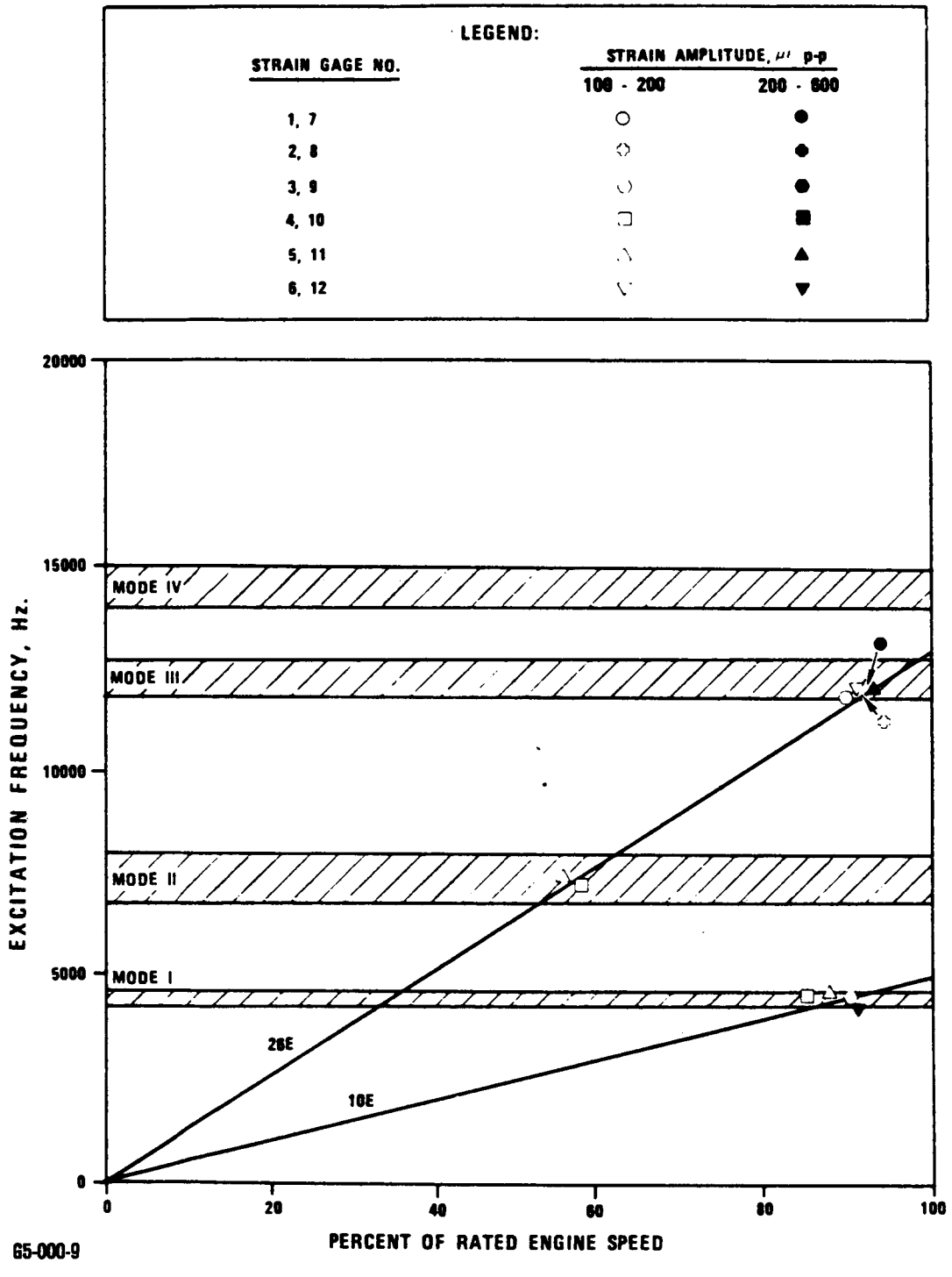

Figure 79. Experimental Campbell Diagram for NASA/MATE MA6000 Blade Excitations.

was the third mode (12320 Hz) excited at 94 percent rated speed at location 5/11, having a maximum amplitude of 516 p-p. In Figure 78, the designations 10E and 26E represent 10 and 26 excitations per engine revolution, respectively. The 26E corresponds to the 26 HP stator vane count. The source of the 10E may be the combustion pattern output. No signs of blades or disk defects were detected by the posttest fluorescent penetrant inspection.

SECTION IX

9.0 COST ANALYSIS

9.1 Introduction

The object of this study is to compare the finished costs of the following three blade designs:

(1) The current uncooled DS MAR-M 247 TFE731-3B production blade. This blade was developed during MATE Project 1.

(2) A hypothetical blade, having the same configuration as the TFE731-3B production blade, but made from the commercially available SC material, CMSX-3. This blade is used for comparison purposes in lieu of the actual Project 3 blade, which was of a slightly different configuration and made from the GTEC-developed SC materials, NASAIR 100 and Alloy 3.

(3) Project 4 uncooled ODS MA6000 blades.

This comparison is based on the production of 2000 to 3000 blades per month during the 1985-1990 time period. Preliminary and final cost studies were completed as part of this task. The key elements of each study are:

- Material cost (raw material for DS and SC blades and bar-stock for MA6000 blades)
- Processing cost
  - Casting

- Machining

- Coating

o Other costs (inspection and handling)

For the relative comparison, the DS MAR-M 247 TFE731-3B production blade cost was given a value of 1.0.

9.2 Preliminary/Final Cost Analysis

9.2.1 DS MAR-M 247 Project 1 Blade

The DS MAR-M 247 solid (uncooled) TFE731-3B turbine blade is a current production part developed under MATE Project 1. For the 1985-1990 time period, cost projections for lots of 2000 to 3000 blades per month were provided by the GTEC financial analysis department. A preliminary cost analysis was performed in late 1982. The final analysis was performed in early 1985 using the same procedure as the preliminary study. Table 28 and Figure 80 summarize the results. Handling and inspection are included in each cost element.

TABLE 28. TURBINE BLADE RELATIVE COST COMPARISON

Material Name	Material	Casting	Machining	Coating	Total
DS MAR-M 247 Uncooled	0.07	0.52	0.32	0.09	1.00
SC CMSX-3 Uncooled	0.11	1.07	0.32	0.18	1.68
ODS MA6000 Uncooled	0.48	0.66**	0.44	0.36*	1.95

*Coating Costs quoted by Vendor
**Casting Equivalent Includes Preform Machining Plus airfoil and Shank ECM.

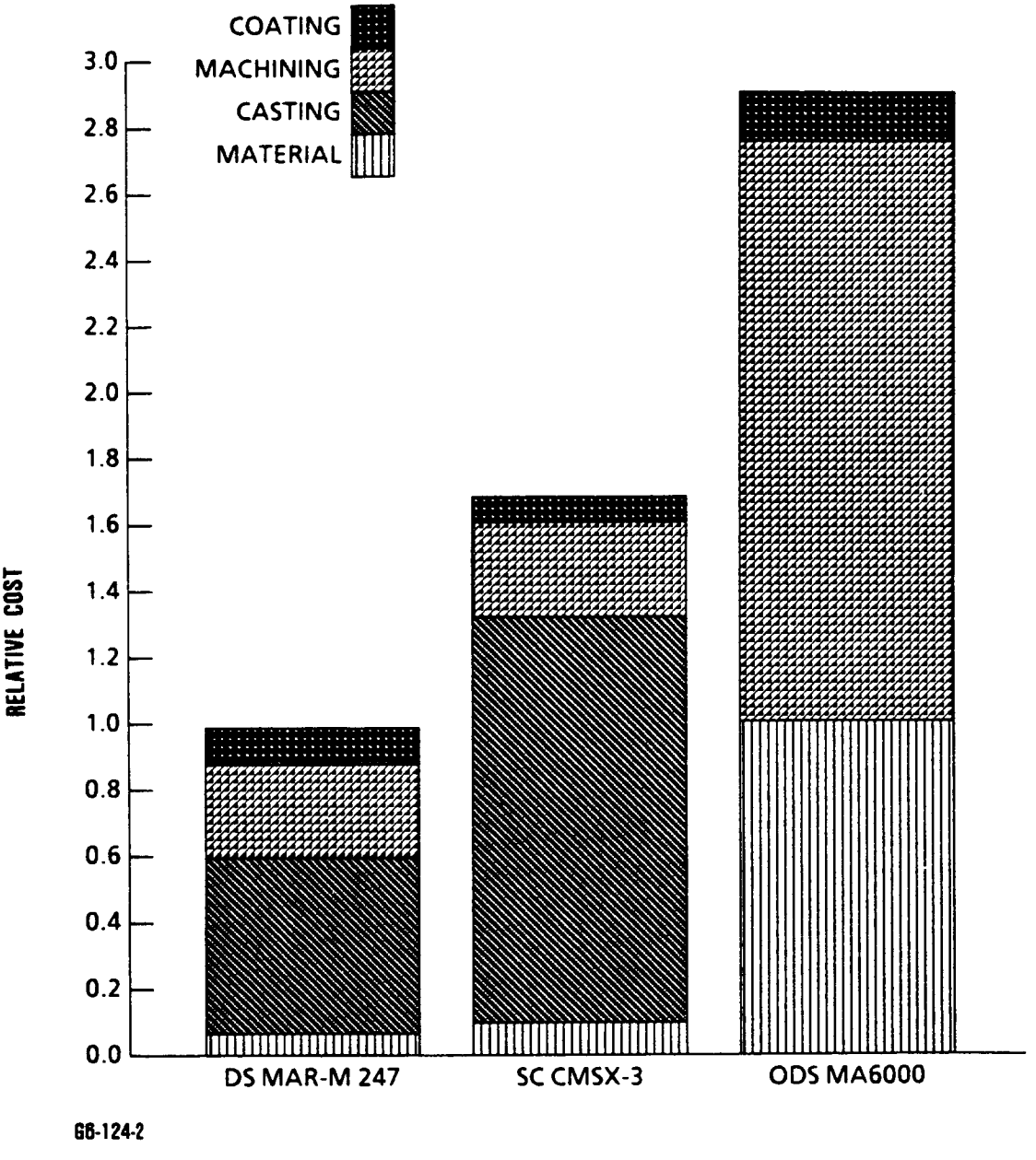

Figure 80. Final Cost Comparison.

9.2.2 SC Project 3 Blade

The same procedure was used for both the preliminary and the final cost studies. However, for the final study, the SC material was changed from NASAIR 100 used in the preliminary study to the more readily available CMSX-3. The cost projections are presented in Table 28 and Figure 80. Inspection and handling charges are included in the costs shown.

9.2.3 MA6000 Project 4 Blade

The preliminary cost analysis of the Project 4 MA6000 blades was conducted in late 1982. This analysis was based on the results of Tasks I and II, GTEC manufacturing cost data, and qualified supplier's experience. This data was updated for the final cost analysis, which was conducted in mid-1986.

9.2.4 Material Costs

In April 1981, based on commercial production and analysis of the learning curve, INCO estimated that the cost to produce fully heat-treated MA6000 barstock was approximately $165/lb. This projected cost was used as the base price in the preliminary cost analysis.

In April 1984, INCO updated their estimate to project the price of hot-rolled MA6000 barstock in the 1985 to 1990 time period. The price was expected to be approximately $80-$100/lb for unrecrystallized barstock and $100-$120/lb for fully heat-treated barstock. The price for fully heat-treated barstock was used in calculating the cost for the final cost analysis. Near net turbine shaped barstock was used to determine the minimum amount of material required to produce a turbine blade.

9.2.5 Processing Cost

Due to unfamiliarity with the MA6000 material, accurate preliminary projections for machining costs were not available from machining vendors to project high volume production of MA6000 blades in the 1985 to 1990 time period. However, the costs were tentatively estimated based on GTEC manufacturing experience and experience gained from the preliminary study on machining the MA6000 material. The preliminary estimate included the costs of machining the barstock to near net shape, ECM of the airfoil and platform pocket, and grinding the firtree.

For the final cost analysis, relative cost estimates for machining the ODS MATE blade were provided by TRW:

1.	Machine preform blade	0.04
2.	ECM airfoil and shank	0.62
3.	Grind firtree and platform, cut to length, and mark	0.44

Items 1 and 2 produce a part that is similar in form to a casting with all surfaces formed except those requiring finish grinding. Therefore, the combined costs of Items 1 and 2 can be compared to the casting cost for DS or SC turbine blades.

The tooling required to produce the high rotor rig and engine test blades was made earlier in the program when the engine test blades were being manufactured. Therefore, no additional tooling charge will be required in the future.

Coating recommendations for MA6000 are based on the test results from Task IV. These results indicate that MA6000 can be effectively coated provided that diffusional stability with the substrate is maintained. NiCrAlY coatings are recommended, based on oxidation resistance and diffusional stability considerations.

Chromalloy Research and Technology Division provided the cost estimate for applying NiCrAlY coating to MA6000 turbine blades. This estimate was based on their experience and high volume production costs. Two methods for applying the coating were suggested: electron beam physical vapor deposition (EB-PVD) and low pressure plasma spray (LPPS). The EB-PVD coating cost estimate was used for this cost comparison, since the LPPS coating cost was almost double the EB-PVD cost.

9.2.6 Inspection Costs

Internal inspection and handling costs were added to the material and processing costs to establish a total manufacturing cost to GTEC. This total cost can be compared with the production costs of the exothermic DS and SC cast TFE731 blades developed in MATE Projects 1 and 3.

Under normal circumstances, none of the blades for production engines are routinely inspected at GTEC. All inspection/quality control is done by the supplier with inspection costs included in the part cost from the supplier. Each supplier is monitored by GTEC Quality Control. The cost of these Quality Reviews are part of the GTEC overall quality assurance cost of operation and is not chargeable to a single part or production source.

The inspection cost for the MA6000 barstock is included in the price estimate from INCO. Similarly, the inspection (ZYGLO and dimensional checks) costs are included in the cost estimate from TRW. Therefore, for comparison purposes, inspection costs are not considered as a separate item.

GTEC handling charges vary from month to month. An average of 10 percent has been selected for this study. Handling costs were included in each cost element for this analysis.

9.2.7 Summary

All the above costs are presented in Table 28 and Figure 80. Results of the final cost study indicate that a MA6000 blade costs approximately twice (1.95) that of a DS cast blade, based on currently available information. The cost projection for production quantities of MA6000 blades in the 1985 to 1990 time period is significantly lower than the preliminary projections (1.95 versus 2.91). This projection reflects the added experience gained by the suppliers with this new material, which has increased their confidence in their ability to control the processing. As more experience is gained with this material, particularly if a pre-ECM forging technique can be developed, the cost of the MA6000 turbine blades is expected to decrease even more.

SECTION X

10.0 SUMMARY OF RESULTS

Process Optimization

Production scale up of the MA6000 alloy was achieved. There is a fair degree of tolerance to nonoptimum processing.

The blade manufacturing process also was optimized. Grinding is used for the firtree area and the blade airfoil shape is generated by electrochemical machining (ECM). The manufacturing process was verified through the manufacture of three complete sets of MA6000 blades and one set of all components needed to test these blades.

Material Properties

The ultimate tensile strength of MA6000 is higher, to about 704C (1300F), but with a corresponding lower tensile elongation compared with DS MAR-M 247. A crossover occurs between 704C (1300F) and 982C (1800F) due to the higher gamma prime volume fraction of MAR-M 247. Above 982C (1800F) MA6000 again has higher strength than DS MAR-M 247. At higher temperatures and lower stresses, MA6000 is clearly superior to DS MAR-M 247.

Based on oxidation resistance and diffusional stability considerations, NiCrAlY coatings are recommended. CoCrAlY coating should be applied on top of a thin NiCrAlY coating if hot corrosion conditions are anticipated.

Blade Design

An MA6000 blade design requires a high taper ratio because of low blade stress. This design utilizes the material's good rupture characteristics to provide improvement in blade life and turbine performance. The design was validated through component evaluation and engine test (Volume II). MA6000 has potential for uncooled turbine blade applications.

Component Testing

The Campbell diagram analysis of the results of the vibration test of the turbine blades indicated maximum alternating strain of less than 520με peak to peak. This strain level is within the acceptable range.

Cost Analysis

In production quantities, the cost of the Project 4 MA6000 blade is estimated to be about twice that of a cast DS MAR-M 247 blade.

General

The significant improvement in metal temperature capability associated with MA6000 will allow increased turbine efficiency in small- to medium-sized turbofan engines for business and commuter aircraft.

APPENDIX A

DETAILED EVALUATION OF MISMACHINED BLADES

The details of the evaluation of the MA6000 blade and attachment life with and without machining errors are present in this appendix. The 2-D model of the firtree is shown in Figure 81. The resulting firtree stresses and their corresponding LCF lives for the following three cases are presented in Table 29:

- Blade as designed
- Blade as manufactured with machining error
- Blade with firtree shifted 0.025 inch toward mismachined shank

As part of this study, the effect of stress concentration, K_T, on shank stresses was analyzed. A 2-D model of the axial section of the blade at Z = 0 was constructed (Figure 82). This section gives the highest moment about the firtree centerline, and due to neglect of shear stress between the axial sections, the calculated stresses are conservative. Table 30 lists the peak firtree and shank stresses for the three cases. Plots of principal stress distribution for the three cases are also provided in Figure 83.

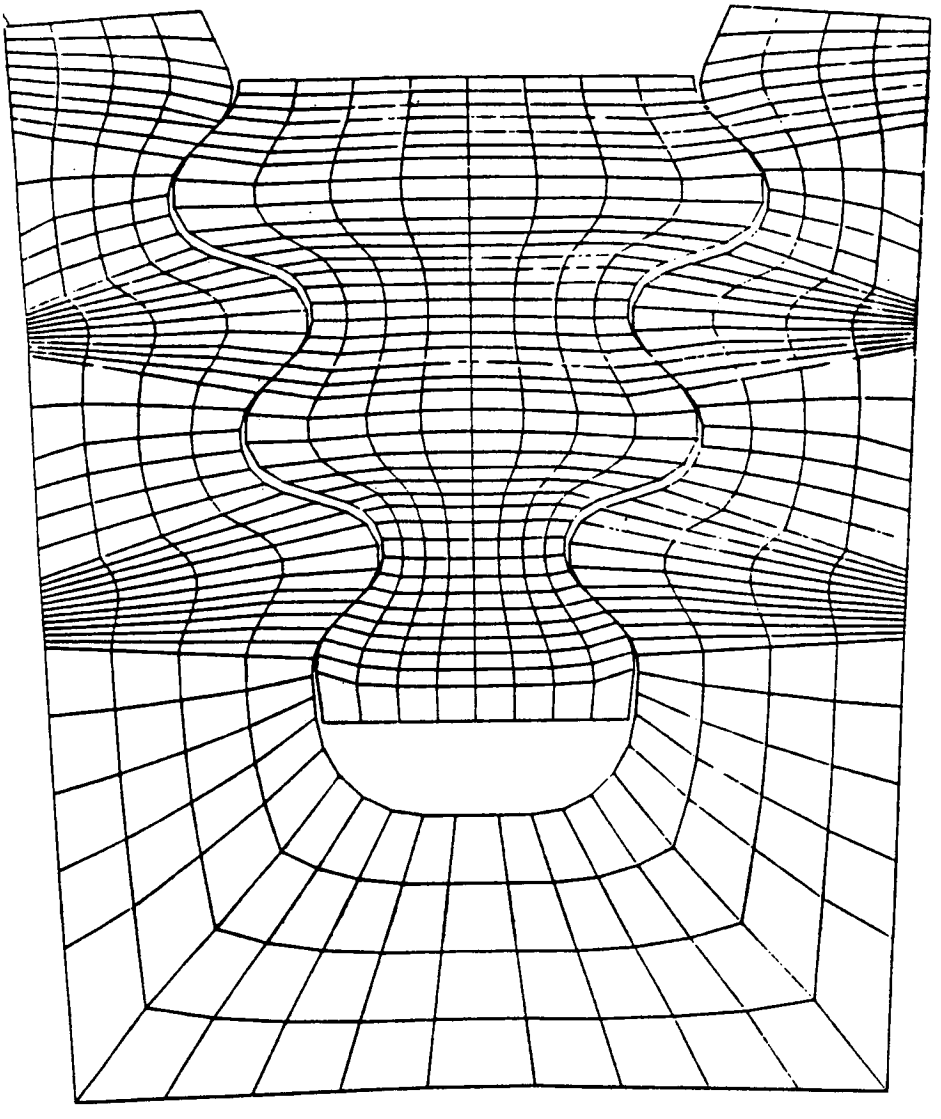

Figure 81. 2-D Mesh Model of the NASA/MATE HP Rotor Attachment.

TABLE 29. SUMMARY OF THE EFFECT OF BLADE SHANK VARIATION ON BLADE LIFE

	Model of the Firtree					Model of the Blades Z = 0 Section					
	P/A (ksi)	M in-lb	Disk σp max.	Blade σp max	Life* Min. (Avg) Cycle	P/A (ksi)	M $\frac{\text{in.lb}}{\text{in depth}}$	Disk σp max	Blade σp max	Shank σp max	Life Min. (Avg) Cycle
I. Blade As Designed	28.2	≈ 0	112.9	90	$>4 \times 10^4$ ($>6 \times 10^6$)	37.2	411.7	263.1	355.3	157.9	103 (163)
II. Blade As Manufactured	28.2	-120.3	116.1	130.8	$>1 \times 10^4$ ($>1 \times 10^5$)	37.9	293.7	212.5	286.2	213.5	184 (332)
III. Blade With 0.025" Shift in Firtree	28.2	≈ 90	≈ 125	≈ 155	>3200 ($>1 \times 10^4$)	38	461.7	282.8	398.5	159.0	84 (127)

*Life is calculated from T = 1400F, R = 1.0, K(T) = 1.0 Strain Controlled LCF data (σy = 120.1, σult = 141.6).

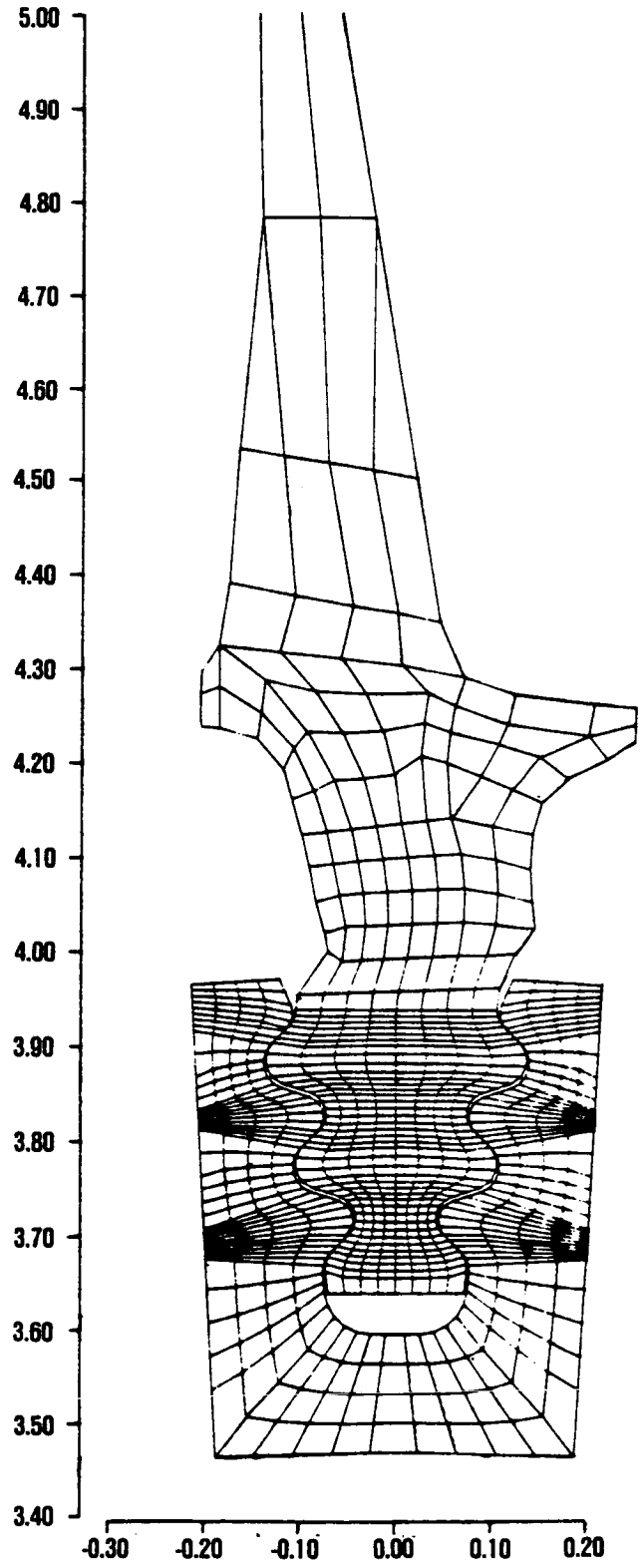

Figure 82. 2-D Model of Z = 0 Section of the Blade.

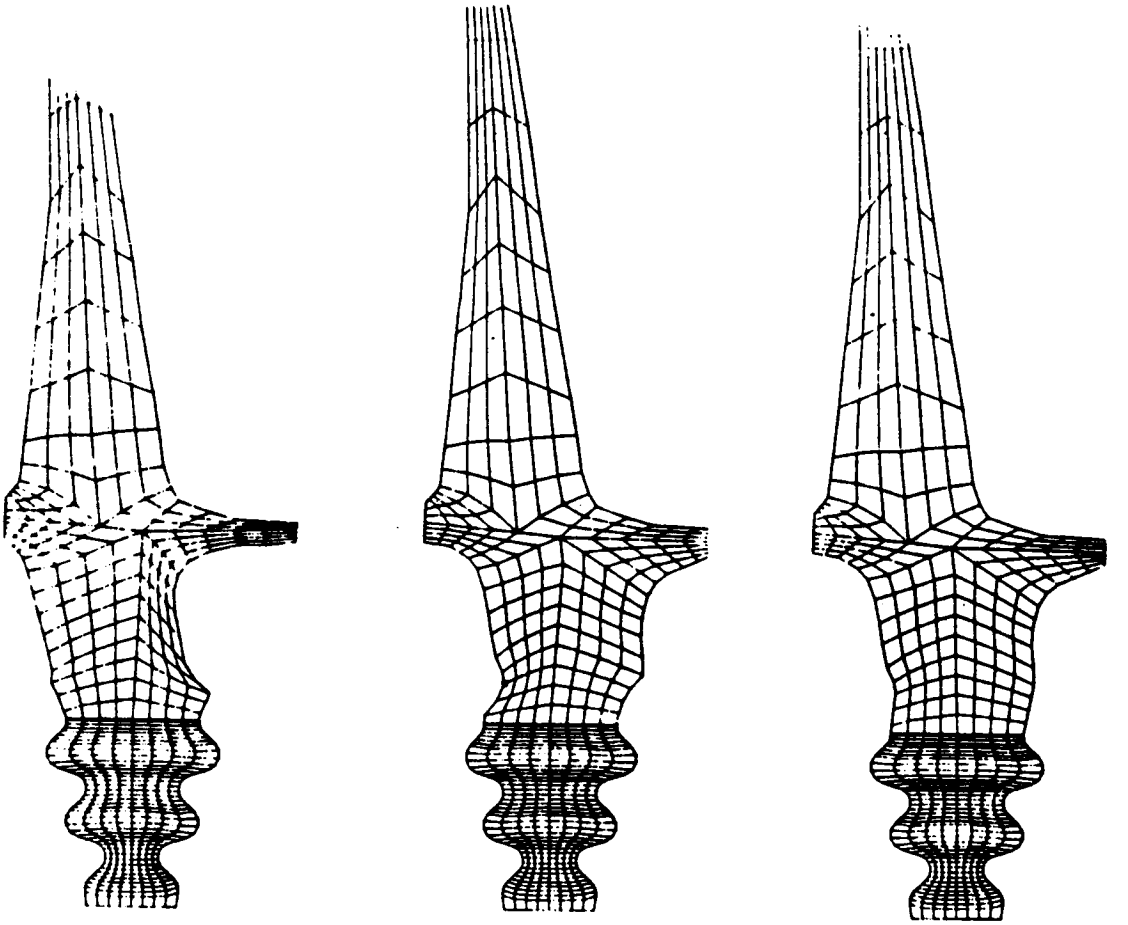

Figure 83. 2-D Model of the Z = 0 Section of Designed and Manufactured Blades.

LIST OF SYMBOLS

T_3	Nozzle exhaust temperature
T_4	Turbine inlet temperature
Y	Gamma phase
Y'	Gamma prime phase
MN	Mega Newton
MPa	Mega Pascal
mm	millimeter
in	inch
ksi	kilopound per square inch
σ	stress
t_f	specimen time at σ
t	expected life at σ
F	sum of fraction lives
$t\sigma$	desired life
σ_t	stress for life of t
KHz	kilo Hertz
K_T	Notch factor
cps	cycles per second
f	frequency
β	Beta phase (CoAl)
N_2	power turbine speed
N_{DESIGN}	design speed
p-p	peak-to-peak
σ_p	principal stress
avg	average
max	maximum
F	degree Fahrenheit
kg	kilogram
lb	pound
C	degree celsius
μmHg	micrometer of mercury

LIST OF SYMBOLS (Contd)

Pa	Pascal
GPa	Grigapascal
psi	pound per square inch
N_f	Total cycles
σ_{ALT}	Alternating stress
σ_{MEAN}	Mean stress
m	meter
mils	milli inch
ppm	parts per million
R	radius
T_5	high pressure turbine discharge temperature
P	radial pull
M	bending moment
F_S	shear force
M_{xp}	bending moment about x plane
M_{zp}	bending moment about z plane
τ_{xp}	x-shear force at blade shank
τ_{zp}	z-shear force at firtree shank
rpm	revolutions per minute
μE	microstrain
σ_y	yield stress
σ_{uH}	Ultimate stress
C	Larson-Miller constant

ATTACHMENT

SPECIFICATION NO. EMS554AD

GARRETT TURBINE ENGINE COMPANY A DIVISION OF THE GARRETT CORPORATION PHOENIX, ARIZONA FSCM 99193	MATERIALS ENGINEERING	SPECIFICATION NO EMS554AD	REV LTR --
CLASSIFICATION Corrosion- and Heat-Resistant		ISSUE DATE	REV DATE

TITLE

BARS, NICKEL ALLOY (MA 6000), MECHANICALLY ALLOYED

REV STATUS																							
	REV	--	--	--	--	--	--	--	--	--													
	PAGE	1	2	3	4	5	6	7	8	9													
	REV																						
	PAGE																						

DRAFT
NOT FOR PRODUCTION

The margins of this specification are marked with a stripe to denote where changes from the previous issue were made. This was done as a convenience only and Garrett assumes no responsibilities whatsoever for any inaccuracies in these notations. Users are cautioned to evaluate the requirements of this document based on the entire content irrespective of the marginal notations and relationship to the last previous issue.

	SIGNATURE	DATE		SIGNATURE	DATE
PREPARER	R. L. Wagner		FAA DER		
MATL ENGR			FAA DER		
OTHER			OTHER		

DRAFT
NOT FOR PRODUCTION

FSCM 99193

SPECIFICATION NO	REV LTR
EMS554AD	--

M300 GTEC SPECIFICATION CHANGE ORDER

RELEASE DATE YY / MM / D

SPECIFICATION NUMBER EMS554AD
SPECIFICATION REVISION LTR. --
CONTROLLED SPECIFICATION G-
C=CONTROLLED G=GENERAL N=NUCLEAR

SPEC. TITLE BARS, NICKEL ALLOY (MA Com), Mech Alloyed
SPEC. SOURCE I
SPEC. TYPE M

DESC.OF CHANGE: New Specification.

REASON FOR CHANGE: New Specification.

** ENTER YES (Y) OR NO (N) **

_ DOCUMENT CHANGE ONLY
_ INTERCHANGEABLE CHANGE INCORPORATE AT DISCRETION OF MANUFACTURING
Y REQUIRED CHANGE. INCORPORATE ON NEXT ORDER
_ MANDATORY CHANGE INCORPORATE WHEN SPECIFICATION RELEASED
_ THIS CHANGE AFFECTS OUTSTANDING PURCHASE ORDERS
_ CUSTOMER NOTIFICATION REQUIRED
SPEC NUMBER NOT ON MASTER FILE - PRESS PF1 KEY TO EXIT

1. SCOPE

1.1 This specification establishes the requirements for MA 6000 bars.

1.1.1 MA 6000 is a directionally recrystallized nickel-base superalloy, strengthened by oxide-dispersion and gamma-prime precipitation.

1.2 This material is used for turbine vanes and blades at temperatures up to 2000°F.

1.3 The product shall be supplied in the following conditions:

Class A - Hot-finished, zone annealed, and fully heat-treated.

Class B - Hot-finished, zone annealed, and solution heat-treated.

If no class is specified, Class B shall be used.

1.4 Definitions

1.4.1 Heat (master powder blend) - A single blend of one or more powder batches manufactured under the producer's fixed process.

1.4.2 Heat number - A number allocated to a heat, assigned and maintained by the supplier.

1.4.3 Lot - All bars cut from a single extrusion, zone annealed, and solution heat treated under the producer's fixed process.

1.4.4 Lot number - A number assigned to a lot and maintained by the supplier.

2. APPLICABLE DOCUMENTS

2.1 Government Documents. The following documents, of issue in effect on date of invitation for bids or request for proposal, form a part of this specification to the extent specified herein.

2.1.1 Federal Standards

Test Method No. 151 - Metals; Test Methods

2.2 Non-Government Documents. The following documents form a part of this specification to the extent specified herein. Unless otherwise indicated, the issue if effect on date of invitation for bids or request for proposal shall apply.

2.2.1 Garrett Turbine Engine Company (GTEC) Specifications

EMS52503 - Source Approval, Melt and Conversion

EMS52309 - Fluorescent Penetrant Inspection

EMS52348 - Radiographic Inspection

EMS52353 - Approval of Material Test Suppliers

PC5006 - Heat Treatment of Quality Assurance Provisions, Control of

2.2.2 Aerospace Materials Specifications

AMS 2269 - Chemical Check Analysis Limits - Wrought Nickel and Cobalt Alloys

2.2.3 American Society for Testing and Materials (ASTM) Standards

E 21 - Elevated Temperature Tension Tests of Metallic Materials

E 139 - Conducting Creep, Creep-Rupture, and Stress-Rupture Tests of Metallic Materials

E 354 - Chemical Analysis of High Temperature, Electrical, Magnetic, and Other Similar Iron, Nickel, and Cobalt Alloys

3. TECHNICAL REQUIREMENTS

3.1 Chemical composition shall conform to the following percentages by weight, determined by wet chemical methods in accordance with ASTM E 354; by spectrographic methods in accordance with Federal Test Method Standard No. 151, Method 112; or by other GTEC-approved instrumentation methods.

COMPOSITION	MIN	MAX
Carbon	---	0.10
Silicon	---	0.50
Manganese	---	0.50
Sulfur	---	0.015
Phosphorus	---	0.015
Chromium	14.0	16.0
Molybdenum	1.5	2.5
Tantalum	1.5	2.5
Titanium	2.0	3.0
Aluminum	4.0	5.0
Iron	---	2.5
Tungsten	3.0	5.0
Boron	0.005	0.015
Zirconium	0.10	0.20
Y_2O_3	0.95	1.25
Nickel	---	Remainder

3.1.1 Composition variations shall meet the requirements of AMS 2269.

3.2 Heat Treatment

Solution Treatment - Heat to 2250° ± 15°F for 0.5 hour ± 3 minutes and rapid air cool.

Initial Age - Heat to 1750° ± 25°F for 8 hours ± 50 minutes and air cool.

Final Age - Heat to 1550° ± 25°F for 24 hours ± 2.5 hours and air cool.

3.2.1 Bars hot-finished, annealed, and heat-treated shall be turned or ground to remove all can material.

3.2.2 Heat treating furnaces and ancillary equipment shall meet the requirements of PC5006.

3.3 Mechanical Property Testing

3.3.1 One tensile and two stress-rupture tests shall be performed on material from each heat-lot combination.

3.3.2 Location of the test specimens shall be near the forward end of the first consolidated bar (extrusion) and the rear end of the last consolidated bar representing the beginning and end of the heat-lot extrusion run.

3.3.3 Material in the fully heat-treated condition shall meet the following minimum mechanical properties when tested at the specified conditions.

TENSILE	1400°F
Ultimate strength (ksi)	120
0.2 percent yield strength (ksi)	100
Elongation (percent in 4D)	5

STRESS-RUPTURE	LIFE
1600°F and 77 ksi	30 hrs min.
2000°F and 32 ksi	30 hrs min.

3.4 Grain Structure

3.4.1 The transverse sections (end faces) on each bar shall have a coarse grain structure. Presence of small equiaxed grains (unrecrystallized areas) on any transverse section shall be rejectable. Acceptable and rejectable grain structures are provided in Figures 1 and 2.

3.4.2 The grain aspect ratio (GAR) in the bar longitudinal direction shall be greater than 10:1.

3.5 Microstructure

3.5.1 The transverse sections on each end of the bar shall be metallographically examined.

3.5.2 The material shall not contain inclusions with dimensions greater than the following:

Nonmetallic inclusions - 10 microns major diameter
Metallic inclusions - 45 microns major diameter

3.5.3 The material shall not contain any unrecrystallized regions.

4. PROCESS CONTROL

This section is not applicable to this specification.

5. IDENTIFICATION AND PACKING

5.1 Individual pieces and bundles of bars shall have attached a metal or plastic tag embossed with the purchase order number, the specification number and its revision letter, nominal size, heat and lot number; or shall be boxed and the box marked with the same information.

5.2 Each bar shall have the heat and lot number stamped on one end of the bar.

6. APPROVAL OR PROCUREMENT

6.1 Suppliers shall procure material only from producers approved by GTEC.

6.2 Engineering source approval for melting and subsequent conversion of material used to produce material to this specification shall be in accordance with EMS52503.

6.3 Chemical analysis and physical- and mechanical-properties testing shall be performed by a source approved by GTEC in accordance with EMS52353.

7. REPORTS

7.1 The supplier of the product shall furnish to GTEC Receiving Inspection a report of mechanical property test and chemical analysis results for each heat in the shipment. The report shall also have a statement as to conformance to the requirements of this specification.

7.1.1 This report shall include, but is not limited to, the purchase order number, lot number, heat number, material specification number and its revision letter, size, quantity, and material heat treat condition.

8. INSPECTION

8.1 The supplier shall perform all testing for conformance to technical requirements.

8.2 Each bar shall be fluorescent-penetrant inspected in accordance with EMS52309, Class 2 and radiographic inspected in accordance with EMS52348. No crack-like indications shall be allowed. Once process control has been established, radiographic sampling may be implemented upon approval by GTEC.

8.2.1 Tensile specimens shall be machined and tested in accordance with ASTM E 21.

8.2.2 Stress-rupture specimens shall be machined and tested in accordance with ASTM E 139.

8.2.3 If any of the destructive test specimens fail to meet minimum properties, two additional specimens for each failed specimen shall be tested. The retest specimens shall be taken from the destructive sample as close as possible to the original test specimen location. If either of the retests falls below the minimums, the material represented by the sample shall be rejected.

8.2.4 All test data shall be reported, including data which does not meet the minimums specified herein.

9. QUALITY ASSURANCE

9.1 The material shall be uniform in quality and condition, sound, and free from internal and external imperfections detrimental to use of the product.

9.2 Materials not conforming to the requirements of this specification shall be rejected.

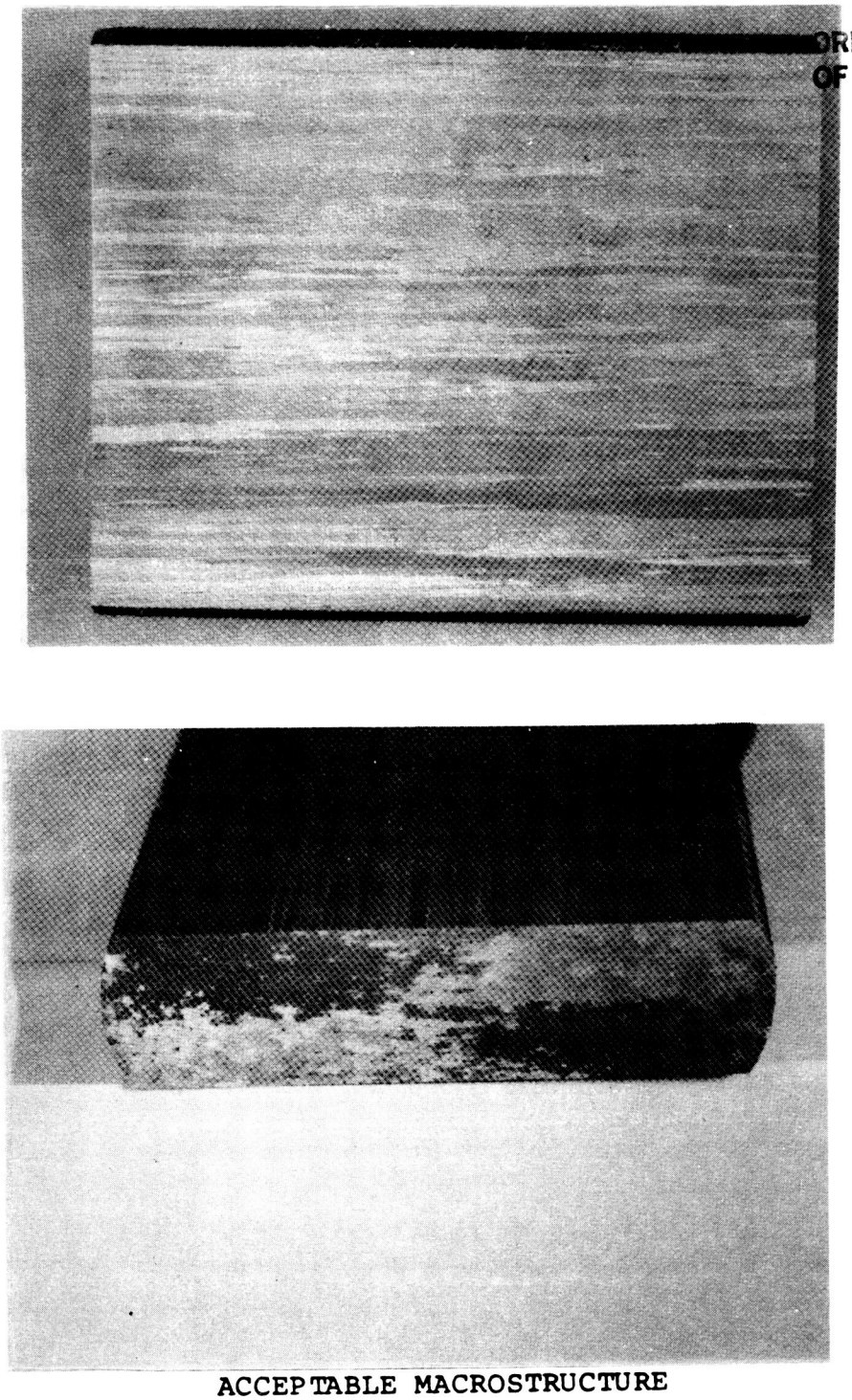

ACCEPTABLE MACROSTRUCTURE

Approximately 1 1/4X

FIGURE 1

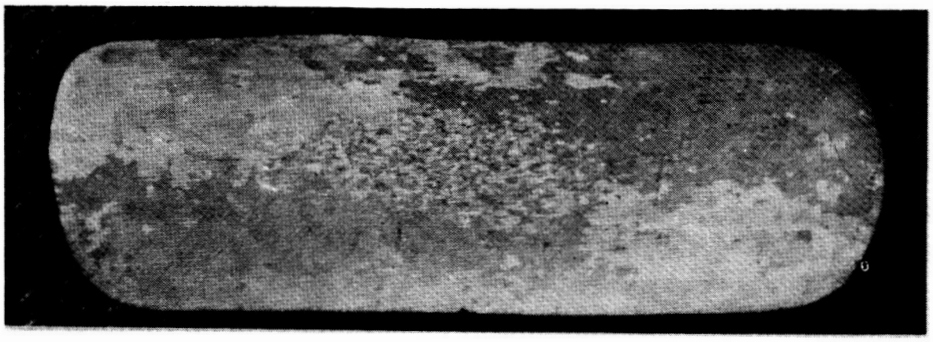

a) Unacceptable - Fine grain core

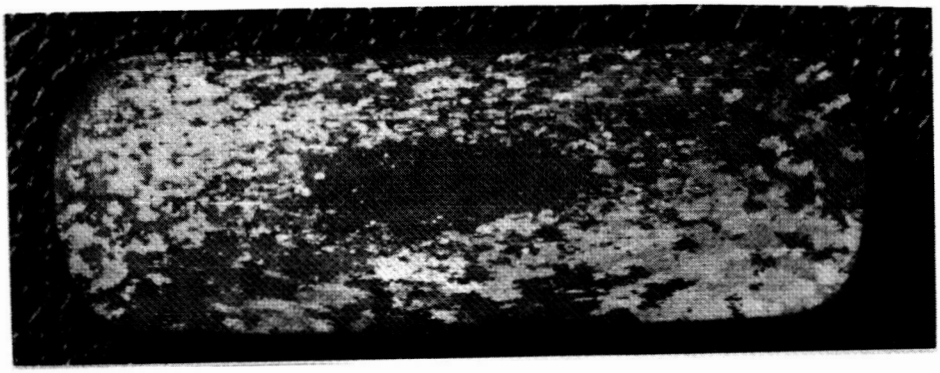

b) Unacceptable - Unrecrystallized core

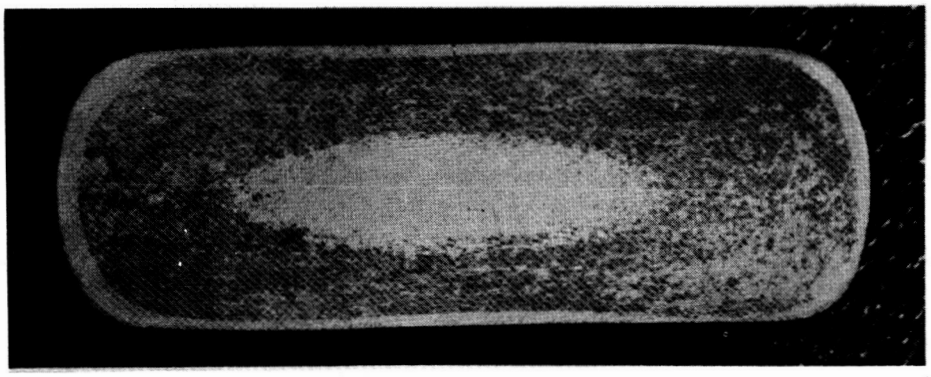

c) Unacceptable - Unrecrystallized core and periphery

FIGURE 2. Unacceptable Macrostructures
Approximately 1.6X

1. Report No.	2. Government Accession No.	3. Recipient's Catalog No.
NASA CR-179537		

4. Title and Subtitle	5. Report Date
Oxide-Dispersion-Strengthened Turbine Blades. Volume I	October 1986
	6. Performing Organization Code
7. Author(s)	8. Performing Organization Report No.
P.P. Millan, Jr. and J.C. Mays	Garrett 21-5278-1
	10. Work Unit No. 505-63-01
9. Performing Organization Name and Address	11. Contract or Grant No.
Garrett Turbine Engine Company A Division of The Garrett Corporation Phoenix, Arizona 85010	NAS3-20073
	13. Type of Report and Period Covered
12. Sponsoring Agency Name and Address	Contractor Report Project 4 Completion Report
National Aeronautics and Space Administration Lewis Research Center Cleveland, Ohio 44135	14. Sponsoring Agency Code

15. Supplementary Notes

Project Manager, Robert L. Dreshfield, Materials Division, NASA Lewis Research Center.

16. Abstract

The overall objective of Project 4 was to develop a high-temperature, uncooled gas turbine blade using MA6000 alloy from the feasibility stage through the engine demonstration test. The program objectives were achieved. Production scale up of the MA6000 alloy was achieved with a fair degree of tolerance to nonoptimum processing. The blade manufacturing process was also optimized. The mechanical, environmental, and physical property evaluations of MA6000 were conducted. The ultimate tensile strength, to about 704 °C (130 °F), is higher than DS MAR-M 247 but with a corresponding lower tensile elongation. Also, above 982 °C (180 °F) MA6000 tensile strength does not decrease as rapidly as MAR-M 247 because the ODS mechanism still remains active. Based on oxidation resistance and diffusional stability considerations, NiCrAlY coatings are recommended. CoCrAlY coating should be applied on top of a thin NiCrAlY coating. Vibration tests, whirlpit tests, and a high-rotor-rig test were conducted to ensure successful completion of the engine test of the MA6000 TFE731 high pressure turbine blades. The results of these tests were acceptable. In production quantities, the cost of the Project 4 MA6000 blade is estimated to be about twice that of a cast DS MAR-M 247 blade.

17. Key Words (Suggested by Author(s))	18. Distribution Statement
Turbine-blade; Oxide-dispersion-strengthened; MA6000; Mechanical alloying; Electrochemical machining	Unclassified - unlimited STAR Category 26

19. Security Classif. (of this report)	20. Security Classif. (of this page)	21. No. of pages	22. Price*
Unclassified	Unclassified	183	A09

*For sale by the National Technical Information Service, Springfield, Virginia 22161

GOVERNMENT PRINTING OFFICE: 1986 - 748120 / 40410